

SERI/TR-631-1330
UC Category: 59c

Analysis of the Adsorption Process and of Desiccant Cooling Systems — A Pseudo- Steady-State Model for Coupled Heat and Mass Transfer

Robert S. Barlow

December 1982

Prepared Under Task No. 1131.00 and 1132.11
WPA Nos. 01-256 and 01-315

Solar Energy Research Institute

A Division of Midwest Research Institute

1617 Cole Boulevard
Golden, Colorado 80401

Prepared for the
U.S. Department of Energy
Contract No. EG-77-C-01-4042

Printed in the United States of America
Available from:
National Technical Information Service
U.S. Department of Commerce
5285 Port Royal Road
Springfield, VA 22161
Price:
Microfiche \$3.00
Printed Copy \$8.00

NOTICE

This report was prepared as an account of work sponsored by the United States Government. Neither the United States nor the United States Department of Energy, nor any of their employees, nor any of their contractors, subcontractors, or their employees, makes any warranty, express or implied, or assumes any legal liability or responsibility for the accuracy, completeness or usefulness of any information, apparatus, product or process disclosed, or represents that its use would not infringe privately owned rights.

PREFACE

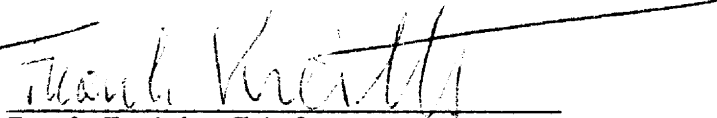
This report documents a computer model that simulates the adiabatic adsorption/desorption process. Developed to predict the performance of desiccant cooling systems, the model has been validated through comparison with experimental data for single-blow adsorption and desorption. This report also contains a literature review on adsorption analysis, detailed discussions of the adsorption process, and an initial assessment of the potential for performance improvement through advanced component development.

This research was performed under task 1131.00 of the Solar Desiccant Cooling Program at the Solar Energy Research Institute during fiscal year 1981. The author would like to acknowledge the contributions of Charles F. Kutscher, in charge of SERI's desiccant laboratory during this work; Harry Pohl, the laboratory technician; and Terry Penney, who provided a detailed and helpful review of the report.

Details of the experimental work completed at SERI to validate the computer model are contained in a separate report, SERI/TR-253-1429.

Approved for

SOLAR ENERGY RESEARCH INSTITUTE



Frank Kreith, Chief
Thermal Research Branch



Barry Butler, Manager
Solar Thermal and Materials Research Division

SUMMARY

OBJECTIVES

The primary objective of the research leading to this report was to develop and validate a computer program for predicting the performance of solar desiccant cooling systems. Major considerations in the development of the simulation model were to make the method of analysis as simple and versatile as possible, while maintaining the level of detail necessary for accurate predictions. The primary objective of this report is to provide complete documentation of this method of analysis and the computer programs. The report serves two additional functions. The first is to provide a detailed description of the adsorption process and the physical behavior of desiccant beds to facilitate a more complete understanding of the operation of the dehumidifier in a desiccant cooling cycle. The second is to provide information for an initial assessment of the potential for performance improvements through the development of advanced, high-performance components.

DISCUSSION

The computer model documented here is called a pseudo-steady-state model, and it uses a new approach to analyzing transient coupled heat and mass transfer as it occurs in adiabatic adsorption. Rather than deriving and solving a set of differential equations, the method uses simple effectiveness equations from the theory of steady-state heat exchangers and mass exchangers within a straightforward finite difference procedure. This simplifies the mathematics of the adsorption problem, makes the model easy to adapt to investigate a variety of adsorption issues, and makes it easier to keep track of the physics of the adsorption process. The body of the report includes a literature review of adsorption analysis and a review of available data and correlations of the properties of regular density silica gel, which appears to be the most suitable available desiccant for solar cooling systems.

The computer model was validated through comparison with experimental data for single-blow adsorption and desorption in packed beds of silica gel. Three data sources were used; the primary one was the SERI Desiccant Test Laboratory. Measured and predicted results for adsorption show agreement well within experimental uncertainty. This demonstrates that the lumped gas-side transfer coefficient, rather than separate gas-side and solid-side resistances to mass transfer, is sufficiently accurate for adsorption cases. Experimental results show that a different effective transfer coefficient must be used during single-blow desorption cases. However, relatively good agreement between measured and predicted results can still be obtained.

A major section of the report deals with the physical behavior of desiccant beds during single-blow adsorption or desorption and during cyclic operation, as in a cooling system. Of particular importance is the fact that adsorption comprises the progression of two heat and mass transfer waves through a desiccant bed. Also important are the differences between the behavior of thick beds, typically used for industrial adsorption applications, and thin beds, as used in desiccant cooling systems. Predicted performance of thin beds is much

more sensitive to errors in transfer coefficients and desiccant property correlations, because only a portion of the second wave front is contained within the bed. The detailed discussion of the adsorption process is intended to facilitate a more complete understanding of the operation of the dehumidifier in a desiccant cooling cycle

The pseudo-steady-state model was incorporated into a computer program for the simulation of a complete desiccant cooling system. Parametric studies were performed on two systems, one representative of existing prototypes and the other containing high effectiveness components. These parametric studies characterize the effect on performance of operating conditions, such as indoor conditions, outdoor conditions, dehumidifier wheel rotation speed, and regeneration temperature. They also provide information on the influence of individual component effectiveness on overall system thermal performance. This permits an initial assessment of the potential gains in performance that could be achieved through the development of advanced, high-effectiveness components.

CONCLUSIONS

Major conclusions include the following:

- A simple computer model for the adiabatic adsorption/desorption process has been developed and validated.
- Close agreement between measured and predicted results for single-blow adsorption demonstrates that a lumped gas-side mass transfer coefficient can be used.
- Effective mass transfer coefficients must be reduced for cases of single-blow desorption, presumably because of a dynamic hysteresis effect in silica gel properties.
- The thermal performance of a desiccant cooling system varies with indoor and outdoor temperature and humidity, and generally decreases as the difference between indoor and outdoor conditions increases.
- COPs above 1.0 are technically feasible if high-effectiveness dehumidifiers and heat exchangers are used.
- With high-performance components, the ventilation mode is clearly superior to the recirculation mode. Thermal COPs in the ventilation mode become relatively insensitive to outdoor conditions when high-effectiveness components are used.

TABLE OF CONTENTS

	<u>Page</u>
1.0 Introduction.....	1
1.1 Background.....	1
1.2 Purpose and Scope.....	2
1.3 Adsorption Process and Desiccant Cooling Cycle.....	3
2.0 Historical Overview.....	5
3.0 Pseudo-Steady-State Model.....	9
3.1 General Description.....	9
3.2 Mass Transfer Calculation.....	10
3.3 Intermediate Energy Balance.....	12
3.4 Heat Transfer Calculation.....	13
3.5 Transfer Coefficients.....	14
3.6 Properties of Moist Air.....	16
3.7 Properties of Silica Gel.....	18
3.7.1 Equilibrium Properties.....	19
3.7.2 Heat of Adsorption.....	27
4.0 Comparison of the Model with Experimental Data.....	31
4.1 Data Sources for Single-Blow Adsorption and Desorption.....	31
4.2 Comparison with SERI Data.....	31
4.3 Comparison with Pesaran Data.....	33
4.4 Comparison with Koh Data.....	52
4.5 Results.....	53
5.0 Desiccant Cooling System Simulation.....	63
5.1 System Configuration.....	63
5.2 Method of Analysis.....	63
5.3 Component Analysis and Equations.....	66
6.0 The Physical Behavior of Desiccant Beds.....	69
6.1 Behavior of Thick Beds During Adiabatic Adsorption.....	69
6.2 Behavior of Thick Beds During Adiabatic Desorption.....	71
6.3 Behavior of Thin Beds.....	75
6.4 Behavior During Cyclic Operation.....	80
7.0 Parametric Studies of Desiccant Cooling Systems.....	85
7.1 Effect of Simulation Parameters in the Dehumidifier Model.....	85
7.2 System Specifications.....	87
7.3 Effect of Outdoor Conditions.....	88
7.4 Effect of Indoor Conditions.....	89

TABLE OF CONTENTS (Concluded)

	<u>Page</u>
7.5 Effect of Regeneration Temperature.....	94
7.6 Effect of Heat Exchanger Effectiveness.....	94
7.7 Effect of Evaporative Cooler 1.....	95
7.8 Summary of Parametric Studies.....	95
8.0 Conclusions and Recommendations.....	99
8.1 Conclusions Regarding the Pseudo-Steady-State Model.....	99
8.2 Conclusions Regarding Cooling System Performance.....	100
8.3 Recommendations.....	100
9.0 References.....	103
Appendix A: Users Guide to Computer Programs.....	107
A-1 Overview of Computer Programs.....	107
A-2 Job Control Files and Input Data.....	108
A-3 A Partial Listing of FORTRAN Variables.....	109
Appendix B: Program Listings.....	115

LIST OF FIGURES

	<u>Page</u>
1-1 IGT Solar-MEC® System in Recirculation Mode.....	4
2-1 Linear Approximation to Properties of Silica Gel and Molecular Sieve.....	6
3-1 Conveyor Belt Concept Used in Computer Model.....	9
3-2 Concentration Profiles for Steady-State Mass Transfer Process.....	11
3-3 (a) Detailed Resistance Model for Mass Transfer.....	14
(b) Gas-Side Resistance Model for Mass Transfer.....	14
3-4 Comparison of Various Mass Transfer Correlations for Packed Beds....	17
3-5 Typical Isotherms for Regular- and Low-Density Silica Gel.....	20
3-6 Isotherms Based on the Bullock and Threlkeld Correlation.....	23
3-7 Comparison of the Close and Banks Complete Correlation with Simplified Correlation Using $f_1(X) = 2.009$	24
3-8 Comparison of the Close and Banks Simplified Expression with Further Simplified Expression Using Linear $f_2(X)$	25
3-9 Comparison of the Rojas Correlation with Eq. 3-30.....	26
3-10 Comparison of Various Correlations and Data for the Heat of Adsorption for Silica Gel.....	29
4-1 Measured and Predicted Outlet Air Conditions During SERI Run 85A (ICORR = 1).....	34
4-2 Measured and Predicted Outlet Air Conditions During SERI Run 85A (ICORR = 2).....	35
4-3 Measured and Predicted Outlet Air Conditions During SERI Run 85A (ICORR = 3).....	36
4-4 Measured and Predicted Outlet Air Conditions During SERI Run 85R (ICORR = 1, Le = 3).....	37
4-5 Measured and Predicted Outlet Air Conditions During SERI RUN 85R (ICORR = 1, Le = 6).....	38
4-6 Measured and Predicted Outlet Air Conditions During SERI Run 85R (ICORR = 1, Le = 9).....	39

LIST OF FIGURES (Continued)

	<u>Page</u>
4-7 Measured and Predicted Outlet Air Conditions During SERI Run 85R (ICORR = 2, Le = 9).....	40
4-8 Measured and Predicted Outlet Air Conditions During SERI Run 85R (ICORR = 3, Le = 9).....	41
4-9 Measured and Predicted Outlet Air Conditions During Pesaran Run 8.....	42
4-10 Measured and Predicted Outlet Air Conditions During Pesaran Run 10.....	43
4-11 Measured and Predicted Outlet Air Conditions During Pesaran Run 11.....	44
4-12 Measured and Predicted Outlet Air Conditions During Pesaran Run 12.....	45
4-13 Measured and Predicted Outlet Air Conditions During Pesaran Run 18 (ICORR = 1).....	46
4-14 Measured and Predicted Outlet Air Conditions During Pesaran Run 18 (ICORR = 2).....	47
4-15 Measured and Predicted Outlet Air Conditions During Pesaran Run 18 (ICORR = 3).....	48
4-16 Measured and Predicted Outlet Air Conditions During Pesaran Run 22.....	49
4-17 Measured and Predicted Outlet Air Conditions During Pesaran Run 24.....	50
4-18 Measured and Predicted Outlet Air Conditions During Koh Run 2.....	54
4-19 Measured and Predicted Outlet Air Conditions During Koh Run 4.....	55
4-20 Measured and Predicted Outlet Air Conditions During Koh Run 6 (ICORR = 2).....	56
4-21 Measured and Predicted Outlet Air Conditions During Koh Run 6 (ICORR = 3).....	57
4-22 Measured and Predicted Outlet Air Conditions During Koh Run 8 (ICORR = 1).....	58
4-23 Measured and Predicted Outlet Air Conditions During Koh Run 9.....	59

LIST OF FIGURES (Continued)

	<u>Page</u>
4-24 Measured and Predicted Outlet Air Conditions During Koh Run 10.....	60
4-25 Measured and Predicted Outlet Air Conditions During Koh Run 15.....	61
5-1 System Schematic and Psychrometric Cycle Diagram for the Ventilation Mode.....	64
5-2 System Schematic and Psychrometric Cycle Diagram for the Recirculation Mode.....	65
5-3 Small Element Used in Simulations of Rotary Dehumidifiers.....	67
6-1 The First Adsorption Wave in a Thick Desiccant Bed.....	70
(a) Desiccant Temperature Profiles.....	70
(b) Desiccant Loading Profiles.....	70
(c) Outlet Air Temperature.....	70
(d) Outlet Air Humidity.....	70
(e) Psychrometric Path of Outlet States.....	70
6-2 Two Adsorption Waves in a Thick Desiccant Bed.....	72
(a) Desiccant Temperature Profiles.....	72
(b) Desiccant Loading Profiles.....	72
(c) Outlet Air Temperature.....	72
(d) Outlet Air Humidity.....	72
(e) Psychrometric Path of Outlet States.....	72
6-3 The First Desorption Wave in a Thick Desiccant Bed.....	73
(a) Desiccant Temperature Profiles.....	73
(b) Desiccant Loading Profiles.....	73
(c) Outlet Air Temperature.....	73
(d) Outlet Air Humidity.....	73
(e) Psychrometric Path of Outlet States.....	73
6-4 Two Desorption Waves in a Thick Desiccant Bed.....	74
(a) Desiccant Temperature Profiles.....	74
(b) Desiccant Loading Profiles.....	74
(c) Outlet Air Temperature.....	74
(d) Outlet Air Humidity.....	74
(e) Psychrometric Path of Outlet States.....	74
6-5 The First Adsorption Wave in a Thin Desiccant Bed.....	76
(a) Desiccant Temperature Profiles.....	76
(b) Desiccant Loading Profiles.....	76
(c) Outlet Air Temperature.....	76
(d) Outlet Air Humidity.....	76
(e) Psychrometric Path of Outlet States.....	76

LIST OF FIGURES (Continued)

	<u>Page</u>
6-6 Two Adsorption Waves in a Thin Desiccant Bed.....	77
(a) Desiccant Temperature Profiles.....	77
(b) Desiccant Loading Profiles.....	77
(c) Outlet Air Temperature.....	77
(d) Outlet Air Humidity.....	77
(e) Psychrometric Path of Outlet States.....	77
6-7 The First Desorption Wave in a Thin Desiccant Bed.....	78
(a) Desiccant Temperature Profiles.....	78
(b) Desiccant Loading Profiles.....	78
(c) Outlet Air Temperature.....	78
(d) Outlet Air Humidity.....	78
(e) Psychrometric Path of Outlet States.....	78
6-8 Two Desorption Waves in a Thin Desiccant Bed.....	79
(a) Desiccant Temperature Profiles.....	79
(b) Desiccant Loading Profiles.....	79
(c) Outlet Air Temperature.....	79
(d) Outlet Air Humidity.....	79
(e) Psychrometric Path of Outlet States.....	79
6-9 Behavior of a Thin Desiccant Bed During Cyclic Operation.....	81
(a) Temperature Profiles During Adsorption.....	81
(b) Loading Profiles During Adsorption.....	81
(c) Outlet Air Temperature During Adsorption.....	81
(d) Outlet Air Humidity During Adsorption.....	81
(e) Temperature Profiles During Desorption.....	82
(f) Loading Profiles During Desorption.....	82
(g) Outlet Air Temperature During Desorption.....	82
(h) Outlet Air Humidity During Desorption.....	82
(i) Psychrometric Paths of Outlet States.....	82
7-1 Predicted COP vs. Simulation Time Step.....	85
7-2 (a) COP vs. Regeneration Lewis Number.....	86
(b) Capacity vs. Regeneration Lewis Number.....	86
7-3 (a) COP vs. Half-Cycle Time.....	87
(b) Capacity vs. Half-Cycle Time.....	87
7-4 Effect of Outdoor Conditions on Performance of the Base System:	
(a) COP vs. T, ambient in Ventilation Mode.....	90
(b) COP vs. T, ambient in Recirculation Mode.....	90
(c) Capacity vs. T, ambient in Ventilation Mode.....	90
(d) Capacity vs. T, ambient in Recirculation Mode.....	90

LIST OF FIGURES (Continued)

	<u>Page</u>
7-5 Effect of Outdoor Conditions on Performance of the High Performance System:.....	91
(a) COP vs. T, ambient in Ventilation Mode.....	91
(b) COP vs. T, ambient in Recirculation Mode.....	91
(c) Capacity vs. T, ambient in Ventilation Mode.....	91
(d) Capacity vs. T, ambient in Recirculation Mode.....	91
7-6 Effect of Indoor Conditions on Performance of the Base System:.....	92
(a) COP vs. T, room in Ventilation Mode.....	92
(b) COP vs. T, room in Recirculation Mode.....	92
(c) Capacity vs. T, room in Ventilation Mode.....	92
(d) Capacity vs. T, room in Recirculation Mode.....	92
7-7 Effect of Indoor Conditions on Performance of the High Performance System:.....	93
(a) COP vs. T, room in Ventilation Mode.....	93
(b) COP vs. T, room in Recirculation Mode.....	93
(c) Capacity vs. T, room in Ventilation Mode.....	93
(d) Capacity vs. T, room in Recirculation Mode.....	93
7-8 (a) Effect of Regeneration Temperature on COP.....	94
(b) Effect of Regeneration Temperature on Capacity.....	94
7-9 (a) Effect of Heat Exchanger Effectiveness on COP.....	95
(b) Effect of Heat Exchanger Effectiveness on Capacity.....	95
7-10 Effect of the Effectiveness of Evaporative Cooler 1 on Performance of the Base System:.....	96
(a) COP.....	96
(b) Capacity.....	96

LIST OF TABLES

	<u>Page</u>
3-1 Typical Properties of Silica Gel.....	19
3-2 Particle Diameter and Surface Area.....	19
3-3 Constants for the Bullock and Threlkeld Correlation for Silica Gel.....	21
4-1 Physical Properties and Dimensions for SERI Experiments.....	32

LIST OF TABLES (Concluded)

	<u>Page</u>
4-2 Summary of Data Runs and Computer Predictions for SERI Experiments on a 3.5-cm Bed.....	33
4-3 Physical Properties and Dimensions for Pesaran Experiments.....	51
4-4 Summary of Data Runs and Predictions for Pesaran Experiments.....	51
4-5 Physical Properties for Koh Experiments.....	52
4-6 Summary of Data Runs and Predictions for Koh Experiments.....	52
7-1 System Specifications for Parametric Studies.....	88
7-2 Nominal Operating Environment for Parametric Studies.....	88

NOMENCLATURE

A_s	Surface area for heat or mass transfer within a packed bed section (m^2)
c_b	Specific heat of desiccant bed ($J/kg^\circ C$)
c_p	Specific heat of air ($J/kg^\circ C$)
c_w	Specific heat of liquid water ($J/kg^\circ C$)
C_{ads}	Capacity rate of air on the adsorption side of the system heat exchanger ($W/^\circ C$)
C_{air}	Capacity rate of air ($W/^\circ C$ or kg/s)
C_{bed}	Capacity rate of desiccant ($W/^\circ C$ or kg/s)
CC	C_{min}/C_{max}
C_{max}	Larger capacity rate ($W/^\circ C$)
C_{min}	Smaller capacity rate ($W/^\circ C$)
C_{reg}	Capacity rate of air on the regeneration side of the system heat exchanger ($W/^\circ C$)
D_p	Particle diameter (m)
E	Effectiveness of exchange process
E_{c1}	Effectiveness of evaporative cooler 1
E_{c2}	Effectiveness of evaporative cooler 2
E_{hx}	Effectiveness of system heat exchanger
g	Mass transfer coefficient (kg/m^2s)
G_a	Mass velocity (kg/m^2s)
h_a	Enthalpy of moist air (J/kg)
h_a	Enthalpy of moist air after mass transfer calculation (J/kg)
h_{ads}	Heat of adsorption of water (J/kg)
h_b	Enthalpy of moist desiccant (J/kg)
h_{vap}	Heat of vaporization of water (J/kg)
Δh_w	Integral heat of wetting

H	Heat transfer coefficient ($\text{W}/^\circ\text{Cm}^2$)
k	Thermal conductivity of air ($\text{W}/^\circ\text{Cm}^2$)
L	Depth of desiccant bed (m)
Le	Lewis number
m	Mass fraction of water vapor in air
\bar{m}	Average mass fraction of water vapor in air
m_s	Mass fraction of water vapor in air at equilibrium with the desiccant surface
$\dot{m}_{\text{H}_2\text{O}}$	Mass flux of water ($\text{kg}/\text{m}^2\text{s}$)
M_a	Dry mass of air chunk (kg)
M_b	Dry mass of bed section (kg)
M_w	Mass of water absorbed (kg)
Ntu	Number of transfer units
Nu	Nusselt number
P_{atm}	Atmospheric pressure (Pa)
P_{sat}	Saturation pressure (Pa)
P_v	Vapor pressure (Pa)
P_{ve}	Equilibrium vapor pressure at desiccant surface (Pa)
Q	Energy transferred (J)
\dot{Q}	Rate of energy transfer (W)
Re	Reynolds number
R_g	Gas-side mass transfer resistance (s/kg)
R_g^*	Modified gas-side mass transfer resistance
RH	Relative humidity
R_s	Solid-side mass transfer resistance ($\text{m}^2\text{s}/\text{kg}$)
Sc	Schmidt number
Δt	Time step (s)

T	Temperature ($^{\circ}\text{C}$)
T_b	Temperature of bed section ($^{\circ}\text{C}$)
$T_b^{\#}$	Intermediate temperature of bed section ($^{\circ}\text{C}$)
T_{in}	Inlet air temperature ($^{\circ}\text{C}$)
T_0	Initial temperature of desiccant bed ($^{\circ}\text{C}$)
T^*	Wet bulb temperature ($^{\circ}\text{C}$)
V	Superficial air velocity (m/s)
w	Humidity ratio (kg/kg dry air)
w_e	Equilibrium humidity ratio at desiccant surface (kg/kg dry air)
w_{in}	Inlet humidity ratio (kg/kg dry air)
w^*	Saturation humidity ratio at wet bulb temperature (kg/kg dry air)
X	Moisture ratio of water in desiccant (kg/kg dry desiccant)
X	Initial moisture content of desiccant (kg/kg dry desiccant)
X_s	Moisture content at desiccant surface (kg/kg dry desiccant)
\bar{X}	Average moisture content of desiccant (kg/kg dry desiccant)
Y	Mass fraction of water in desiccant ($X/1 + X$)
ϵ_v	Void fraction
μ	Dynamic viscosity of air (kg/m s)
ρ	Density of air (kg/m^3)
ρ_b	Density of desiccant bed (kg/m^3)

SUBSCRIPTS

e	Exit
i	Inlet
1	State at beginning of time step
2	State at end of time step

SECTION 1.0

INTRODUCTION

1.1 BACKGROUND

Desiccants have been used for many years to provide dry air for a variety of industrial and commercial processes. Several manufacturers have marketed desiccant air conditioning systems for special situations requiring very low relative humidities ($<10\%$) which cannot be provided by vapor compression equipment. Because there has been little competition in this market, the energy efficiency of drying equipment has not been a primary concern. The thermal efficiency of industrial and commercial drying equipment tends to be low, and parasitic power requirements tend to be high. A significant difference between solar cooling systems and commercial drying systems is that solar cooling must compete with conventional vapor compression cooling. Thus, the thermal coefficient of performance must be high and parasitic power requirements must be low.

Although Löf [1] proposed an open-cycle, liquid-desiccant, solar-cooling system in 1955 and Dunkle [2] proposed an open-cycle, solid-desiccant, solar-cooling system in 1965, active research in desiccant cooling did not begin until the mid-1970s. Lunde [3] developed preliminary designs for a cooling system using silica gel. Nelson [4] investigated the feasibility of solar desiccant cooling using a simple desiccant model in seasonal simulations. Because of an emphasis on the rapid commercialization of solar technologies, the national desiccant cooling research program moved quickly from these initial studies toward the development of prototype cooling systems in the capacity range of 5 to 10 kW (17000 to 34000 Btu/h) for residential and small commercial applications. Solid desiccant systems are a promising alternative for these smaller-scale applications because they are mechanically simple, can be driven by flat-plate collectors, and use air as the transport fluid and water as the refrigerant.

Three prototype systems were designed and built under U.S. Department of Energy (DOE) contracts beginning in 1977. The Institute of Gas Technology (IGT) uses a molecular sieve impregnated wheel in its Solar-MEC® system [5]. AiResearch uses a thin rotating drum packed with silica gel particles in its SODAC system [6]. The Illinois Institute of Technology (IIT) uses Teflon® bonded silica gel sheets in fixed, cross-cooled adsorbers [7]. All three systems have performed with COPs between 0.5 and 0.6 under ARI standard operating conditions.

A recent report evaluating residential and commercial solar/gas heating and cooling technologies, written by Booz-Allen and Hamilton for the Gas Research Institute [8], has indicated that advanced desiccant cooling systems with COPs near 1.2 would be competitive with vapor compression systems in the 1990s and would be the solar cooling system of choice for residential applications in regions having moderate heating and cooling loads. The current emphasis of the desiccant cooling program is to expand on experience gained with first-generation prototypes and to perform basic research and development on new concepts and advanced components that will lead to advanced desiccant systems with this prescribed performance.

1.2 PURPOSE AND SCOPE

This report documents a computer model for adsorption/desorption that was developed as a research tool to investigate a variety of technical areas concerning the behavior of desiccant beds and the performance of cooling systems. This model fills a need for a general-purpose desiccant simulation program to evaluate alternatives for advanced components. Specific issues that the model has been or will be used to investigate involve the effects of desiccant bed geometry, of modifying desiccant properties,* and of component performance on the system coefficient of performance (COP). The model uses a new approach to simulation of transient coupled heat and mass transfer in that simple equations for steady-state heat and mass exchangers are used. Hence, it is referred to as a pseudo-steady-state model. This approach simplifies the mathematics of the analysis and is intended to make the model easy to adapt to a variety of adsorption problems. It also should make the model more acceptable and thus more useful to engineers and research scientists who are not specialists in numerical analysis.

The report is divided into eight sections. In the last portion of this introduction is a brief description of the physics of the adsorption problem, intended primarily for those with little or no experience with desiccants. Section 2.0 provides a detailed historical overview of adsorption analysis that summarizes the different mathematical approaches that various investigators have taken. Section 3.0 describes the new pseudo-steady-state adsorption model, presents the equations used, and gives correlations for the properties of moist air and silica gel. Section 4.0 compares predictions using this model with experimentally measured outlet air conditions for single-blow adsorption and desorption experiments with packed beds of silica gel. Three independent data sources are used to provide a thorough assessment of the validity of the model. Section 5.0 outlines the simulation of complete desiccant cooling systems, giving equations for analysis of components other than the dehumidifier and describing the program logic. Section 6.0 describes the physical behavior of desiccant beds, both in single-blow operation and cyclic system operation. This description is qualitative but detailed. It is intended to facilitate a better understanding of the way the desiccant cooling cycle works and the factors that affect the performance of the desiccant bed, an understanding essential to making sound research decisions. Section 7.0 presents results of parametric studies on the performance of two cooling systems, one representative of existing prototypes and the other containing advanced, high-effectiveness components. Section 8.0 presents conclusions and recommendations. A practical user's guide to the programs for single-blow simulations, system simulations, and parametric studies is included as Appendix A. Program listings are also included, as Appendix B.

As reported here, the computer model only includes property data of regular density silica gel in a packed-bed geometry. The capabilities of the model will be expanded to include properties of other desiccant materials, such as molecular sieve, and to simulate heat and mass transfer in parallel-passage, laminar flow desiccant beds in the near future.

*See SERI/TP-631-1157 [Ref. 49].

1.3 ADSORPTION PROCESS AND DESICCANT COOLING CYCLE

Few people in the solar community are familiar with desiccants or the adsorption process. Therefore, a brief description of both is included here as an introduction.

Desiccants are a class of adsorbents/absorbents that have a high affinity for water. They can be either liquids or solids. Examples of liquid desiccants are salt solutions, such as lithium chloride or calcium chloride, and some organic liquids, such as triethylene glycol. Examples of solid desiccants are silica gel, molecular sieves, and natural zeolites. This report is concerned only with solid desiccants and, specifically, regular density silica gel. However, the methods used here can be applied to a wide variety of coupled heat and mass transfer problems. Generally, solid desiccants are highly porous materials that adsorb water by mechanisms of chemical adsorption of water molecules onto sites on the walls of the pores, physical adsorption of successive layers of water molecules, and capillary condensation within the pores. The amount of water that a desiccant will hold at equilibrium is a function of its temperature and the water vapor pressure or humidity of the air that surrounds it. At high temperatures and low humidities, a desiccant will contain almost no sorbed water. At room temperature in saturated air, silica gel will pick up 35% to 40% of its weight in moisture.

The desiccant cooling cycle takes advantage of this moisture cycling capacity to dehumidify air. Figure 1-1 is a diagram of the Solar-MEC® desiccant cooling system. It consists of a dehumidifier, sensible heat exchanger, two evaporative coolers, a solar heating coil, and an auxiliary gas burner.

In essence, the desiccant cycle permits evaporative cooling to be used in humid climates by turning hot, humid air into hot, dry air before it is sent through an evaporator pad. The heart of a desiccant system and the component that is most difficult to simulate mathematically is the dehumidifier or desiccant wheel. This wheel rotates between two counter-flowing air streams, adsorbing moisture from the conditioning stream and desorbing that moisture to the solar-heated air of the regeneration stream.

Consider a dehumidifier wheel constructed of a thin, packed bed of desiccant particles held between two metal screens (the construction used by AiResearch). On the adsorption side of the system, warm, moist air is exposed to relatively dry desiccant. Water molecules in the air at the surface of the particles are adsorbed. This creates a humidity gradient in the air stream and causes other water molecules to migrate toward the surface where they, in turn, are adsorbed as the air flows through the bed. This is a convective mass transfer process. A second mass transport process takes place simultaneously within the desiccant particles. During dehumidification, the water concentration in the desiccant near the surface of the desiccant particle is higher than it is at the center. This concentration gradient causes water to diffuse inward.

Thus, there are two mass transfer resistances, a gas-side resistance and a solid-side resistance, that determine the rate of transfer of water between the air and the desiccant. Both resistances are important in packed beds and must be accounted for in simulations.

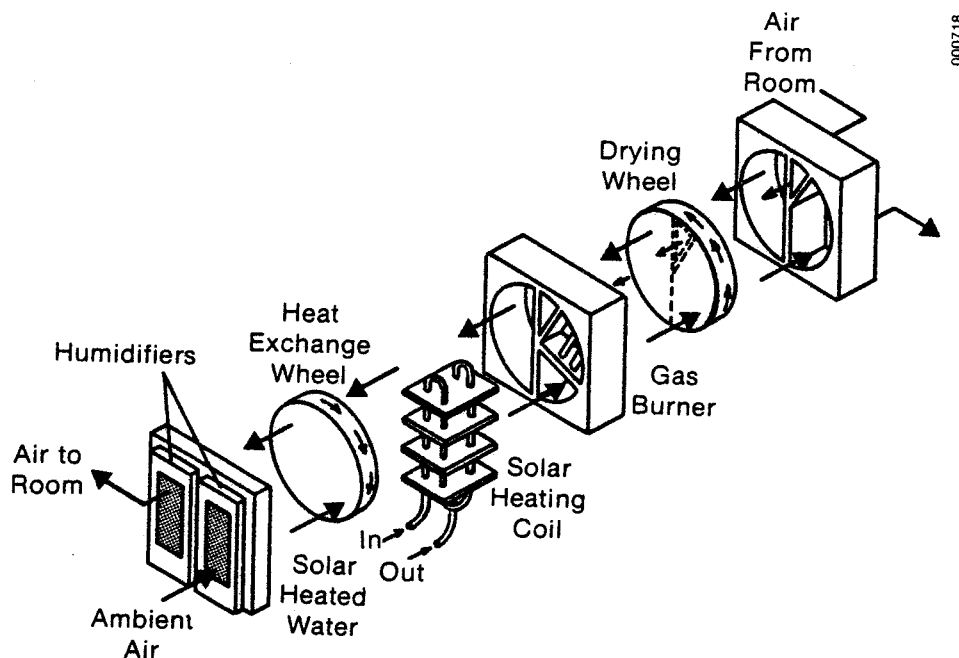


Fig. 1-1. IGT Solar-MEC® System in the Recirculation Mode [Ref. 5]

In addition to the mass transfer problem, the adiabatic dehumidification process involves a heat transfer problem. When water is adsorbed by the desiccant, energy is released. For silica gel, the amount of energy, called the heat of adsorption, is typically 10% to 15% greater than the heat of condensation of water. This energy release elevates the temperature of the desiccant and causes heat to be transferred to the air stream. Fortunately, the thermal conductivity of most desiccants is high enough so that temperature gradients within the particles can be neglected, and only a single resistance to heat transfer, the convective resistance, need be considered. In summary, adsorption comprises simultaneous heat and mass transfer processes that are coupled by the equilibrium properties of the desiccant and during which thermal energy is generated as a consequence of the mass transfer.

When the desiccant wheel passes to the regeneration side, all processes listed above are reversed. Energy is transferred from the solar-heated air stream to the desiccant. As the temperature of the desiccant increases, water at the surface is desorbed and picked up by the air. Water from the interior of the particle diffuses toward the surface where it is desorbed.

SECTION 2.0

HISTORICAL OVERVIEW

Desiccants have been used for many years to dehumidify air for industrial processes. The analysis of air drying also has a long history, dating back to the late 1940s. Beyond the drying application, adsorption has many applications in the chemical industry. The governing transport equations are the same whether we use silica gel to remove water vapor from air or activated carbon to remove methane from helium. As a result, researchers have contributed to the state of the art of analysis in a variety of fields. Despite this long history, few modeling attempts have been completely successful, for two reasons. First, the mathematical formulation of the adsorption process as described above includes five differential equations for the conservation of mass and energy. These equations are coupled nonlinearly by additional equations describing the properties of the desiccant. This set of equations must be solved numerically, and even with today's computers, their solution is computationally expensive. Second, differential equations include transport coefficients that must be determined experimentally. The experiments are difficult to perform, and few data are available for some of these transport coefficients. This is especially true with regard to diffusion coefficients for water within solid desiccants. The accuracy of any model is limited by the accuracy of the data supplied to it.

To make the problem manageable, the first investigators of the adsorption process made sets of fairly restrictive assumptions about the adsorption process and desiccant properties. The history of modeling has been a process of relaxing these assumptions step by step. The first modeling work in air drying was conducted by Hougen and Marshall [9]. They developed an analytical solution for isothermal adsorption where the relationship between the vapor pressure in the air and the equilibrium water content of the desiccant is linear. Figure 2-1 compares linear isotherms with typical isotherms for molecular sieve and silica gel. The linear approximation is relatively good for silica gel below relative humidities of about 50%. However, it is a poor approximation for molecular sieves. Hougen and Marshall also proposed graphical methods to deal with nonlinear desiccant properties, and with adiabatic adsorption where the heat generated during adsorption is significant and must be included. An underlying assumption in this work was that a single, air-side mass transfer coefficient could be used, and that the effect of diffusion in the solid could be included in this lumped coefficient. Hougen and Marshall used data from Ahlberg [10] to produce empirical correlations for heat and mass transfer coefficients in packed beds of silica gel. Subsequently, several other authors have used these correlations. However, because the data set on which they are based is relatively limited and includes considerable scatter, these coefficients should probably be used only as a starting point. Additional problems with the correlations are discussed in Sec. 3.5.

Rosen [11,12] expanded the isothermal model to include the separate effects of mass transfer across a fluid boundary layer and diffusion of the adsorbate into spherical adsorbent particles. This analytical approach leads to a series solution that can be evaluated numerically. However, it is still

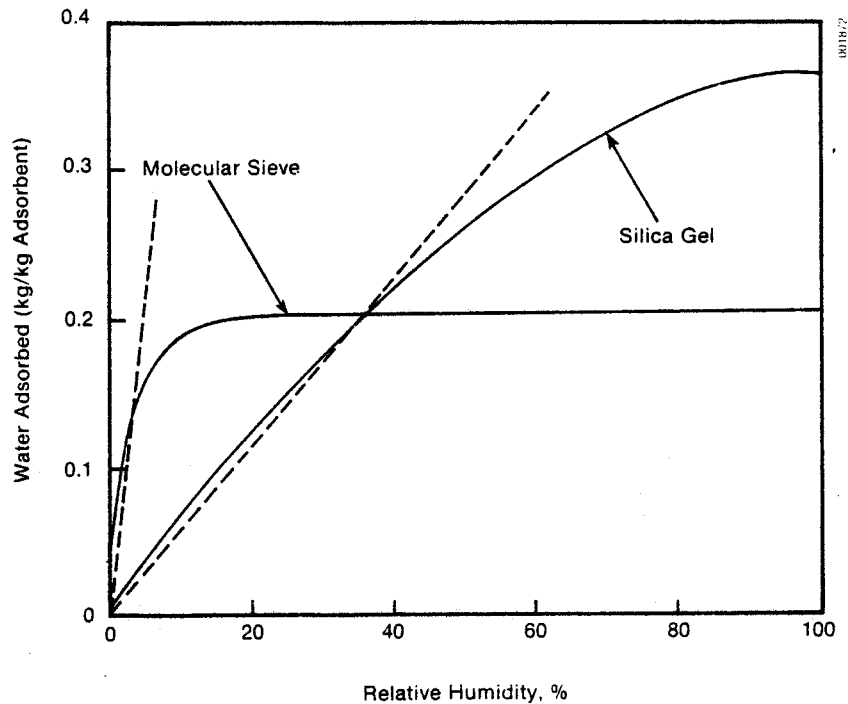


Fig. 2-1. Linear Approximation to Properties of Silica Gel and Molecular Sieve

limited to linear isotherms and applies only to cases in which the desiccant bed is initially uniformly dry. An alternative approach used by Eagleton and Bliss [13] allows for the concentration gradient in the adsorbent by means of a hypothetical solid film coefficient. That is, the mass transfer rate in the solid is assumed to be proportional to the difference between the surface concentration and the average concentration of the adsorbate in the particle. They maintained the assumption of a linear isotherm, but allowed for a non-zero intercept. Antonson [14] obtained relatively good agreement with experimental results for the isothermal case by considering diffusion in the solid as the only resistance to mass transfer in a helium/ethane/molecular sieve system.

After comparing the relative success of the previous approaches and concluding that a two-resistance model is preferable [15-17], Carter extended Rosen's work to include the adiabatic case [18,19]. Carter assumed a simple exponential relationship between vapor pressure and the equilibrium loading of the adsorbent. He used finite difference techniques to solve the resulting set of equations and obtained good agreement between experimental and calculated results for adsorption of water vapor by activated alumina. Meyer and Weber [20] increased the complexity and generality of adsorption modeling in a study of the adsorption of methane from helium by activated carbon. They included internal and external resistances to heat transfer as well as mass transfer and used a general equation for equilibrium properties containing eight curve-fitting parameters. Although this is a very detailed model, it

attained only limited success, presumably because of inaccuracies in the experimentally measured values of the diffusion coefficient of methane in activated carbon.

Noting the difficulty of obtaining accurate values for the intraparticle diffusion coefficient, Bullock and Threlkeld [21] used the lumped, effective external heat and mass transfer coefficients reported by Hougen and Marshall for the adiabatic drying of air by silica gel. To facilitate computation, they expressed the equilibrium data for silica gel presented by Hubbard [22] as polynomials in temperature and moisture content. Chi and Wasan [23] used the same approach to study air drying by a porous matrix impregnated with lithium chloride. More recently, Koh [24] investigated the use of solar energy for the regeneration of silica gel used for grain drying. Following the methods of Bullock and Chi, but modifying the transfer coefficients of Hougen and Marshall, Koh was moderately successful in matching experimental and predicted results for the adiabatic desorption process.

All the researchers mentioned have investigated single-blow adsorption or desorption in fixed beds. Concerns about energy conservation and renewable resources over the past decade have stimulated research in coupled heat and mass transfer in total heat regenerators or enthalpy exchangers and in desiccant dehumidifiers for solar cooling. Maclaine-cross, Banks, and Close [25,26,27,28] used the method of characteristics to reexpress the governing equations for adsorption in terms of combined potentials. These equations are analogous to those for transfer alone, and existing solutions for rotary heat exchangers can be applied. This analogy method is approximate because linearizations are made at several points in its derivation. However, it is very efficient computationally. Pla-Barby [29], Holmberg [30], Barker and Kettleborough [31], and Mathiprakasham and Lavan [32] have each analyzed the performance of adiabatic silica gel dehumidifiers but without comparing predictions with experimental data. Mathiprakasham [33] predicted the performance of a cross-cooled silica gel dehumidifier.

SERIO 

SECTION 3.0

PSEUDO-STEADY-STATE MODEL

3.1 GENERAL DESCRIPTION

Most of the analytical approaches described in the previous section involve the derivation of a set of differential equations for conservation of mass and energy within the adsorption system, and the solution of that set of equations by finite difference techniques. The pseudo-steady-state model developed in this study uses an approach that simplifies the mathematics of the adsorption problem. As illustrated in Fig. 3-1, the Desiccant Simulation computer model (DESSIM) can be thought of as a conveyor belt that carries one chunk of air at a time through the desiccant bed. The passage of each air chunk through the bed corresponds to a single time step. The bed is divided into equal sections, and as the air chunk is exposed to each section, mass and heat transfer calculations are performed in an uncoupled manner.

First, all temperatures are held constant while the amount of moisture transferred between the air and the bed section during the time step is determined, and the humidity ratio of the air chunk and moisture content of the desiccant section are revised. Second, an energy balance is performed that accounts for the amount of energy released when the water is adsorbed and determines an intermediate temperature for the bed section. Finally, a heat-transfer calculation is performed using this intermediate bed temperature and the original air temperature. Temperatures for the air and the bed are updated, and the air chunk is moved to the next bed section.

Although the sorption process is a transient one, these mass transfer and heat transfer calculations are done using equations for steady-state, counterflow mass exchangers and heat exchangers; hence, the name pseudo-steady state. Conceptually, the model carries along a counterflow mass exchanger and a counterflow heat exchanger that each have surface areas for transfer equal to the surface area in each bed section. Final moisture contents and temperatures for the air chunk and the bed section at the end of each time step are taken to be the same as the outlet moisture contents and temperatures from simple counterflow exchangers. These have steady flows of air and desiccant material with inlet conditions equal to the initial conditions of the air

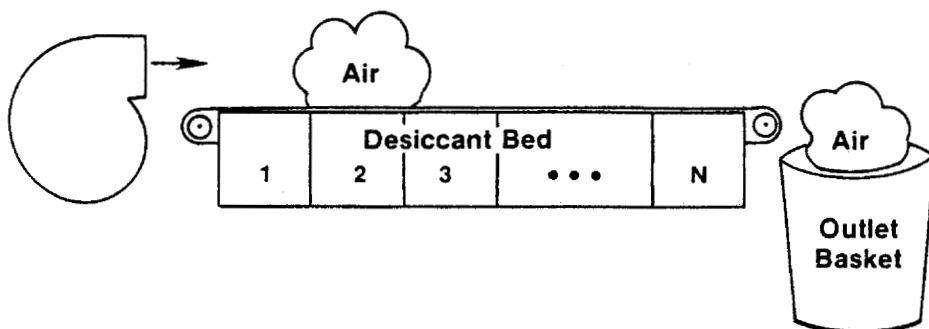


Fig. 3-1. Conveyor Belt Concept Used in Computer Model

chunk and the bed section. Applying these exchanger equations during time steps that are short compared to the duration of the complete process preserves the transient character. The fact that the exchanger equations are analytical solutions describing the approach of an exchange process toward a maximum effectiveness allows relatively large time and space increments to be used without complicated numerical techniques. This permits simulations to be carried out at a very reasonable computational cost.

In the remainder of this section, we outline the equations used in the computer model.

3.2 MASS TRANSFER CALCULATION

The mass transfer calculation that is performed as each air chunk is exposed to a bed section is adapted from the effectiveness equations for a counterflow gas/liquid mass exchanger [46]. The configuration from which these equations are derived is shown in Fig. 3-2.

The air at the desiccant surface is assumed to be in equilibrium with the desiccant. All temperatures are assumed to be constant. The moisture ratio in the desiccant is assumed to be uniform in the direction perpendicular to flow, and the transfer process is assumed to be controlled by a gas film resistance, which is modified to account approximately for the effect of a solid-side resistance to the diffusion of water. The applicability of these last two assumptions is discussed in Sec. 3.5.

The rate of mass transfer per unit surface area at any point in the exchanger is given by

$$\dot{m}_{H_2O} = g(m - m_s) \quad (3-1)$$

where

m = bulk vapor mass fraction in air

$m_s = f(X, T_b)$, equilibrium vapor mass fraction at the desiccant surface

g = effective gas-side mass transfer coefficient

X = moisture ratio in desiccant (kg water/kg dry desiccant)

T_b = temperature of bed section

Defining the effectiveness E of the exchanger as the actual moisture transfer divided by the maximum possible moisture transfer, we have

$$E = \frac{1 - \exp[-Ntu(1-CC)]}{1 - CC \exp[-Ntu(1-CC)]} \quad (3-2)$$

where

$Ntu = gA_s / C_{min}$

A_s = surface area for mass transfer within the bed section

$CC = C_{min} / C_{max}$

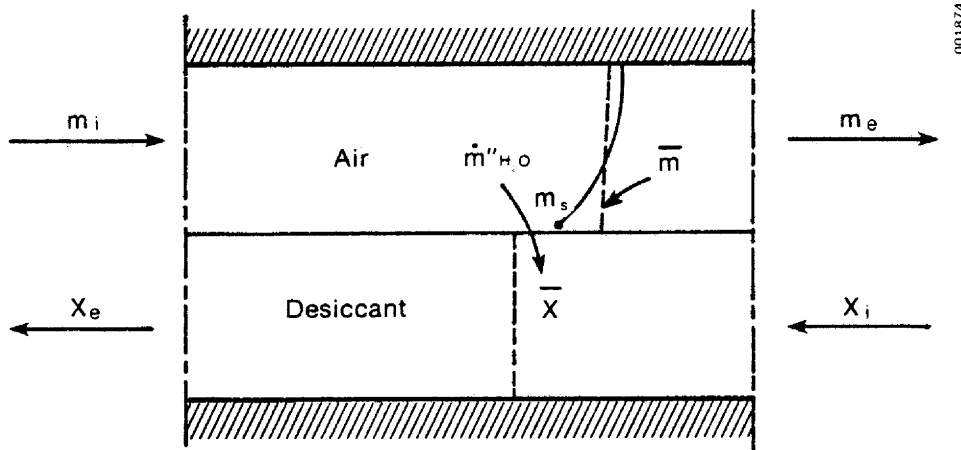


Fig. 3-2. Concentration Profiles for Steady-State Mass Transfer Process

C_{\min} and C_{\max} are the smaller and larger of the capacity rates of the two streams flowing through the hypothetical exchanger. The capacity rate for the air is

$$\begin{aligned} C_{\text{air}} &= \dot{m}_{\text{gas}}, \text{ for the steady-state case} \\ &= M_a (1 + w_1)/\Delta t, \text{ for the pseudo-steady-state case.} \end{aligned} \quad (3-3)$$

The capacity rate for the desiccant material is

$$C_{\text{bed}} = M_b (1 + X) \left[\frac{\partial Y}{\partial m_s} \right]_T / \Delta t, \quad (3-4)$$

where

M_a = dry mass of air chunk

M_b = dry mass of bed section i

Y = water mass fraction in desiccant, $X/(1+X)$

Δt = time step defined for the simulation.

The partial derivative of the mass fraction of water in the desiccant with respect to the equilibrium vapor mass fraction at the surface replaces the inverse of the Henry number used in gas/liquid mass exchanger analysis, and is analogous to the specific heat in the expression for heat exchanger capacity rates. The calculation of this quantity is discussed in Sec. 3.6.

With the effectiveness known, the mass fraction for the outlet air is

$$m_2 = m_1 - E(m_1 - m_s) \quad (3-5)$$

and the outlet humidity ratio is

$$w_2 = m_2 / (1 - m_2) \quad . \quad (3-6)$$

The amount of water transferred to the bed section during one time step is

$$M_w = M_a (w_1 - w_2) \quad , \quad (3-7)$$

so the new moisture ratio in the bed is

$$X_2 = (X_1 M_b + M_w) / M_b \quad . \quad (3-8)$$

3.3 INTERMEDIATE ENERGY BALANCE

When water is adsorbed by a desiccant, energy is released. This heat of adsorption is usually greater than the heat of vaporization of water, and is a function of the water content in the desiccant. In the pseudo-steady-state model, an energy balance is performed after the mass transfer calculation to determine the change in the bed section temperature due to the adsorption or desorption of water. The temperature of the air is assumed to remain constant.

The overall sorption process is assumed to be adiabatic, and no work is involved. Therefore, the energy balance on the air chunk and the bed section can be written simply as

$$M_a (h_a^* - h_{a1}) + M_b (h_b^* - h_{b1}) = 0 \quad . \quad (3-9)$$

Here, all enthalpies are in terms of energy per unit dry mass of air or bed material, and 1 and * refer to states before and after the adsorption or desorption of the amount of water determined by Eq. 3-7. Correlations for the enthalpy of moist air (Sec. 3.6) use dry air and liquid water at 0°C as a base. Therefore, the heat of vaporization is included implicitly in the enthalpies. Enthalpies for the desiccant bed can be defined using the same base, 0°C and liquid water. However, water in the bed is in the sorbed state, not the liquid state. The energy difference between the liquid and sorbed states can be accounted for either by including a term for the integral heat of wetting directly into the expression for the enthalpy of the desiccant or by including an extra term in the energy balance, which accounts for the difference between the heat of adsorption and the heat of vaporization. The latter approach is used in this analysis. Hence, the enthalpy of the bed is defined as

$$h_b = (c_b + X c_w) T_b \quad , \quad (3-10)$$

where the temperature is in degrees Celsius. Equation 3-9 becomes

$$M_a (h_a^* - h_{a1}) - M_w (h_{ads} - h_{vap}) + M_b [(c_b + X_2 c_w) T_b^* - (c_b + X_1 c_w) T_{b1}] = 0 \quad (3-11)$$

$$\text{where } h_a^* = h_a (T_{a1}, w_{a2}) \quad .$$

Solving for the intermediate bed temperature $T_b^\#$,

$$T_b^\# = \frac{M_b(c_b + X_1 c_w) T_{b1} - M_a(h_a^* - h_{a1}) + M_w[(h_{ads} - h_{vap}) - 1]}{M_b(c_b + X_2 c_w)} \quad (3-12)$$

This is the initial bed temperature for the heat transfer calculation. Correlations for the ratio of the heat of adsorption and the heat of vaporization are given in Sec. 3.7.

3.4 HEAT TRANSFER CALCULATION

After the temperature change of the bed section caused by the heat of adsorption is determined, a heat transfer calculation is performed. As with the mass transfer calculation, equations for a counterflow exchanger are applied and the steady-state outlet temperatures are used as the final average temperatures of the air chunk and the bed section at the end of the time step. Again, the equation for the exchanger effectiveness is

$$E = \frac{1 - \exp[-Ntu(1 - CC)]}{1 - CC \exp[-Ntu(1 - CC)]}$$

where, for the heat exchange problem,

$$Ntu = H A_s / C_{\min}$$

$$CC = C_{\max} / C_{\min}$$

$$C_{air} = M_a c_p / \Delta t$$

$$C_{bed} = M_b(c_b + X_2 c_w) / \Delta t$$

H = average heat transfer coefficient.

Since the effectiveness is the ratio of actual energy transfer to the maximum possible energy transfer, the total energy transfer from the air to the bed section during the time increment is

$$Q = EC_{\min}(T_b^\# - T_{a1})\Delta t \quad (3-13)$$

Applying simple energy balances, new temperatures for the air chunk and bed section are

$$T_{a2} = T_{a1} + Q / (M_a c_p) \quad (3-14)$$

$$T_{b2} = T_b^\# - Q / (M_b(c_b + X_2 c_w)) \quad (3-15)$$

The conditions of the bed section are stored and the air chunk is sent to the next bed section, where this series of calculations is repeated.

3.5 TRANSFER COEFFICIENTS

In both the mass transfer and heat transfer calculations, the rates of transfer are assumed to be controlled by single resistances in the gas film adjacent to the desiccant surface. This assumption is a good one for the heat transfer calculation because the heat transfer Biot number is small for typical packed-bed situations, and the temperature gradient within the particles would be minor. However, there is wide agreement that for silica gel particles of the size used in packed beds, there is a significant resistance to mass diffusion within the solid particle. The appropriate resistance model for the overall mass transfer process is shown in Fig. 3-3a. Here, R_g and R_s are the gas-side and solid-side resistances, respectively. In this case, the rate of mass transfer would be

$$\dot{m}_{H_2O} = \frac{\bar{m} - m_s}{R_g} = \frac{X_s - X_o}{R_s}.$$

Solving for a value of the moisture ratio at the desiccant surface that is different from the average value adds significantly to the complexity and cost of a numerical solution to the sorption problem. Furthermore, there may be little benefit in accurate predictions, because diffusion coefficients for desiccants are difficult to measure accurately or predict theoretically.

To simplify the analysis, the mass transfer rate is calculated as if it were strictly a gas-side-controlled process. However, the gas-side resistance is modified to account approximately for the resistance to moisture diffusion within the desiccant particles. This gas-side resistance model is shown in Fig. 3-3b.



Fig. 3-3. (a) Detailed Resistance Model for Mass Transfer
(b) Gas-Side Resistance Model for Mass Transfer

The particle is assumed to have a uniform moisture content and the equilibrium vapor mass fraction of the air at the surface is calculated using the average moisture content of the desiccant. The convective mass transfer coefficient g is then reduced by some factor, which can be determined experimentally or approximated on the basis of theory.

Hougen and Marshall [9], who were the first researchers to analyze the adiabatic adsorption process, used experimental data from Ahlberg [10] to develop the following correlations for effective mass transfer and heat transfer coefficients for adsorption in packed beds of silica gel.

$$\begin{aligned} g &= 0.704 G_a \left[\frac{D_p G_a}{\mu} \right]^{-0.51} \\ H &= 0.617 G_a c_p \left[\frac{D_p G_a}{\mu} \right]^{-0.51} \end{aligned} \quad (3-16)$$

These transfer coefficients have been used by Bullock and Threlkeld [21], Chi and Wasan [23], Pla-Barby et al. [29], Koh [24], and Nienberg [34]. However, the original Ahlberg data contain a considerable amount of scatter, which leads to significant uncertainty. Also, the correlations of Hougen and Marshall modify the heat transfer coefficient, as well as the mass transfer coefficient, to preserve a Lewis number close to unity. The Lewis number, defined as

$$Le = H/gc_p, \quad (3-17)$$

is close to unity for an air/water mixture in a strictly convective problem. However, in our case, there is no reason to modify the heat transfer coefficient, and consequently, modification of the mass transfer correlation results in an effective Lewis number greater than unity.

Since the heat transfer process is gas-side controlled in typical packed-bed situations, a correlation for heat transfer alone is used in the pseudo-steady-state model. The correlation given by Handley and Heggs [35] for the Nusselt number is

$$Nu = 0.23 Re^{2/3} / \epsilon_v, \quad (3-18)$$

where

$$Nu = H D_p / k$$

$$Re = \rho V D_p / \mu$$

$$\epsilon_v = \text{void fraction.}$$

Manufacturers' data give a void fraction of 0.4, so the expression for the heat transfer coefficient used in the model is

$$H = 0.58 k \left[\frac{\rho V D_p}{\mu} \right]^{0.67} / D_p. \quad (3-19)$$

The mass transfer coefficient is then

$$g = H/c_p Le \quad , \quad (3-20)$$

where Le is an effective Lewis number that depends on the parameters of the sorption situation.

Close and Banks [27] have used this same approach for calculating mass transfer coefficients in silica gel beds. Recently, van Leersum [47] has carried out an analysis to determine appropriate values of the effective Lewis number for rotary dehumidifiers. This analysis adapts Hausen's correction for the heat transfer coefficient in thermal regenerators that have a resistance to heat transfer within the solid matrix, and includes considerations of the convective transfer coefficient, the diffusivity of moisture in silica gel, the particle diameter, the equilibrium properties of silica gel, and the typical operating conditions of a rotating dehumidifier within a desiccant cooling system. Van Leersum's results indicate that a value between $Le = 3$ and $Le = 4$ would be an appropriate average for rotary system simulations. However, the effective Lewis number is a function of several parameters and different values may be appropriate for single-blow simulations.

Figure 3-4 compares several correlations for mass transfer in packed beds. Clearly, there is a considerable degree of uncertainty in characterizing this type of transport phenomenon. Mass transfer relationships based on the Handley and Heggs heat transfer correlation are included in Fig. 3-4 for three values of the effective Lewis number; 1, 3, and 9. With $Le = 1$, the Handley and Heggs correlation is grouped with the majority of the other correlations. With $Le = 3$, it is similar to the Hougen and Marshall correlation, which is based on silica gel adsorption data. With $Le = 9$ at low Re , it is relatively close to the Eagleton and Bliss correlation, which is also based on silica gel adsorption data. Thus, the use of an effective Lewis number as large as 9 is not out of line with previously reported mass transfer correlations.

3.6 PROPERTIES OF MOIST AIR

The properties of air that are used at various points in the calculation procedure are enthalpy, specific heat, thermal conductivity, and dynamic viscosity. The following expression for the enthalpy of moist air was reported by MacLaine-cross [37]:

$$h_a = (1005.22 + 0.02615 T) T + w (2500800 + 1868 T) \quad . \quad (3-21)$$

Here, temperature T is in degrees Celsius and the enthalpy is units of joules per kilogram. The reported accuracy of this equation is 0.05%, as compared to standard tables. In the simulation of complete cooling systems, outlet temperatures from the sensible heat exchanger must be calculated from known values of enthalpy and humidity ratio. Solving Eq. 3-21 for temperature gives us

$$T = -D + [D^2 + (h_a - 2500800 w)/0.02615] \quad , \quad (3-22)$$

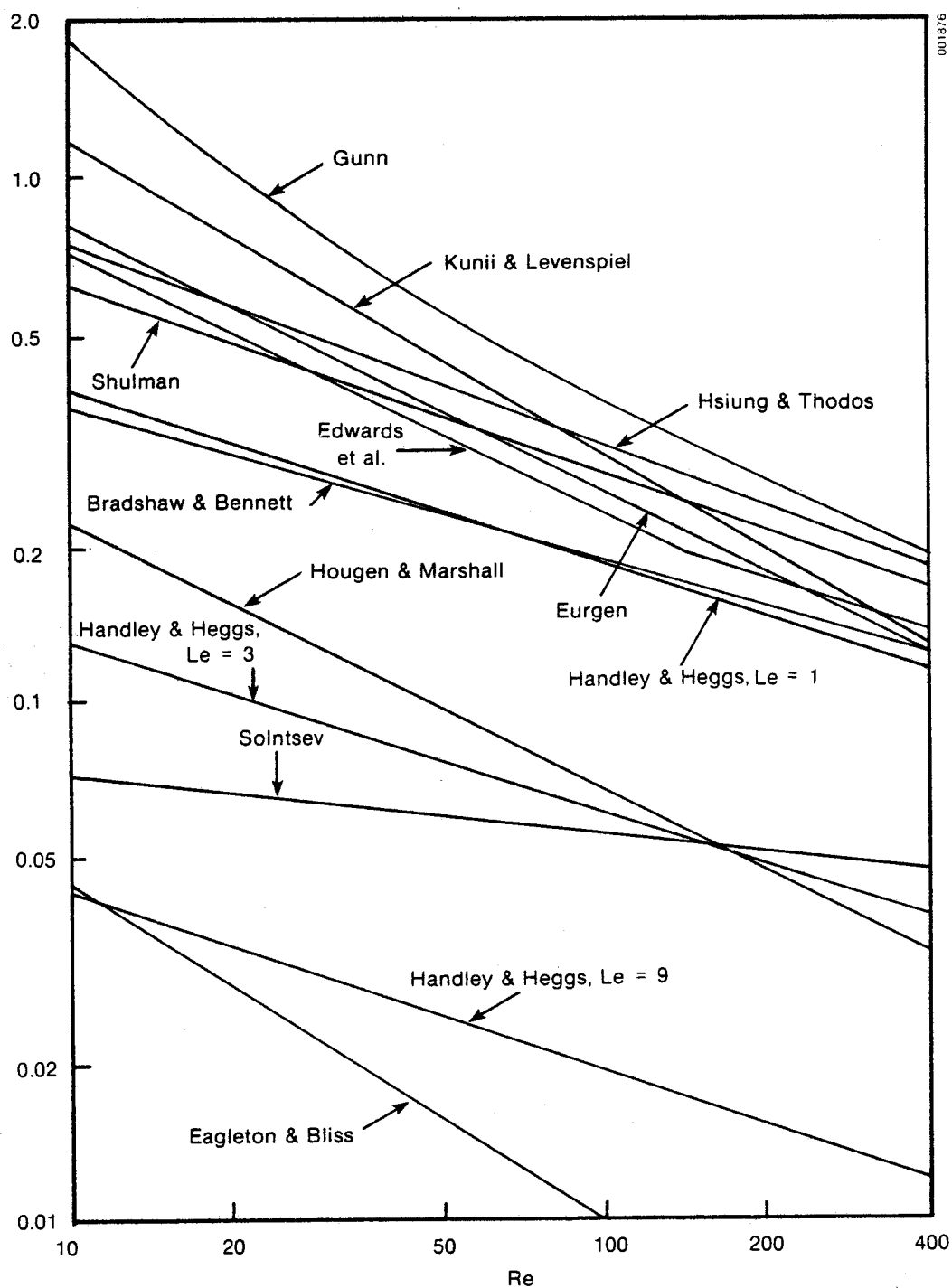


Fig. 3-4. Comparison of Various Mass Transfer Correlations for Packed Beds. ($Sc = 0.61$, adapted from Pesaran [36]).

where

$$D = (1005.22 + 1868 w)/0.0523 \quad .$$

The specific heat of moist air is also derived from Eq. 3-21:

$$c_p = \left[\frac{\partial h}{\partial T} \right]_p = 1005.22 + 0.0523 T + 1868 w \quad . \quad (3-23)$$

Specific heat, conductivity, and viscosity appear in the correlation for the heat and mass transfer coefficients. Because of the inherent uncertainty in this type of correlation, highly accurate expressions for air properties are not warranted. Properties of dry air at the inlet temperature to the bed are, therefore, used in calculating transfer coefficients. A constant specific heat and linear interpolation are used to calculate conductivity and viscosity from data in Holman [38] for the temperature range of interest.

$$c_p = 1006 \text{ J/kg}^\circ\text{C} \quad (3-24)$$

$$k = 0.02624 + 7.58 \times 10^{-5} (T - 27) \text{ W/m}^\circ\text{C} \quad (3-25)$$

$$\mu = 1.859 \times 10^{-5} + 4.32 \times 10^{-8} (T - 27) \text{ kg/m} \cdot \text{s} \quad . \quad (3-26)$$

The following standard psychrometric equations are also used:

$$\text{humidity ratio } w = .622 P_v / (P_{\text{atm}} - P_v) \quad (3-27)$$

$$\text{relative Humidity RH} = P_{\text{atm}} w / [(0.622 + w) P_{\text{sat}}] \quad . \quad (3-28)$$

where P_v is the vapor pressure, P_{atm} is the ambient pressure, and P_{sat} is the saturation pressure at a given temperature.

The saturation pressure (N/m^2) is calculated using the simple but accurate correlation reported by Maclaine-cross [37]. The reported accuracy of this equation is 0.08% as compared with standard tables.

$$P_{\text{sat}} = \exp[23.28199 - 3780.82/(T + 273) - 225805/(T + 273)^2] \quad (3-29)$$

3.7 PROPERTIES OF SILICA GEL

Silica gel is a highly porous, granular, amorphous form of silica that is manufactured by reacting sodium silicate with sulfuric acid. The internal structure of silica gel consists of a vast number of small pores. When used as a desiccant, standard grades of gel can hold up to 40% of their weight in water by mechanisms of physical adsorption and capillary condensation. Many different grades of silica gel are manufactured whose physical and equilibrium properties vary between grades. Regular-density gel, such as Davison PA40 or Syloid® 63, is more appropriate than low-density gel for solar cooling applications because it demonstrates a favorable and relatively steep isotherm shape in the range of relative humidities typically found in desiccant cooling. Figure 3-5 shows this qualitative difference in gel properties.

The physical properties of regular-density silica gel are summarized in Tables 3-1 and 3-2.

Table 3-1. Typical Properties of Silica Gel (Manufacturer's Data, Grace & Co. [43])

Specific heat (c_b)	921 J/kg°C
Apparent bulk density (ρ_b)	720 kg/m ³
Void fraction (ϵ_v)	0.4

Table 3-2. Particle Diameter and Surface Area [24]

Tyler Mesh Size	Average Particle Diameter (m)	External Surface Area (m ² /m ³)
2-4	0.00671	384
4-6	0.00390	663
6-8	0.00277	931
8-10	0.00193	1335
10-12	0.00176	1470
10-14	0.00136	1890
14-20	0.00098	2641
20-28	0.00069	3740

3.7.1 Equilibrium Properties

Critical information for the simulation of the adsorption process is an expression for the equilibrium properties of the desiccant being modeled; i.e., an expression for the equilibrium vapor pressure at the desiccant surface as a function of the desiccant temperature and moisture content. There are several correlations available for the equilibrium properties of silica gel. Lunde and Kester [39] used a multilayer adsorption model along with experimental data for a moderate range of moisture content to predict complete isotherms. Rojas [40] measured the equilibrium characteristics of four grades of silica gel of different porosity, and fit polynomial expressions of the form

$$X = A_0 + A_1 \left[\frac{P_v}{P_{sat}} \right] + A_2 \left[\frac{P_v}{P_{sat}} \right]^2 + A_3 \left[\frac{P_v}{P_{sat}} \right]^3 + A_4 \left[\frac{P_v}{P_{sat}} \right]^4 \quad (3-30)$$

to this data. One of the gels investigated by Rojas is Davison grade PA-40, the same silica gel used in current adsorption experiments at SERI.

Jury and Edwards [41] fit the following equation to their data:

$$X = \frac{2R}{1 + 13.33R} + \frac{10.15R^{3.3}}{1 + 46.7R^{3.3}},$$

$$\text{where } \left[R = \frac{P_v}{P_{sat}} \right]^{(T + 273)/273}.$$

(3-31)

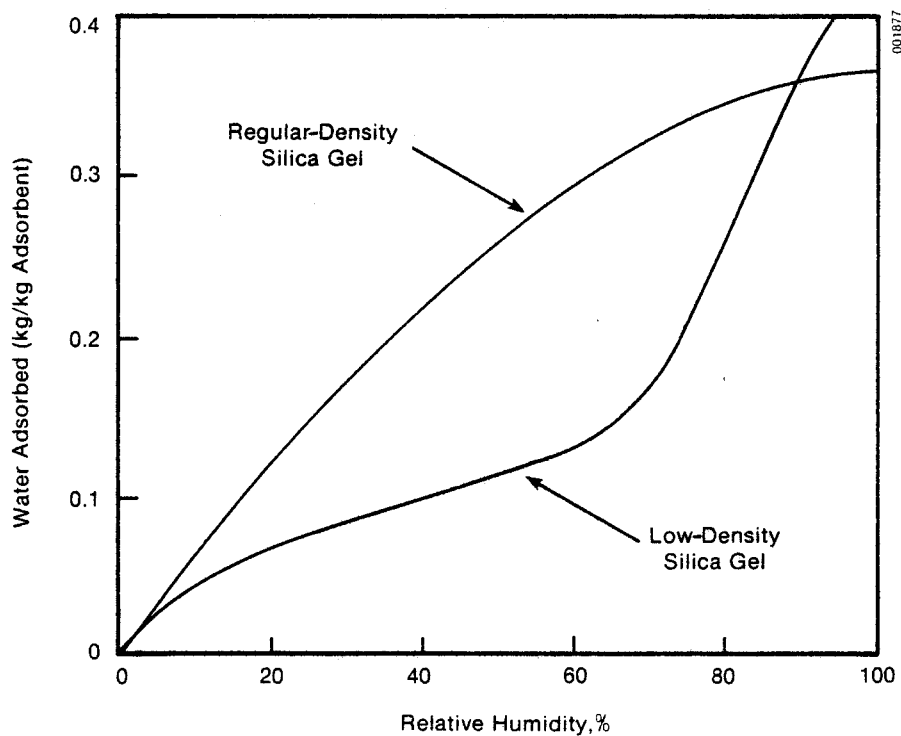


Fig. 3-5. Typical Isotherms for Regular- and Low-Density Silica Gel

Hubard [22] reported equilibrium data for the silica-gel/air-water system for temperatures between 4°C and 93°C (40°F and 200°F), and moisture contents between 1.5% and 35%. Bullock and Threlkeld [21] represented these data as polynomials of the form

$$P_{ve} = (C_1T^3 + C_2T^2 + C_3T + C_4)X^m + (C_5T^3 + C_6T^2 + C_7T + C_8)X^n, \quad (3-32)$$

where

P_{ve} = equilibrium vapor pressure (in Hg)

T = silica gel temperature (°F)

X = silica gel moisture content (lb water/lb dry gel).

The constants C_1 through C_8 are given in Table 3-3; $m = 2$ and $n = 1$ for X less than 0.05; and $m = 1$ and $n = 0$ for X greater than 0.05.

Table 3-3. Constants for the Bullock and Threlkeld Correlation for Silica Gel

Range of Moisture Content (X)	$C_1 \cdot 10^6$	$C_2 \cdot 10^4$	C_3	C_4
$0 < x < 0.05$	402.263374	-893.827167	7.06882716	-182.15263
$0.05 < x < 0.10$	-7.80864197	43.1023703	-0.484787037	17.2044753
$0.10 < x < 0.15$	20.833333	-38.25	0.255416667	-4.6825
$0.15 < x < 0.20$	53.333333	-138.0	1.26466667	-38.0
$0.20 < x < 0.25$	-81.666667	213.5	-1.75233333	47.6
$0.25 < x < 0.30$	40.0	-81.0	0.599	-14.1
$0.30 < x < 0.35$	20.0	-37.0	0.291	-6.9

Range of Moisture Content (X)	C_5	$C_6 \cdot 10^4$	C_7	C_8
$0 < x < 0.05$	11.86211399	32.6790123	0.322929012	-10.4143621
$0.05 < x < 0.35$	1.98919753	-6.02453703	0.0580578703	-1.83632253
$0.10 < x < 0.15$	-0.875	2.1125	-0.159625	0.352375
$0.15 < x < 0.20$	-5.75	17.075	-0.16735	5.35
$0.20 < x < 0.25$	21.25	-53.225	0.43605	-11.77
$0.25 < x < 0.30$	-9.16666667	20.4	-0.151783333	3.655
$0.30 < x < 0.35$	-3.16666667	7.2	-0.0593833333	1.495

Close and Banks [27] plotted Hubbard's data in the form of Othmer charts and, by applying the Clausius-Clapeyron equation, obtained

$$P_v(\text{atm}) = \frac{1}{29.91} [29.91 f_1(X) P_{\text{sat}}]^{f_2(X)}, \quad (3-33)$$

where $f_1(X)$ and $f_2(X)$ are polynomials, and $f_2(X)$ is the ratio of the heat of adsorption to the heat of vaporization. They recommended the simplification of replacing $f_1(X)$ with the simple linear function $2.009X$.

The polynomial expression of Bullock and Threlkeld was originally chosen for this study, because of the convenience of calculating $\left[\frac{\partial Y}{\partial m}\right]_T$. However, it was later determined that this correlation gave erroneous results when a combination of high temperature and high moisture content was encountered. Figure 3-6 shows a series of isotherms based on the equations of Bullock and Threlkeld. This demonstrates that the correlation should not be used when the gel moisture content is greater than 20% and the temperature is greater than about 50°C.

Once this was discovered, other correlations were investigated more closely. Isotherms from the Close and Banks complete correlation and the simplified one using $f_1(X) = 2.009X$ are compared in Fig. 3-7. This correlation was further simplified to facilitate the calculation of $\left(\frac{\partial Y}{\partial m}\right)_T$ by using linear equations for $h_{\text{ads}}/h_{\text{vap}}$, which are discussed in the next section. Figure 3-8 shows that this further simplification produces almost no change in the isotherms. The Rojas correlation for grade PA-40 is included for comparison in both figures. The Rojas data demonstrate an upper limit on the capacity of this grade of silica gel of about 37%, which is typical of regular-density gels. The other correlations do not taper off toward such a limit. However, the Rojas correlation does not include the fanning of isotherms at different temperatures, which is displayed in his data and by the other correlations. To combine both characteristics, the Rojas equation was recast to give vapor pressure as a function of moisture content, and an additional temperature dependence was included.

$$P_v = P_{\text{sat}} \frac{(0.616238X + 16.7916X^2 - 74.34228X^3 + 116.6834X^4)}{[1 - (T - 40)/300]} \quad (3-34)$$

Isotherms from this equation are shown in Fig. 3-9.

The equilibrium vapor mass function at the surface m_s used in the mass transfer calculation is determined from the equilibrium vapor pressure using the following psychrometric relationships:

$$w_e = 0.622 P_{ve} / (P_{\text{atm}} - P_{ve}) \quad (3-35)$$

$$m_s = w_e / (1 + w_e) \quad (3-36)$$

Also required in the mass transfer calculation is the partial derivative of the water mass fraction in the desiccant with respect to the equilibrium vapor mass fraction of the air at the surface. Reexpressing the derivative,

$$\left[\frac{\partial Y}{\partial m_s}\right]_T = \left[\frac{\partial X}{\partial P_{ve}}\right]_T \cdot \frac{dY}{dX} \cdot \frac{dP_{ve}}{dm_s} \quad (3-37)$$

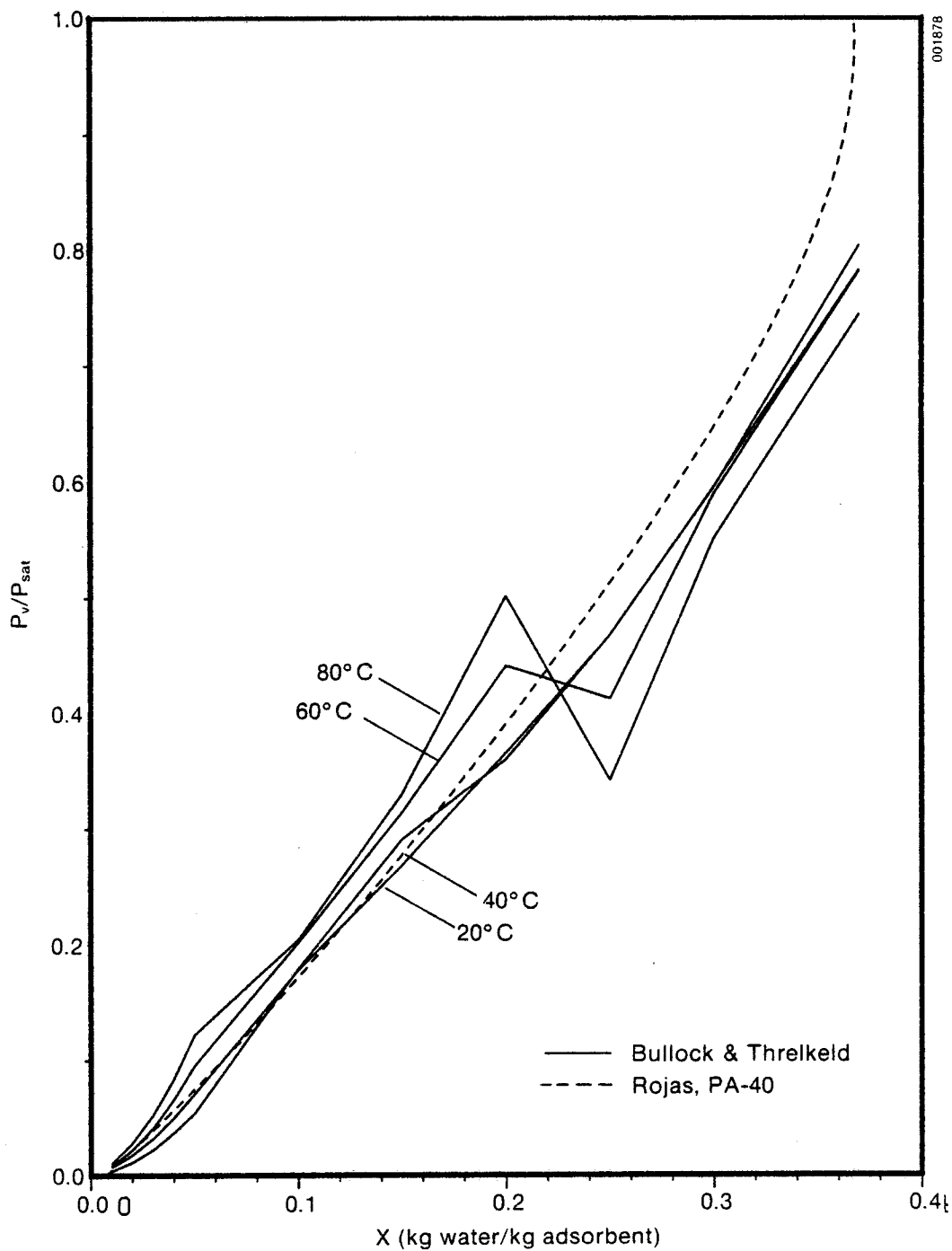


Fig. 3-6. Isotherms Based on the Bullock and Threlkeld Correlation

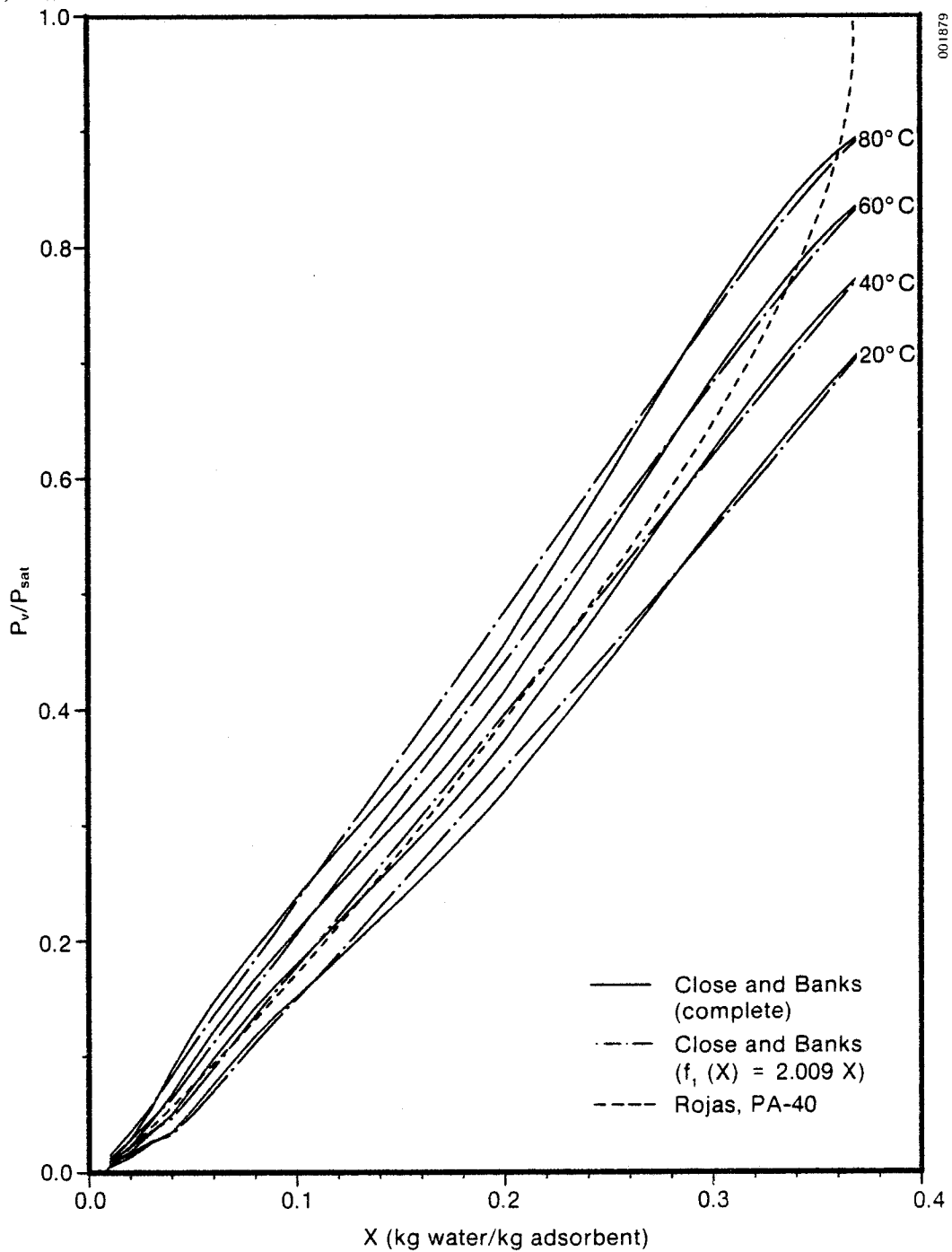


Fig. 3-7. Comparison of the Close and Banks Complete Correlation with Simplified Correlation Using $f_1(X) = 2.009$

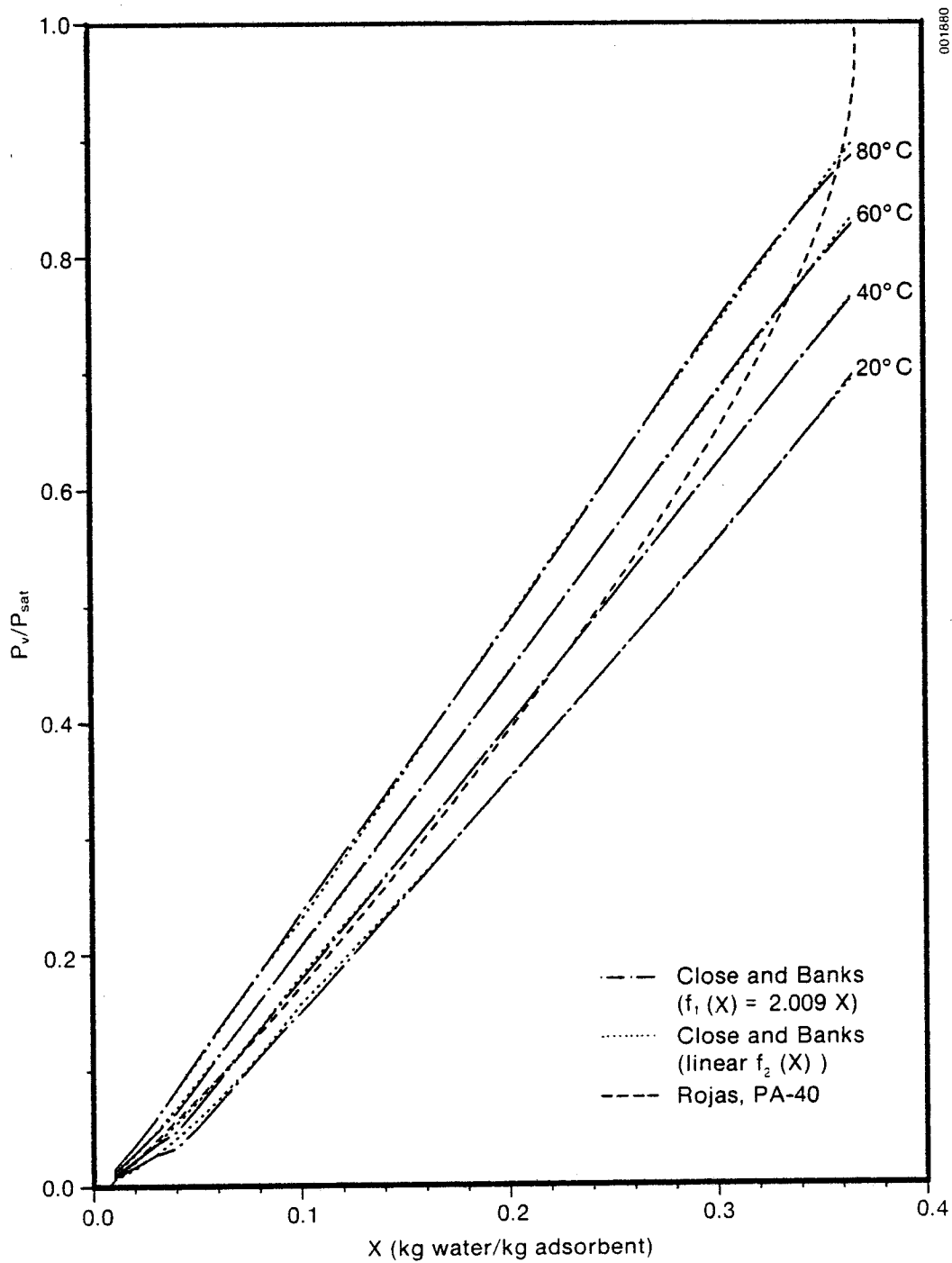


Fig. 3-8. Comparison of the Close and Banks Simplified Expression with Further Simplified Expression Using Linear $f_2(X)$

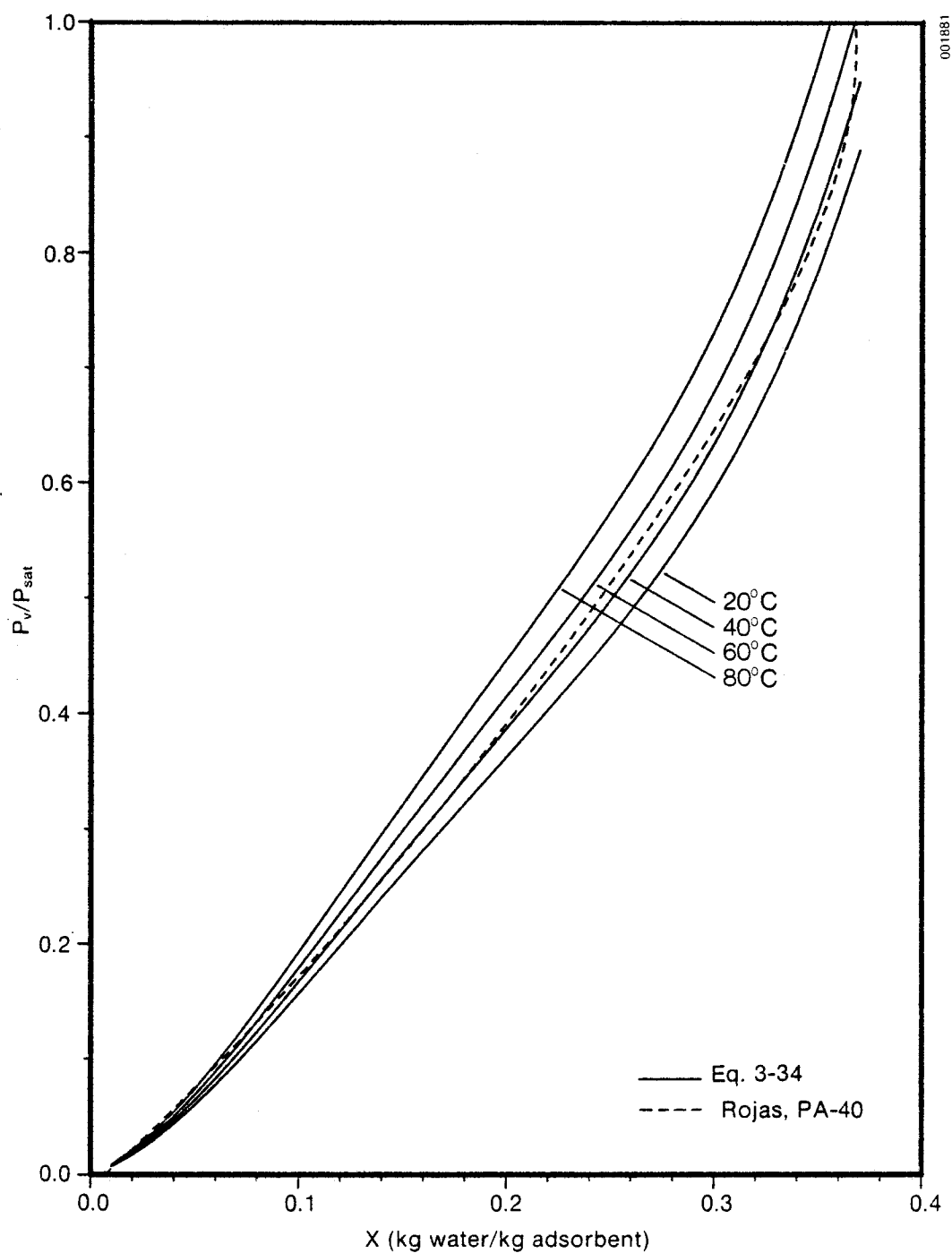


Fig. 3-9. Comparison of the Rojas Correlation with Eq. 3-30

Here, Y , the water mass fraction in the desiccant, is

$$Y = X/(1 + X); \text{ kg water}/(\text{kg water} + \text{kg gel}) ,$$

so

$$\frac{dY}{dX} = \frac{1}{(1 + X)^2} .$$

Equations 3-35 and 3-36 combine to give us

$$m_s = 0.622 P_{ve}/(P_{atm} + 0.378 P_{ve}) ,$$

so

$$\frac{dP_{ve}}{dm_s} = 0.622 P_{atm}/(0.622 + 0.378 m_s)^2 .$$

The partial derivative $(\partial X/\partial P_{ve})_T$ can be evaluated by differentiating the appropriate equation for P_{ve} with respect to X and taking the inverse of the result. The reader is referred to the program listings in Appendix B for specific equations.

The value of $(\partial Y/\partial m_s)_T$ is determined by combining these results in Eq. 3-37.

3.7.2 Heat of Adsorption

The heat of adsorption of water on silica gel is a function of the water content of the gel. Close and Banks [27] plotted Hubbard's data in the form of an Othmer chart to determine the ratio of the heat of adsorption to the heat of vaporization for water contents between 1% and 35%. Results were presented as polynomial curve fits, which were used in this study in combination with the equilibrium correlations of Bullock and Threlkeld.

$$0 < X < 0.04,$$

$$h_{ads}/h_{vap} = 8533 X^3 - 542 X^2 + 11.79 X + 1.1557$$

$$0.04 < X < 0.1,$$

$$h_{ads}/h_{vap} = 45.4 X^2 - 8.97 X + 1.5922$$

$$0.1 < X < 0.35$$

$$h_{ads}/h_{vap} = -9.1553 X^3 + 7.048 X^2 - 1.8966 X + 1.2789 . \quad (3-38)$$

Close and Banks [27] also applied the Clausius-Clapeyron equation to the vapor pressure data of Hougen, Watson, and Ragatz to obtain heat of adsorption information. Their conclusion was that these data must have been for a grade of silica gel other than the regular density type. Rojas [40] reported heat of adsorption data for four grades of silica gel. Of particular interest is

his data for regular-density Grade PA-40. Low-density grades exhibit a lower heat of adsorption similar to the data of Hougen et al. Bullock and Threlkeld [21] fit two polynomials to Ewing's and Bauer's data for the integral heat of wetting. The polynomials are

$$\begin{aligned} X < 0.05 \\ \Delta h_w (\text{kJ/kg}) &= 552425X^3 - 53498X^2 + 2131X \\ X > 0.05 \\ \Delta h_w (\text{kJ/kg}) &= 1068.63X^3 - 1392.45X^2 + 658.49X + 12.29 \quad . \quad (3-39) \end{aligned}$$

When these equations are differentiated with respect to X and the heat of vaporization is added, the heat of adsorption is obtained. A discontinuity in the heat of adsorption results from a discontinuity in slope at the intersection of the above equations. Nienberg [34] fit a linear equation to data reported by Beecher [42].

Figure 3-10 is a graph of the ratio of the heat of adsorption to the heat of vaporization, $h_{\text{ads}}/h_{\text{vap}}$ versus gel moisture content, which compares all the sources above. Agreement for regular density gel is within 5% for values of X between 0.1 and 0.25. However, for X less than 0.1 there is a large uncertainty. The following linear equations, which are shown as dashed lines in Fig. 3-10, were considered to give the best combination of accuracy and computational convenience and are used in this study in combination with the equilibrium correlations of Close and Banks and those based on the Rojas data.

$$\begin{aligned} X < 0.1, \quad h_{\text{ads}}/h_{\text{vap}} &= 1.3 - 1.75 X \\ X > 0.1, \quad h_{\text{ads}}/h_{\text{vap}} &= 1.14 - 0.15 X \quad . \quad (3-40) \end{aligned}$$

In summary, the computer program includes three sets of correlations for equilibrium properties and the heat of adsorption. The first set combines the Bullock and Threlkeld polynomials for equilibrium vapor pressure with the Close and Banks equations for $h_{\text{ads}}/h_{\text{vap}}$. The second set combines the Close and Banks equation for equilibrium vapor pressure with the above linear expressions for $h_{\text{ads}}/h_{\text{vap}}$. The third set combines the modified equation for Rojas' equilibrium data with the linear expressions for $h_{\text{ads}}/h_{\text{vap}}$. These three correlation sets were included to allow comparison of the relative success of the different correlations in predicting experimental results.

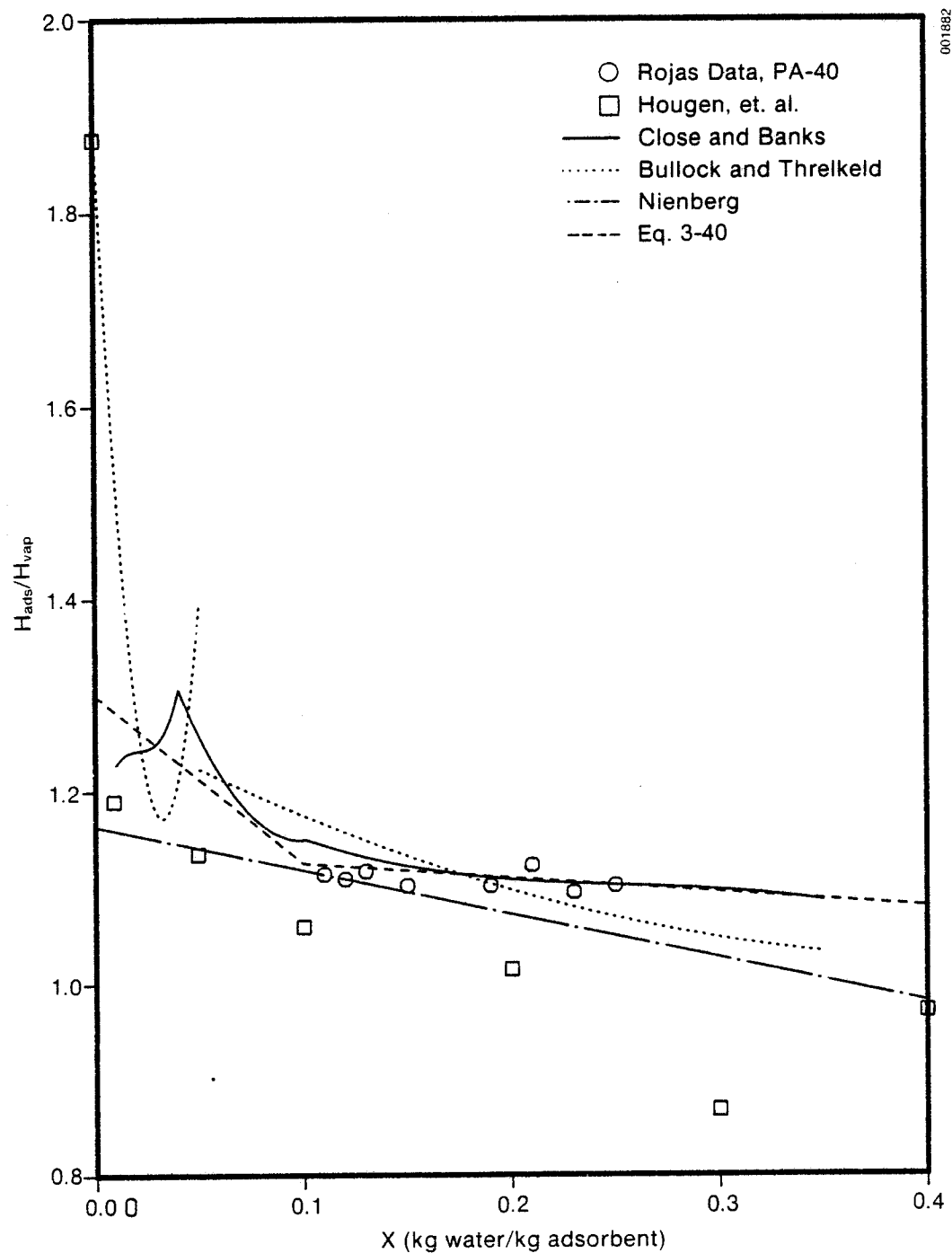


Fig. 3-10. Comparison of Various Correlations and Data for the Heat of Adsorption for Silica Gel



SECTION 4.0

COMPARISON OF THE MODEL WITH EXPERIMENTAL DATA

4.1 DATA SOURCES FOR SINGLE-BLOW ADSORPTION AND DESORPTION

In terms of both analytical and experimental work, it is most convenient to deal with single-blow adsorption or desorption; i.e., the case where the desiccant bed is initially at some uniform state of temperature and moisture content, and air of constant temperature, humidity, and flow rate is passed through the bed. If an analytical model can predict the outlet conditions of process air during single-blow experiments, then the same model can be used to predict the periodic performance of desiccant beds in cooling systems. This reduces the need for complex and costly experiments on rotary desiccant wheels or complete cooling system prototypes.

Simulation of the single-blow case is a straightforward application of the pseudo-steady-state calculation procedure described in Sec. 3.0. The physical properties and dimensions of the desiccant bed are specified, along with the initial conditions of the bed and the inlet conditions of the air. Outlet conditions of the air at each point in time are simply the final conditions of each air chunk after being exposed to the last bed section.

In this section, predictions of the pseudo-steady-state model are compared to experimental data for single-blow adsorption and desorption cases. Three data sources are used to provide a thorough assessment of the validity of the model and the supporting information on silica gel properties and transport coefficients. The first data source is the Desiccant Test Laboratory at SERI. The second is Pesaran's master's thesis on "Air Dehumidification in Packed Silica Gel Beds" [36]. The third data source is Koh's doctoral dissertation on the regeneration of silica gel used for grain drying [24]. For each of these data sources, predictions using each of the three sets of property correlations described in Secs. 3.6 and 3.7 are compared.

4.2 COMPARISON WITH SERI DATA

The SERI desiccant test laboratory was designed to test the performance of desiccants under operating conditions that would exist in desiccant cooling systems [48]. The data reported here were taken for a thin, packed bed of Davison Grade PA-40 regular density silica gel, which was held between two metal screens. The materials used, the dimensions of the bed, the flow rates, and the inlet air conditions were all chosen to be similar to those found in the AiResearch prototype cooling system. The physical properties of the silica gel and the dimensions of the bed are given in Table 4-1.

**Table 4-1. Physical Properties and Dimensions
for SERI Experiments**

Desiccant type:	Davison Grade PA-40 Silica Gel
Particle diameter:	$0.00193 \text{ m}^\#$ (8-10 mesh)
Void fraction:	$0.4^\#$
Bulk density:	850 kg/m^3^*
Surface area:	$1335 \text{ m}^2/\text{m}^3^\#$
Specific heat:	$921 \text{ J/kg } ^\circ\text{C}^\#$
Bed thickness:	0.035 m
Face area:	0.412 m^2

$^\#$ From manufacturer's data.

* Measured after settling. Note that this value is different from the nominal one reported in the manufacturer's data.

Data from only two experimental runs, one adsorption run and one desorption run, are reported here. (See Ref. [48] for a complete report on the SERI desiccant test laboratory and a complete comparison of measured and predicted results.) For the adsorption run, data are compared with predictions using each of the three sets of silica gel property correlations described in Secs. 3.6 and 3.7. For the desorption run, data are compared with predictions using the Bullock and Threlkeld correlations with Lewis numbers of 3, 6, and 9. Data are also compared with predictions using the other two correlations (ICORR = 2,3) and a Lewis number of 9.

Table 4-2 presents a summary of the parameters for these comparisons, and graphical results are shown in Figs. 4-1 through 4-8. ICORR indicates which correlations are used in the simulation. ICORR = 1 is for the Bullock and Threlkeld equilibrium correlation with the Close and Banks polynomial equations for $h_{\text{ads}}/h_{\text{vap}}$. ICORR = 2 is for the Close and Banks equilibrium correlation with linear equations for $h_{\text{ads}}/h_{\text{vap}}$. ICORR = 3 is for the correlation adapted from the Rojas data with linear equations for $h_{\text{ads}}/h_{\text{vap}}$.

Data presented here are typical of all the data obtained in the SERI desiccant test laboratory. Data obtained during the first one or two minutes are unreliable, however, because of the response characteristics of the optical dew point hygrometers. After this initial transient, the data follow smooth paths with very little scatter. The relationship between data and predictions is also typical in that agreement is closer for adsorption than for desorption. Figures 4-1 through 4-3 show predictions for the adsorption run using the three sets of property correlations. These figures demonstrate that there is little difference between these correlations in predicting outlet air conditions during adsorption. An effective Lewis number of 3.0 was used in

Table 4-2. Summary of Data Runs and Computer Predictions for SERI Experiments on a 3.5-cm Bed^a

Data Run	T_{in} (°C)	W_{in} (kg/kg)	Previous Adsorption or Regeneration Conditions		Simulation Parameters				
			T (°C)	W	G_a (kg/m ² s)	T_0 (°C)	x_0^b (kg/kg)	ICORR	Le
85A	40.0	0.0184	80.0	.0097	0.505	60.0	0.0195	1	3.0
					0.505		0.0167	2	3.0
					0.505		0.0241	3	3.0
85R	80.4	0.0106	40.0	.0184	0.597	40.0	0.178	1	3.0
					0.597		0.178	1	6.0
					0.597		0.178	1	9.0
					0.597		0.171	2	9.0
					0.597		0.174	3	9.0

^a p_{atm} = 83.4 kPa. Two-second time step and 10 bed sections used in simulations.

^bCalculated from the previous adsorption or regeneration conditions using the indicated equilibrium correlations.

each simulation and provided a better fit to the data than 2.5 or 4.0. However, these changes in Lewis number produced only small changes in the predicted breakthrough curve.

To obtain reasonable agreement between predicted and measured outlet condition during desorption, the effective Lewis number had to be increased significantly. Figures 4-4 thru 4-6 compare data to predictions using Lewis numbers of 3, 6, and 9 with the first correlation set. $Le = 9$ provides the best fit to the data, although this fit is not as good as that obtained for adsorption. Figures 4-7 and 4-8 show prediction using the second and third correlation sets. Differences between the predictions using the three correlations are larger than in the adsorption case. However, the differences are not major. These results are discussed in greater detail in Sec. 4.5.

4.3 COMPARISON WITH PESARAN DATA

Pesaran [36] conducted single-blow adsorption experiments on regular density silica gel in packed beds. He performed experiments with two particle sizes and three bed thicknesses. His range of inlet air conditions is somewhat limited, with inlet temperatures near room temperature and relatively low inlet humidities between 0.003 and 0.011 kg/kg. Predictions using the pseudo-steady-state model are compared with data from seven of Pesaran's runs in Figs. 4-9 thru 4-17. Most of these runs were performed using the Bullock and Threlkeld correlation before the limitation of that correlation was discovered. Predictions using the other two correlations are given for Pesaran's Run 18. Again, with these operating conditions, the different correlations give very similar predictions.

The physical properties of the silica gel and the dimensions of the bed as reported by Pesaran are summarized in Table 4-3. A summary of the parameters of each run is given in Table 4-4.

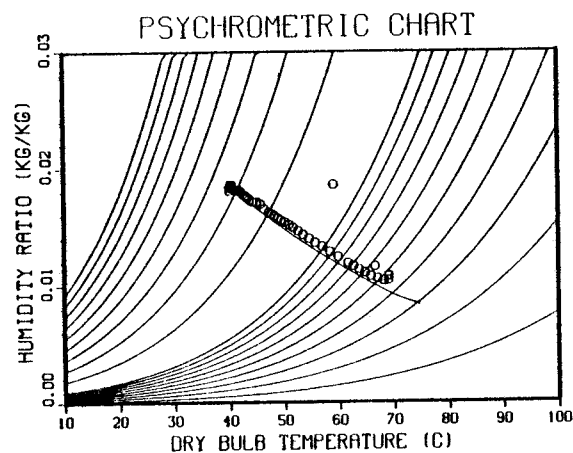
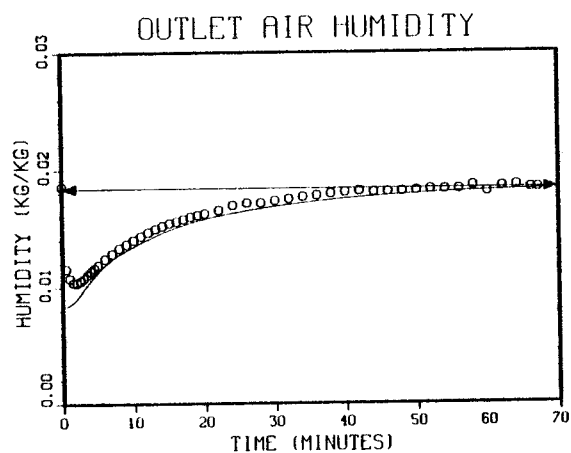
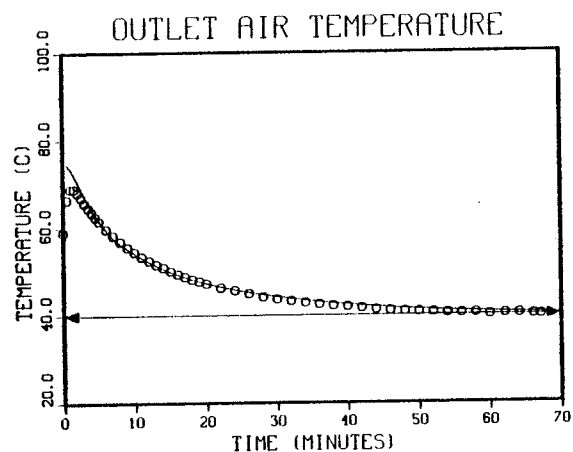
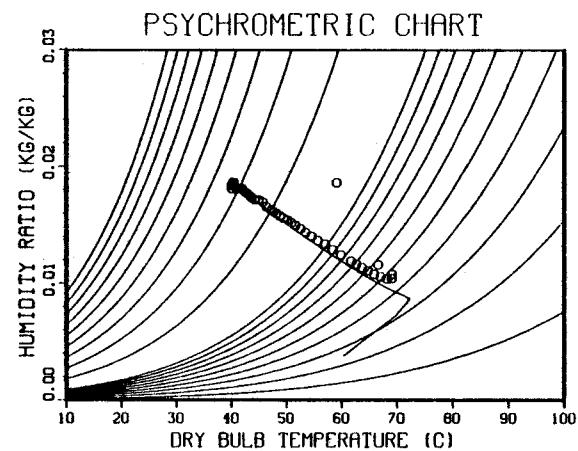
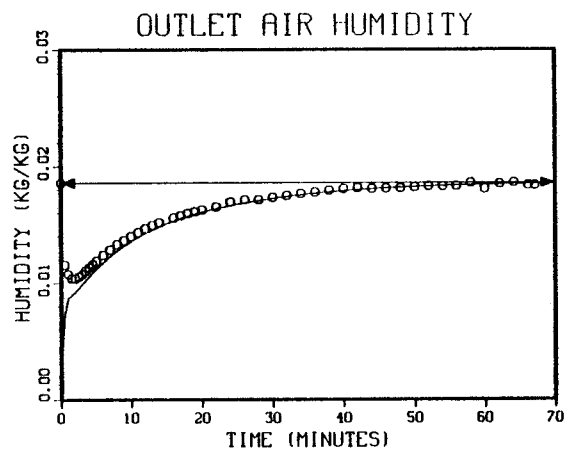
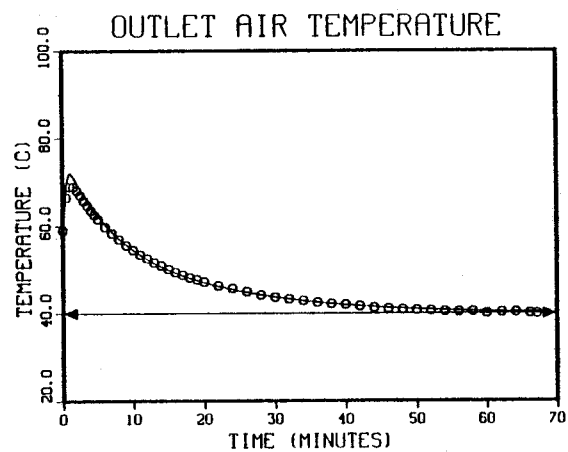


Fig. 4-1. Measured and Predicted Outlet Air Conditions During SERI Run 85A.

$T_{in} = 40.0^{\circ}\text{C}$, $W_{in} = 0.0184$, $T_o = 60.0^{\circ}\text{C}$, $X_o = 0.0195$, $G_a = 0.505$ $\text{kg/m}^2\text{s}$, $ICORR = 1$, $Le = 3$.

001883



001854

Fig. 4-2. Measured and Predicted Outlet Air Conditions During SERI Run 85A.

$T_{in} = 40.0^{\circ}\text{C}$, $W_{in} = 0.0184$, $T_o = 60.0^{\circ}\text{C}$, $X_o = 0.0167$, $Ga = 0.505$
 $\text{kg/m}^2\text{s}$, $ICORR = 2$, $Le = 3$.

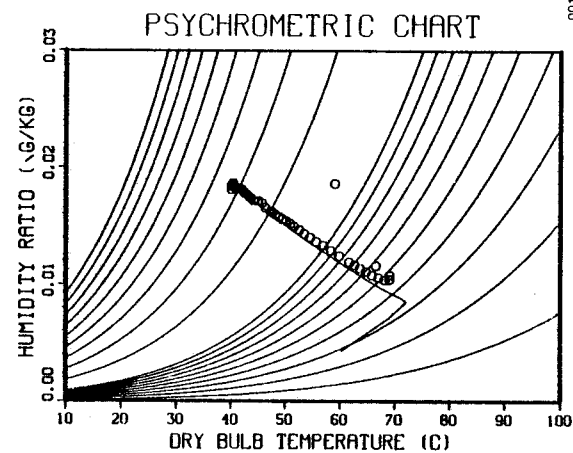
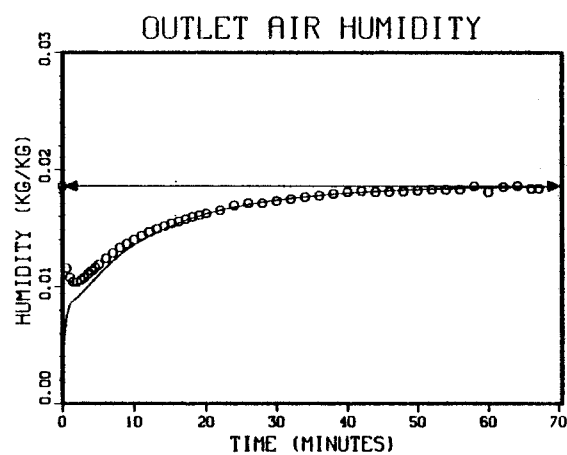
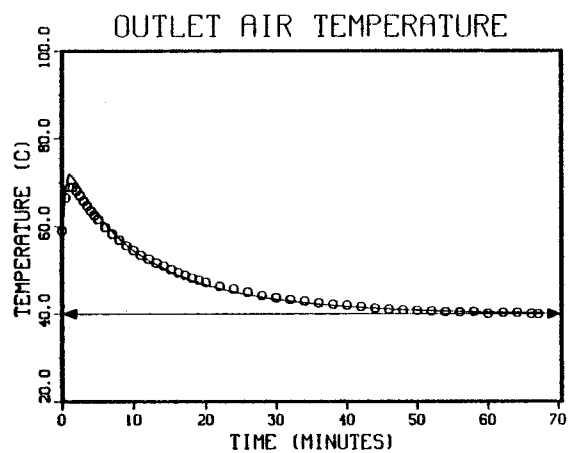


Fig. 4-3. Measured and Predicted Outlet Air Conditions During SERI Run 85A.

$T_{in} = 40.0^{\circ}\text{C}$, $W_{in} = 0.0184$, $T_o = 60.0^{\circ}\text{C}$, $X_o = 0.0241$, $G_a = 0.505$ $\text{kg/m}^2\text{s}$, $\text{ICORR} = 3$, $\text{Le} = 3$.

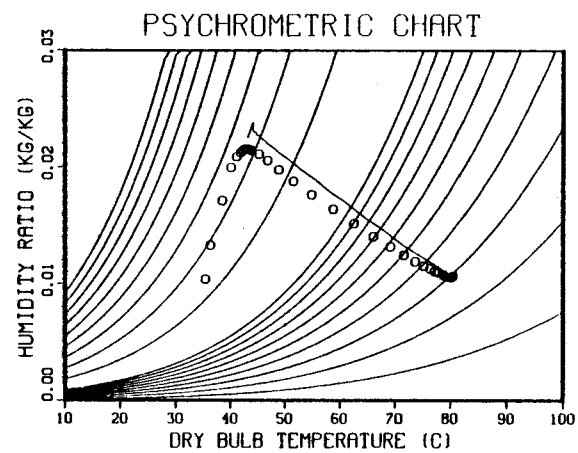
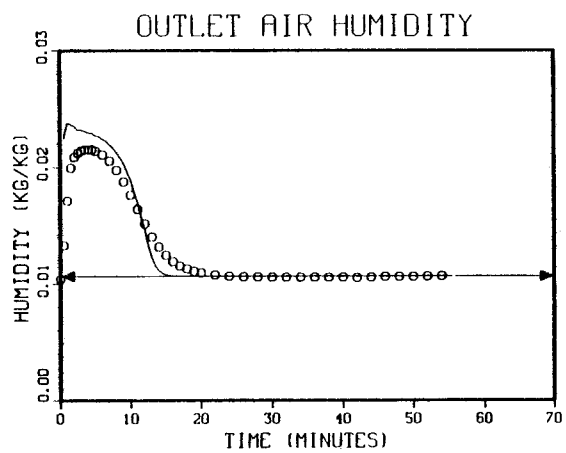
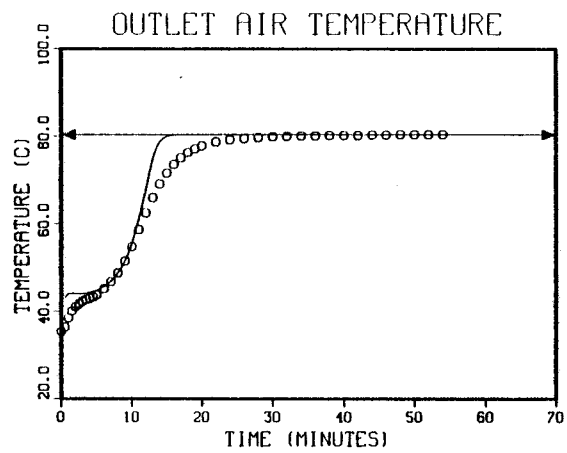


Fig. 4-4. Measured and Predicted Outlet Air Conditions During SERI Run 85R.

$T_{in} = 80.4^{\circ}\text{C}$, $W_{in} = 0.0106$, $T_o = 40.0^{\circ}\text{C}$, $X_o = 0.178$, $Ga = 0.597$
 $\text{kg/m}^2\text{s}$, $ICORR = 1$, $Le = 3$.

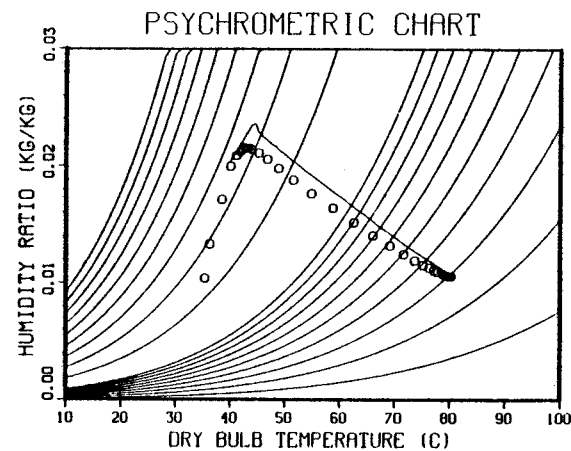
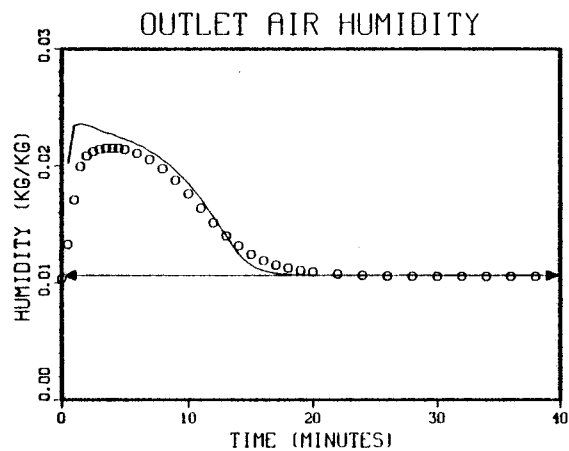
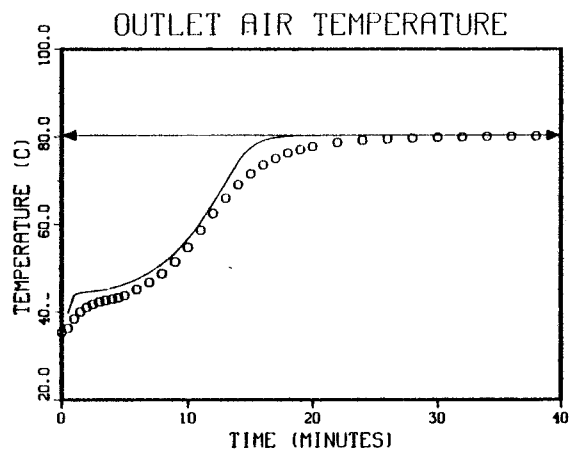


Fig. 4-5. Measured and Predicted Outlet Air Conditions During SERI Run 85R.

$T_{in} = 80.4^{\circ}\text{C}$, $W_{in} = 0.0106$, $T_o = 40.0^{\circ}\text{C}$, $X_o = 0.0178$, $Ga = 0.597$
 $\text{kg/m}^2\text{s}$, $ICORR = 1$, $Le = 6$.

001887

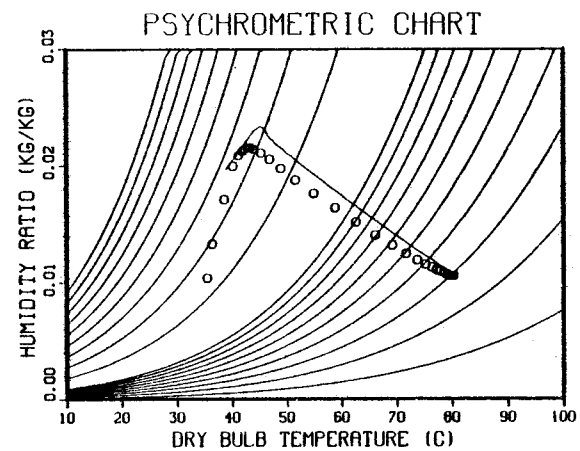
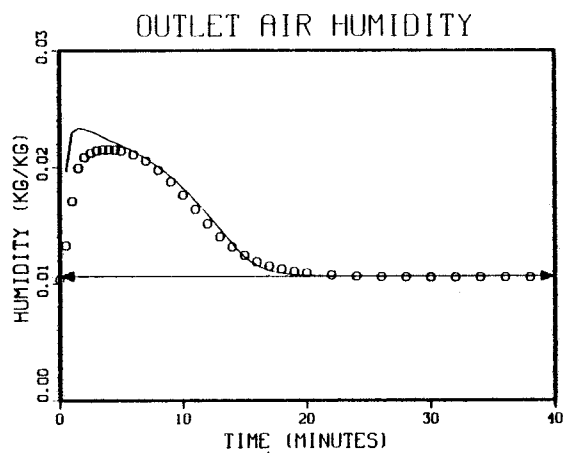
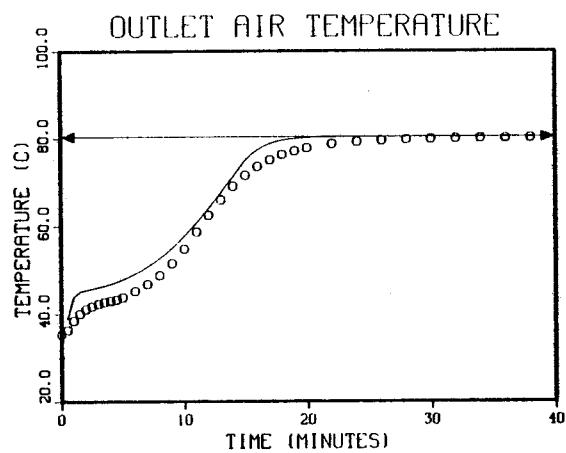
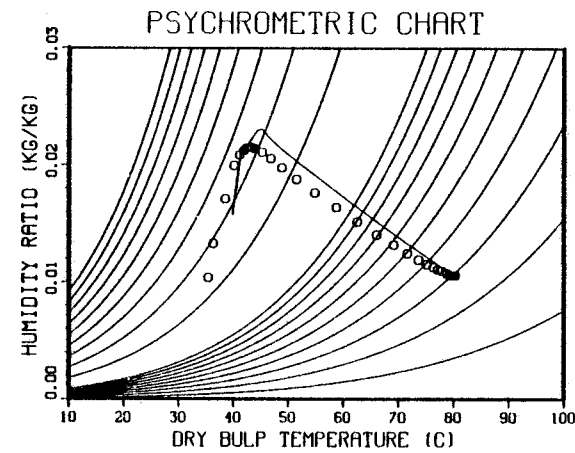
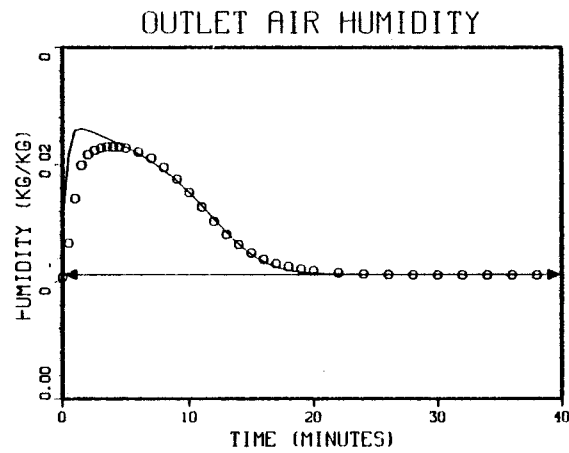
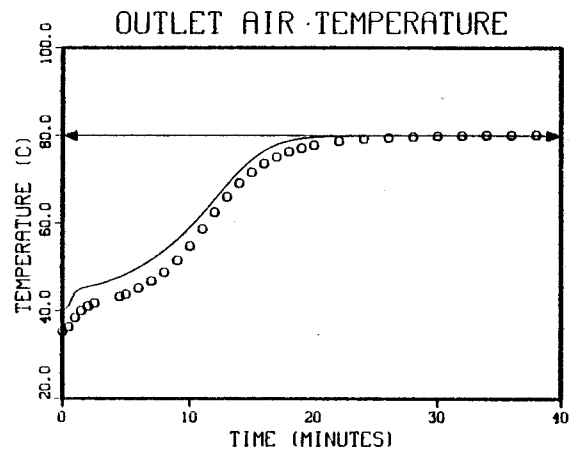


Fig. 4-6. Measured and Predicted Outlet Air Conditions During SERI Run 85R.

$T_{in} = 80.4^{\circ}\text{C}$, $W_{in} = 0.0106$, $T_o = 40.0^{\circ}\text{C}$, $X_o = 0.178$, $Ga = 0.597$
 $\text{kg/m}^2\text{s}$, $ICORR = 1$, $Le = 9$.

001886



6881889

Fig. 4-7. Measured and Predicted Outlet Air Conditions During SERI Run 85R.

$T_{in} = 80.4^{\circ}\text{C}$, $W_{in} = 0.0106$, $T_o = 40.0^{\circ}\text{C}$, $x_o = 0.171$, $Ga = 0.597$ $\text{kg/m}^2\text{s}$, $ICORR = 2$, $Le = 9$.

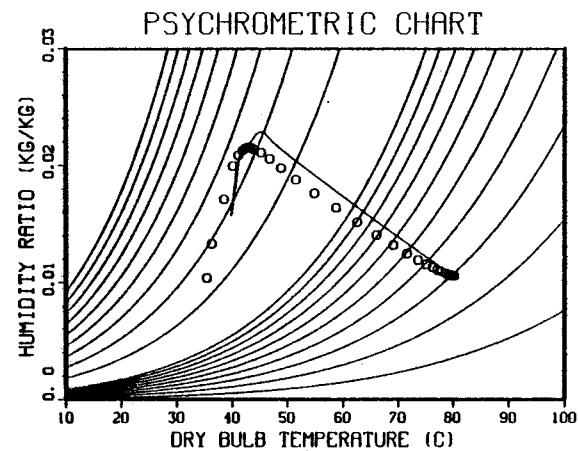
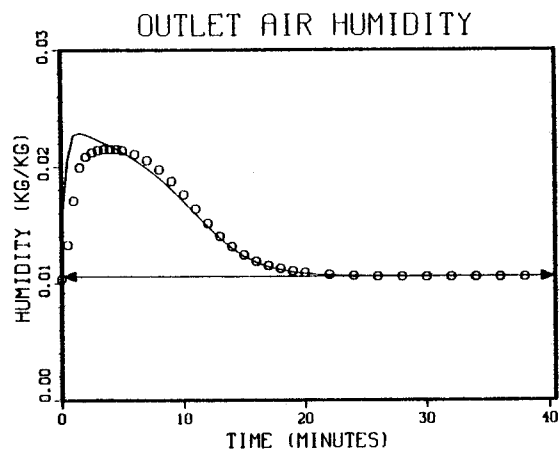
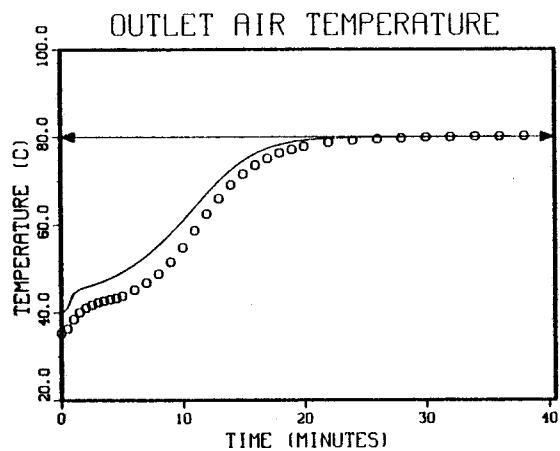


Fig. 4-8. Measured and Predicted Outlet Air Conditions During SERI Run 85R.

$T_{in} = 80.4^{\circ}\text{C}$, $W_{in} = 0.0106$, $T_o = 40.0^{\circ}\text{C}$, $X_o = 0.174$, $Ga = 0.597$
 $\text{kg/m}^2\text{s}$, $ICORR = 3$, $Le = 9$.

068100

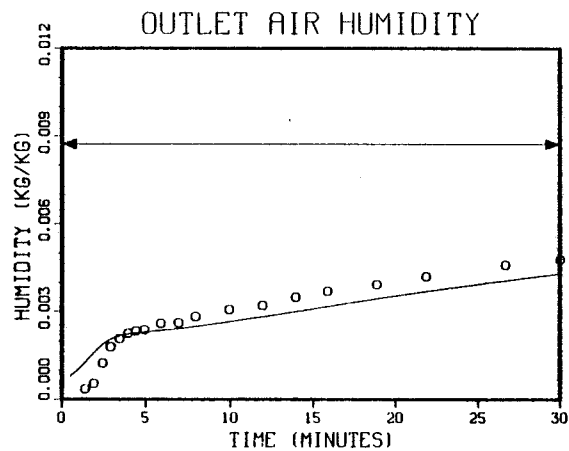
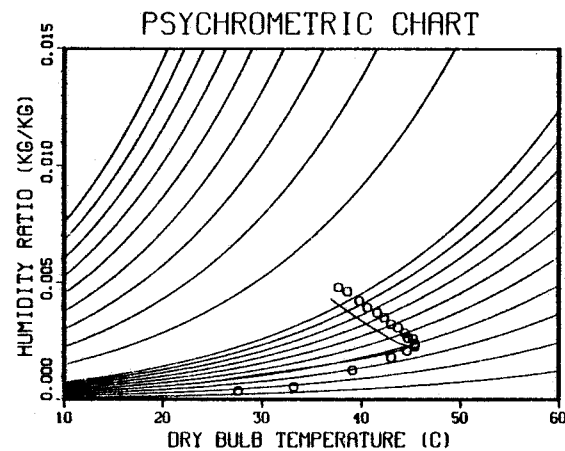
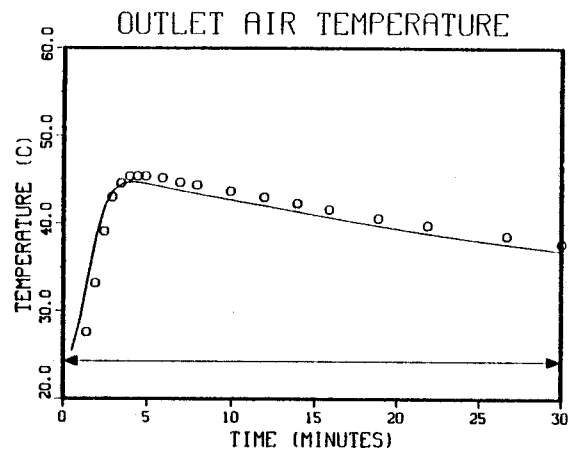


Fig. 4-9. Measured and Predicted Outlet Air Conditions During Pesaran Run 8.

$L = 0.07$ m, $D_p = 0.0039$ m, $T_{in} = 24.3^\circ\text{C}$, $W_{in} = 0.00873$, $T_o = 24^\circ\text{C}$,
 $X_o = 0.028$, $G_a = 0.408$ kg/m²s,
 $ICORR = 1$, $Le = 3$.

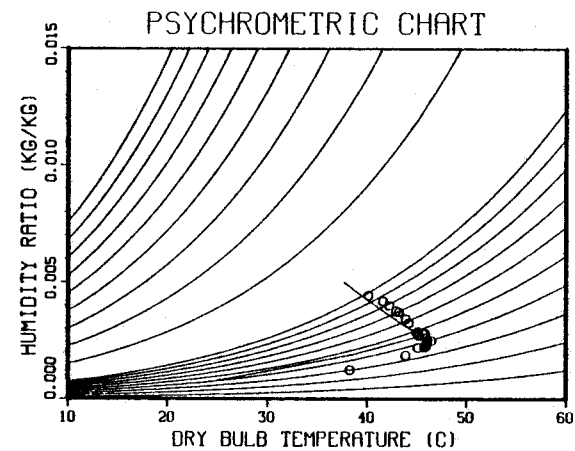
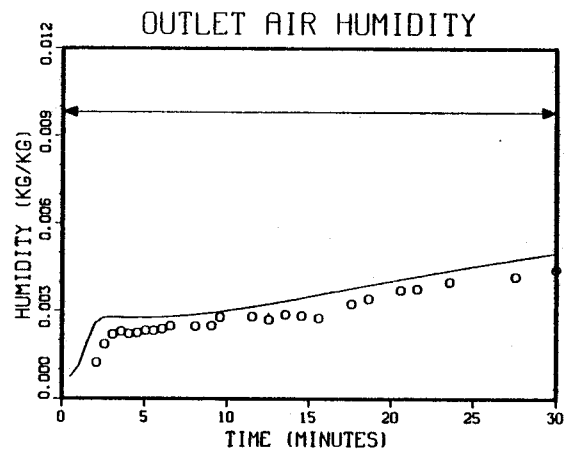
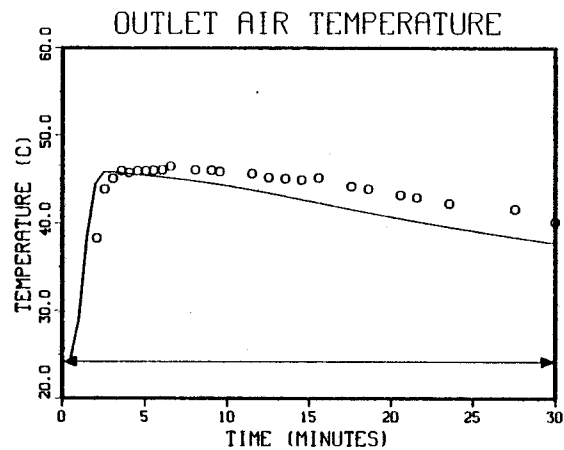


Fig. 4-10. Measured and Predicted Outlet Air Conditions During Pesaran Run 10.

$L = 0.065$ m, $D_p = 0.0021$ m, $T_{in} = 24.2$, $W_{in} = 0.00982$, $T_o = 24^\circ\text{C}$, $X_o = 0.0343$, $Ga = 0.456$ kg/m²s, ICORR = 1, Le = 3.

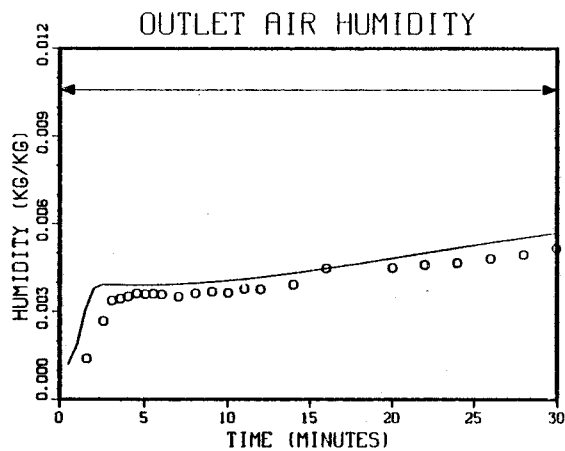
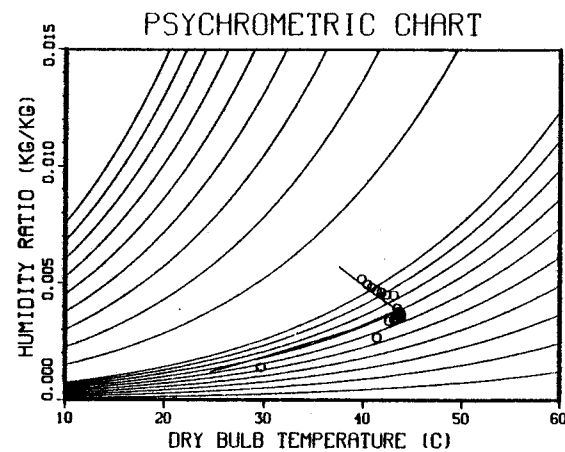
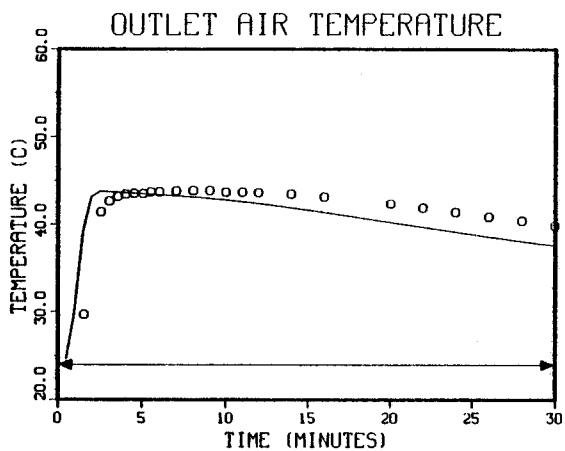
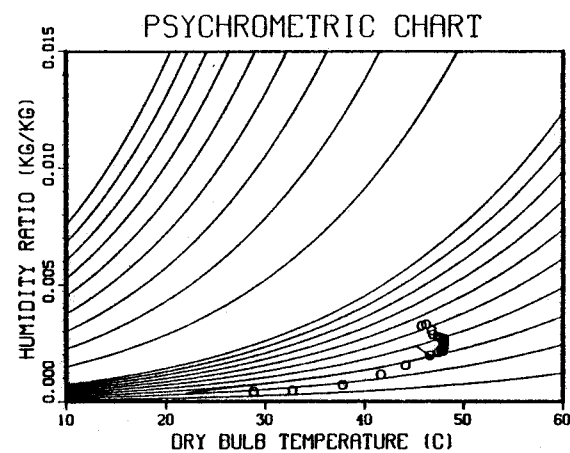
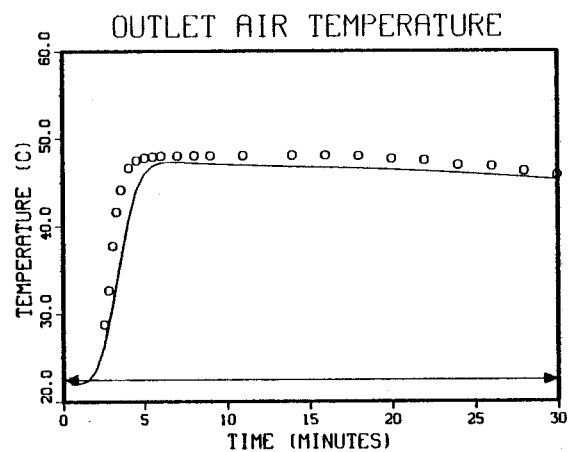


Fig. 4-11. Measured and Predicted Outlet Air Conditions During Pesaran Run 11.

$L = 0.065 \text{ m}$, $D_p = 0.0021 \text{ m}$, $T_{in} = 24.0$, $W_{in} = 0.01059$, $T_o = 24^\circ\text{C}$, $X_o = 0.0463$, $Ga = 0.0472$, $ICORR = 1$, $Le = 3$.



001894

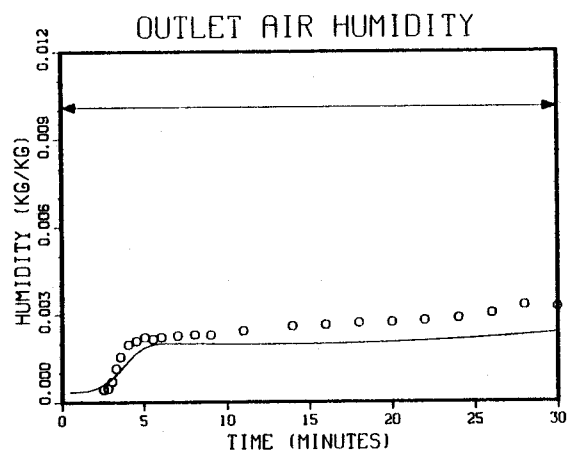


Fig. 4-12. Measured and Predicted Outlet Air Conditions During Pesaran Run 12.

$L = 0.10$ m, $D_p = 0.0021$ m, $T_{in} = 22.5$, $W_{in} = 0.0101$, $T_o = 22^\circ\text{C}$, $X_o = 0.0263$, $Ga = 0.292$, $ICORR = 1$, $Le = 3$.

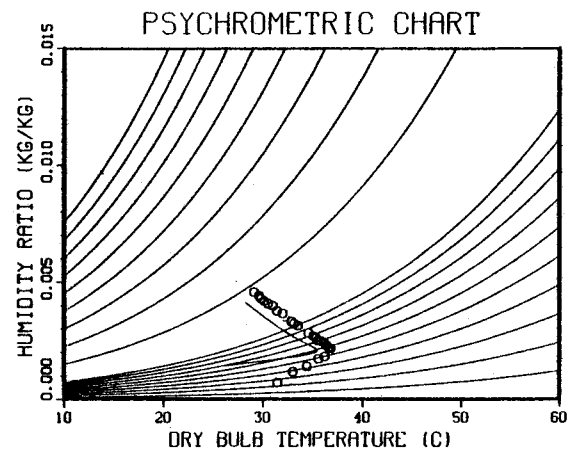
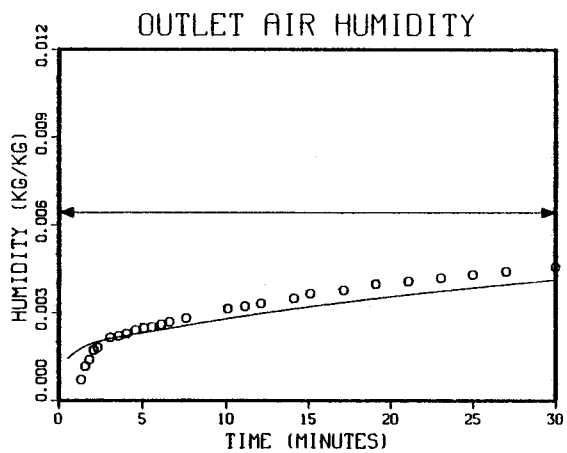
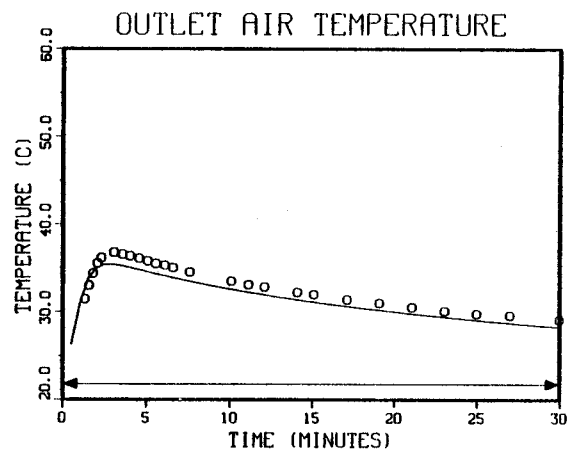


Fig. 4-13. Measured and Predicted Outlet Air Conditions During Pesaran Run 18.

$L = 0.0375$ m, $D_p = 0.0039$ m, $T_{in} = 21.8$, $W_{in} = 0.00643$, $T_o = 22^\circ\text{C}$, $X_o = 0.0295$, $Ga = 0.411$, $ICORR = 1$, $Le = 3$.

568100

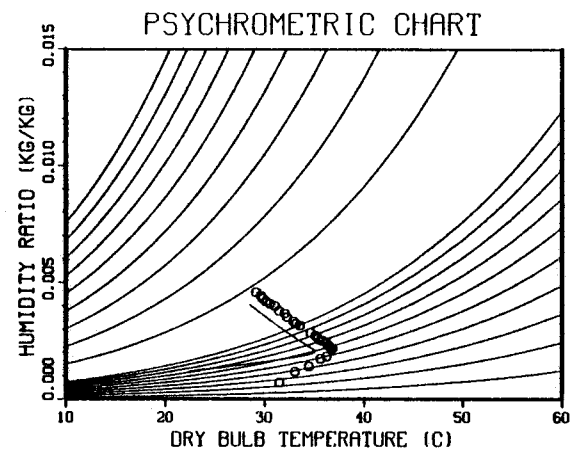
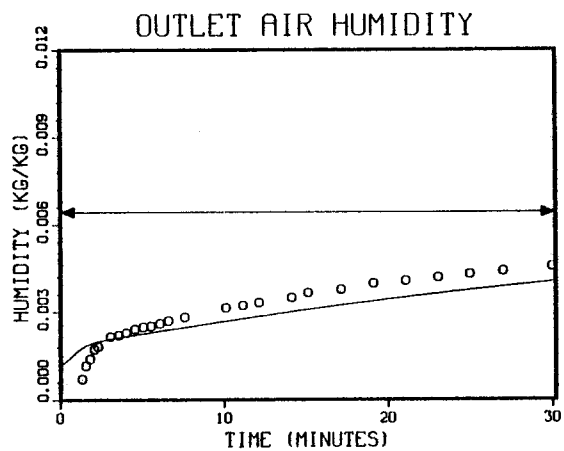
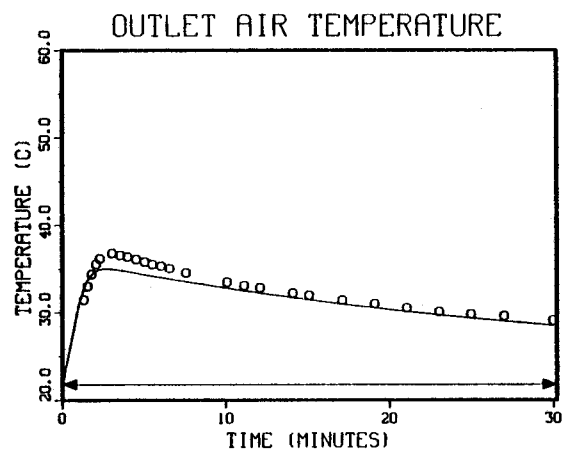


Fig. 4-14. Measured and Predicted Outlet Air Conditions During Pesaran Run 18.

$L = 0.0375$ m, $D_p = 0.0039$ m, $T_{in} = 21.8$, $W_{in} = 0.00643$, $T_o = 22^\circ\text{C}$, $X_o = 0.0295$, $Ga = 0.411$, $ICORR = 2$, $Le = 3$.

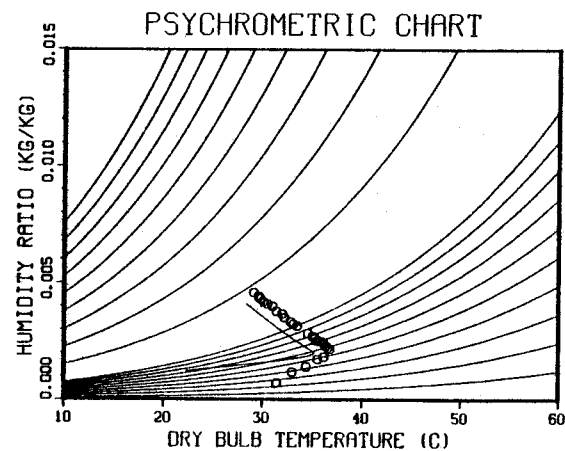
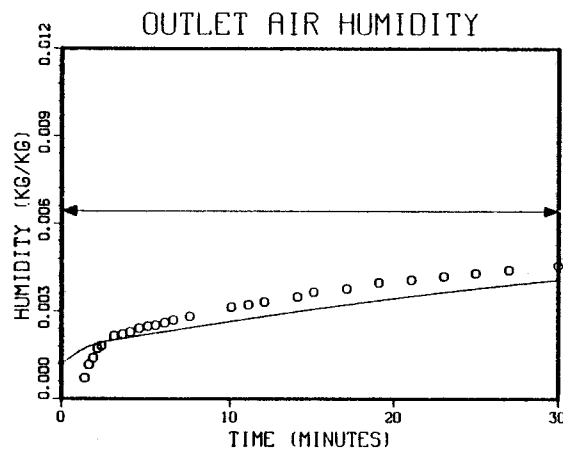
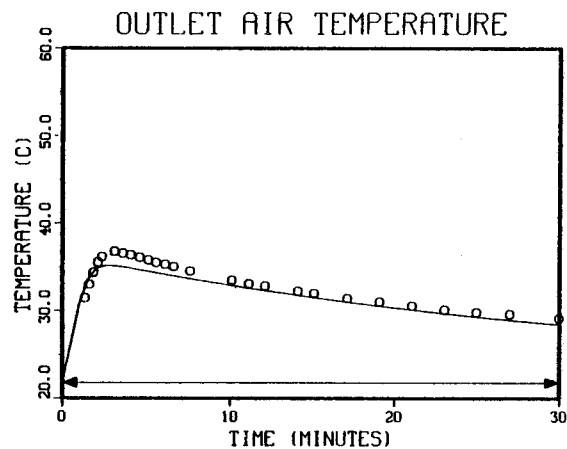


Fig. 4-15. Measured and Predicted Outlet Air Conditions During Pesaran Run 18.

$L = 0.0375$ m, $D_p = 0.0039$ m, $T_{in} = 21.8$, $W_{in} = 0.00643$, $T_o = 22^\circ\text{C}$, $X_o = .0295$, $Ga = 0.411$, $ICORR = 3$, $Le = 3$.

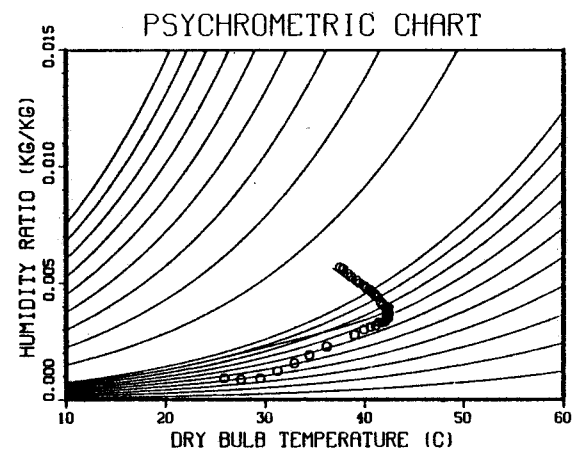
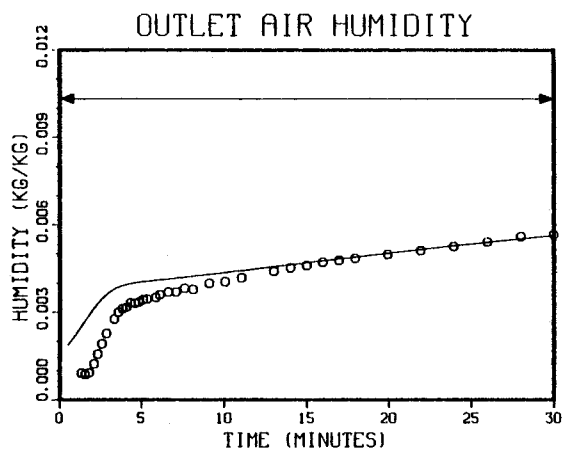
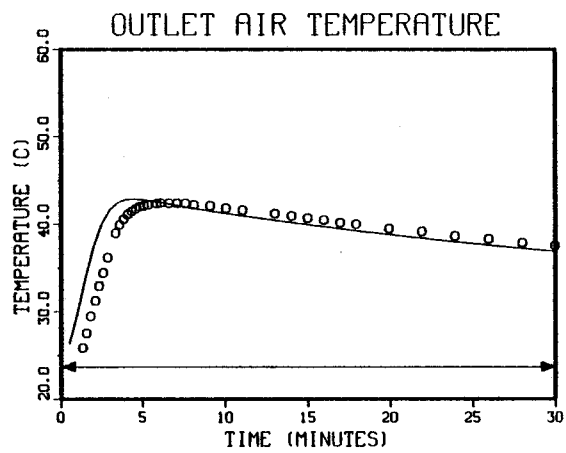


Fig. 4-16. Measured and Predicted Outlet Air Conditions During Pesaran Run 22.

$L = 0.0375$ m, $D_p = 0.0039$ m, $T_{in} = 23.7$, $W_{in} = 0.01033$, $T_o = 24^\circ\text{C}$, $X_o = 0.0418$, $Ga = 0.198$, $ICORR = 1$, $Le = 3$.

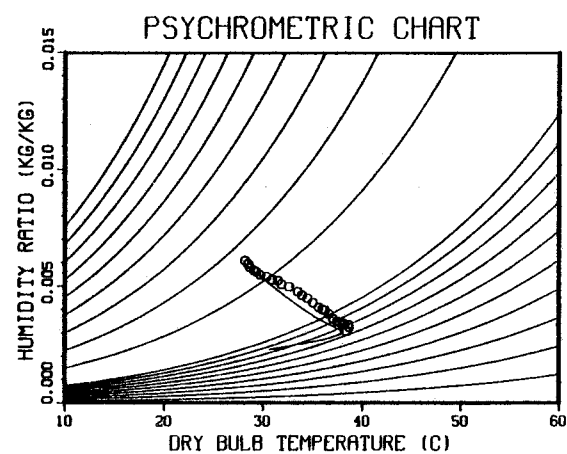
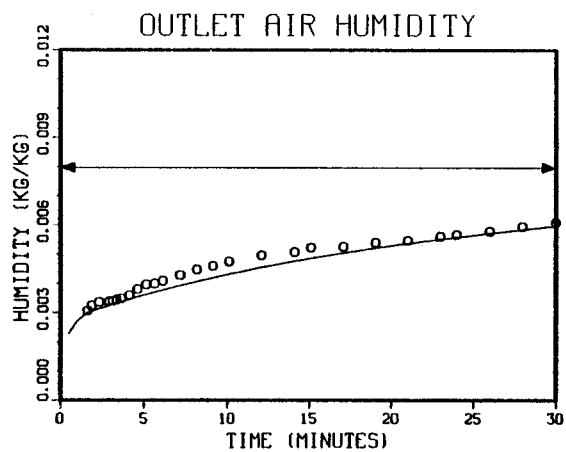
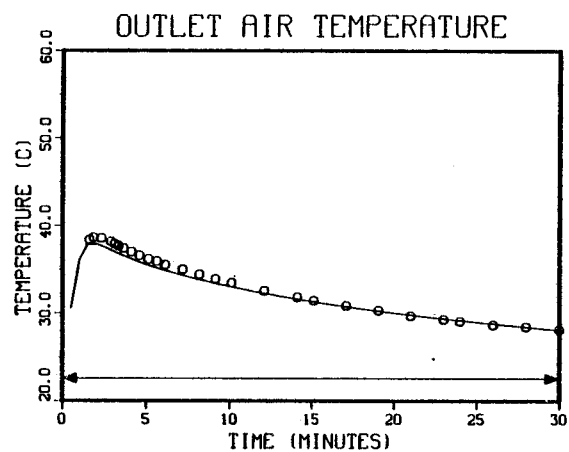


Fig. 4-17. Measured and Predicted Outlet Air Conditions During Pesaran Run 24.

$L = 0.0375$ m, $D_p = 0.0039$ m, $T_{in} = 22.6$, $W_{in} = 0.00797$, $T_o = 23^\circ\text{C}$, $X_o = 0.346$, $Ga = 0.595$, $ICORR = 1$, $Le = 3$.

**Table 4-3. Physical Properties and Dimensions
for Pesaran Experiments [36]**

Specific heat: 921 J/kg °C		
Void fraction: 0.4		
Bulk density: 745 kg/m ³		
Face area: 0.01327 m ²		
Tyler mesh:	3-8	6-12
Surface area:	919 m ² /m ³	1690 m ² /m ³
Particle diameter:	0.0039 m	0.0021 m

Table 4-4. Summary of Data Runs and Predictions for Pesaran Experiments

Data Run	Gel Mesh	Bed Depth	T _{in} (°C)	W _{in} (kg/kg)	T ₀ (°C)	X ₀ (kg/kg)	Ga (kg/m ² s)	Simulation Parameters	
								ICORR	Le
8	3-8	0.070	24.3	0.00873	24	0.028	0.408	1	3
10	6-12	0.065	24.2	0.00982	24	0.0343	0.456	1	3
11	6-12	0.065	24.0	0.01059	24	0.0463	0.472	1	3
12	6-12	0.100	22.5	0.0101	22	0.0263	0.292	1	3
18	3-8	0.0375	21.8	0.00643	22	0.0295	0.411	1	3
18	3-8	0.0375	21.8	0.00643	22	0.0295	0.411	2	3
18	3-8	0.0375	21.8	0.00643	22	0.0295	0.411	3	3
22	3-8	0.0375	23.7	0.01033	24	0.0413	0.198	1	3
24	3-8	0.0375	22.6	0.00797	23	0.0346	0.595	1	3

P_{atm} = 101235 Pa. Two-second time step and 10 bed sections used in simulations.

Results show relatively good agreement between data and predictions, although agreement is not as close as with the SERI data. A discrepancy that repeats itself is that the second predicted process line on the psychrometric chart, the one that is similar to a constant enthalpy line, runs parallel to the data but is displaced to a lower humidity in several runs. This indicates the possibility that reported inlet conditions for these runs are inaccurate, because the psychrometric process line must terminate at the inlet air state once the bed is saturated.

4.4 COMPARISON WITH KOH DATA

To study the potential of using solar energy to regenerate silica gel used for grain drying, Koh performed single-blow desorption experiments on packed beds. The packed beds Koh studied were thick compared to those used in desiccant cooling, but his regeneration temperatures are in a range of interest. The physical properties of the silica gel reported by Koh are given in Table 4-5. A summary of the parameters from each run included here is given in Table 4-6.

Table 4-5. Physical Properties for Koh Experiments

Particle diameter:	0.00176 m
Surface area:	1440 m ² /m ³
Void fraction:	0.4
Bulk density:	740 kg/m ³
Specific heat:	921 J/kg °C

Table 4-6. Summary of Data Runs and Predictions for Koh Experiments

Data Run	Bed Depth	T _{in} (°C)	W _{in} (kg/kg)	T ₀ (°C)	X ₀ (kg/kg)	Ga (kg/m ² s)	Simulation Parameters	
							ICORR	Le
2	0.089	48.9	0.01078	23.3	0.2782	0.0860	1	9
4	0.089	65.6	0.01575	27.2	0.2377	0.9852	1	9
6	0.089	82.2	0.01421	26.7	0.2575	0.0844	2	9
6	0.089	82.2	0.01421	26.7	0.2575	0.0844	3	9
8	0.178	48.9	0.00487	21.7	0.2652	0.0780	1	9
9	0.178	65.6	0.00493	18.3	0.1681	0.0774	1	9
10	0.178	65.6	0.00775	22.5	0.2867	0.0765	1	9
15	0.267	48.9	0.00392	17.8	0.2484	0.0741	1	9

P_{atm} = 98200 Pa. Ten-second time step and ten bed sections used in simulations.

The Koh data exhibit more scatter, particularly in humidity, than the other two data sources. There is generally good agreement between data and predictions on the trajectories of the psychrometric process lines. However, in almost all cases the predicted breakthrough curve is steeper than that measured. An effective Lewis number of 9 was used in the simulations, because it gave a good fit to the SERI data. Koh used finite difference methods to

obtain computer predictions for his experimental runs. Beginning with the heat and mass transfer correlations of Hougen and Marshall (see Fig. 3-4), he found it necessary to divide both transfer coefficients by five to obtain reasonable agreement between predicted and experimental breakthrough curves. Reynolds numbers for most of Koh's data runs were less than 10; therefore, axial dispersion may have contributed to the spreading of the moisture wave that is observed [44] (see Figs. 4-18 through 4-25).

4.5 RESULTS

In summary, the pseudo-steady-state model and the associated correlations for equilibrium properties and transfer coefficients give predictions that are very close to measured results for adsorption cases. Based on these results, it may be concluded that the use of a lumped, gas-side mass transfer coefficient is satisfactory for the simulation of water vapor adsorption by silica gel in packed-bed situations with conditions in the range of interest in desiccant cooling. The desiccant cooling cycle, of course, includes both adsorption and desorption. Results for desorption are not nearly as satisfactory as those for adsorption. On the whole, far fewer data are available for desorption than for adsorption, and other investigators have had similar difficulty in matching predictions with experimental data. Close [44] used the analogy method for heat transfer to predict single-blow adsorption and desorption, achieving relatively good agreement with adsorption data but poor agreement with desorption data. He attributed this discrepancy primarily to variations in properties of the silica gel/air/water system that are not fully accounted for by the analogy method. However, the pseudo-steady-state model accounts for any property variations included in currently available equilibrium correlations. Furthermore, this study has demonstrated that the use of different property correlations has little effect on the predicted breakthrough curves. Thus, it seems that variation or uncertainty in equilibrium properties during the adsorption/desorption process cannot explain the need to use a large effective Lewis number to obtain reasonable predictions for desorption.

Some silica gels exhibit a hysteresis loop in their relationship between moisture content and vapor pressure between adsorption and desorption. However, Rojas' data for PA-40 silica gel indicate that there is little or no hysteresis in the equilibrium properties of this gel [40]. Therefore, the fact that desorption cannot be predicted accurately by a gas-side resistance model using the same effective Lewis number as for adsorption indicates that there may be a dynamic hysteresis that acts to slow the desorption process but does not affect equilibrium data. This does not mean that a two-resistance model is necessary. The transport of water molecules within silica gel is not a simple solid diffusion problem, but a combination of pore diffusion, surface diffusion, repeated adsorption/desorption along the pore walls, and evaporation within capillaries. Consequently, a two-resistance model using a single diffusion coefficient may offer little improvement in accuracy over the lumped, gas-side resistance model. Relatively good results can be obtained with the pseudo-steady-state model once the appropriate value for the effective Lewis number has been determined. However, the above results show that, at least for desorption in packed beds, it will be necessary to determine these values experimentally.

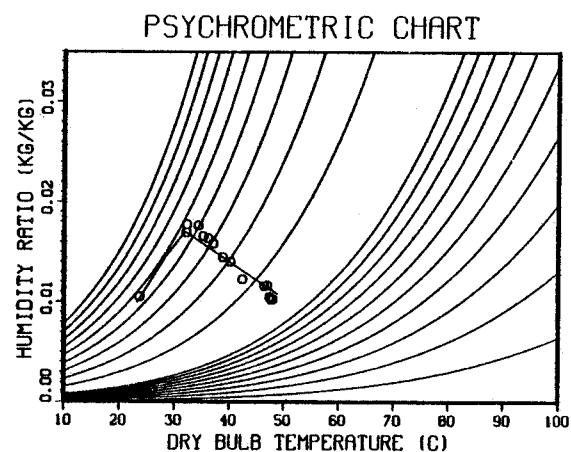
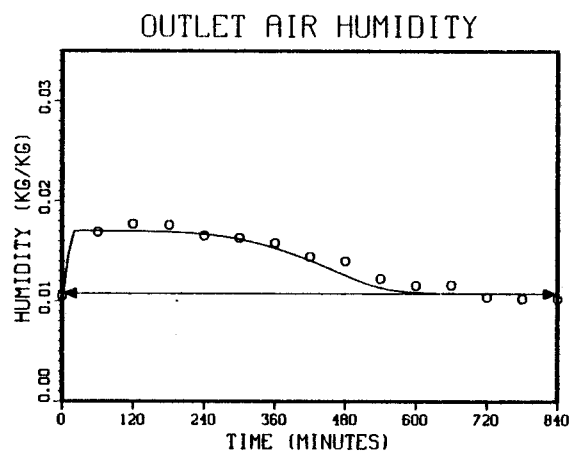
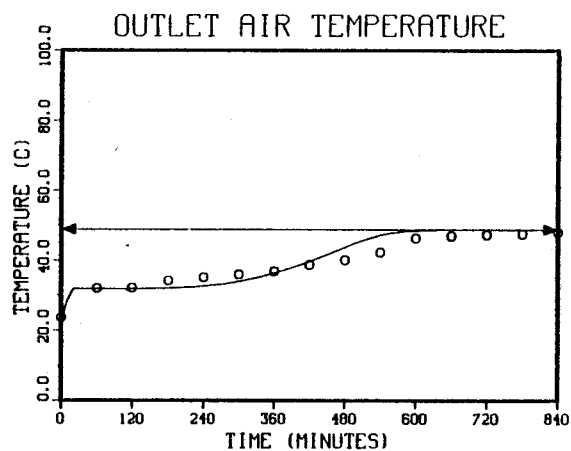


Fig. 4-18. Measured and Predicted Outlet Air Conditions During Koh Run 2. $L = 0.0889 \text{ m}$, $T_{in} = 48.9^\circ\text{C}$, $W_{in} = 0.01078$, $T_o = 23.3^\circ\text{C}$, $X_o = 2782$, $Ga = 0.0860 \text{ kg/m}^2\text{s}$, $ICORR = 1$, $Le = 9$.

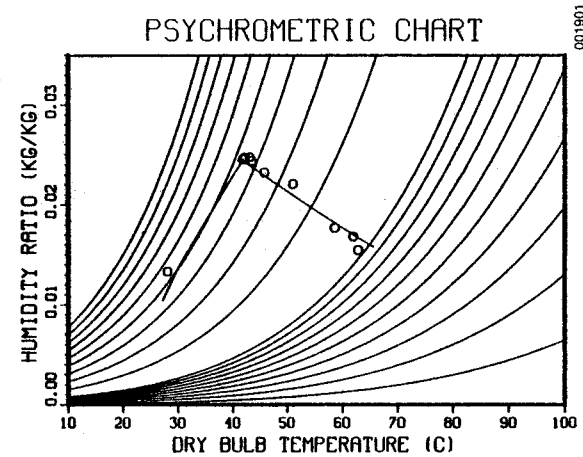
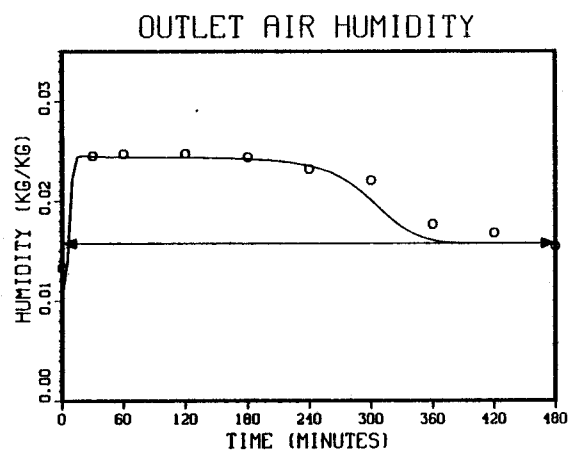
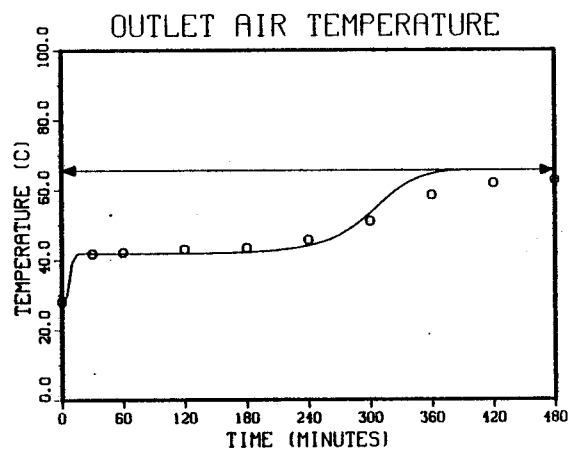


Fig. 4-19. Measured and Predicted Outlet Air Conditions During Koh Run 4. $L = 0.0889$ m, $T_{in} = 465.6^{\circ}\text{C}$, $W_{in} = 0.01575$, $T_o = 27.2^{\circ}\text{C}$, $X_o = 2377$, $G_a = 0.0852$ kg/m²s, $ICORR = 1$, $Le = 9$.

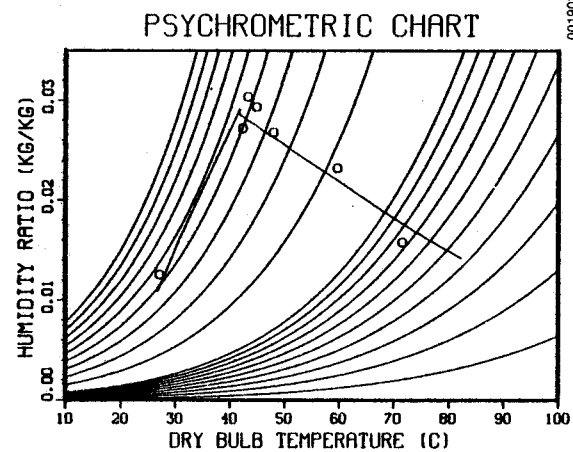
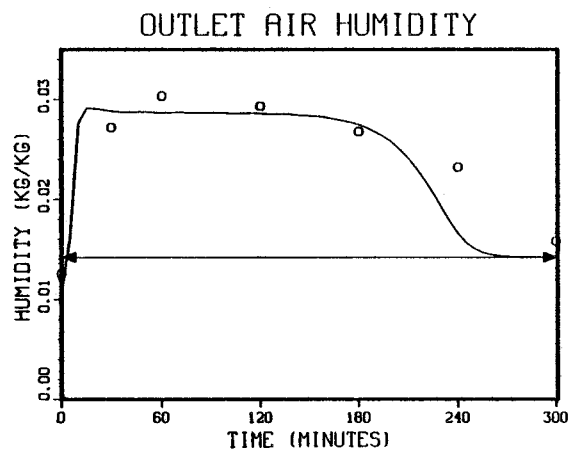
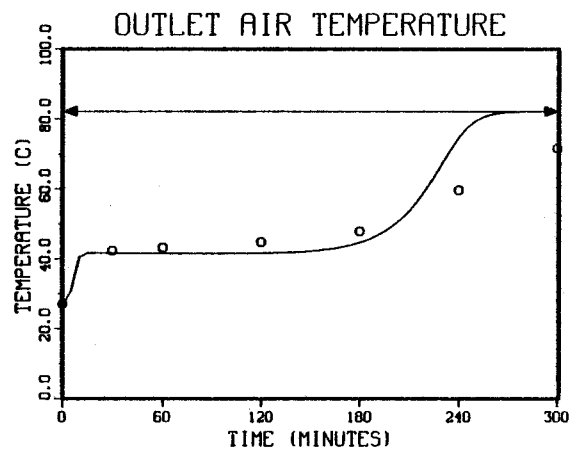


Fig. 4-20. Measured and Predicted Outlet Air Conditions During Koh Run 6. $L = 0.0889$ m, $T_{in} = 82.2^{\circ}\text{C}$, $W_{in} = 0.01421$, $T_o = 26.7^{\circ}\text{C}$, $X_o = 2575$, $Ga = 0.0844$ kg/m²s, $ICORR = 2$, $Le = 9$.

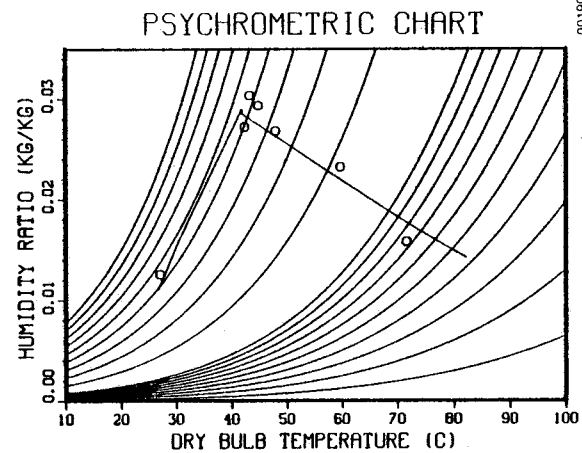
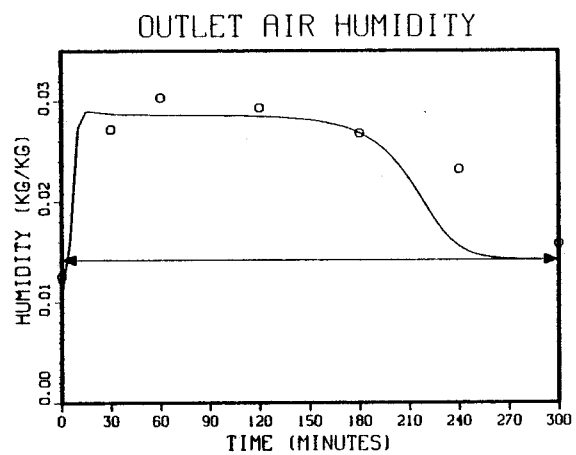
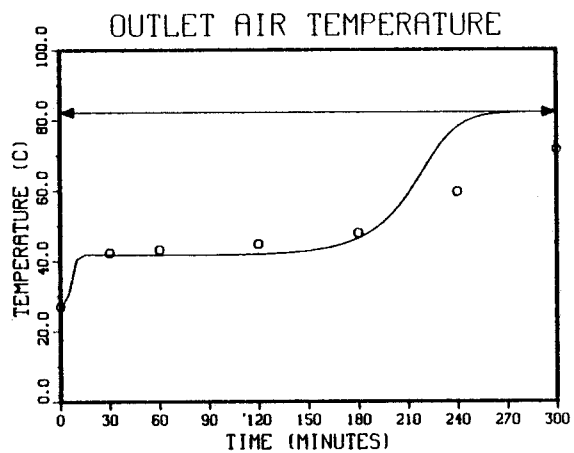


Fig. 4-21. Measured and Predicted Outlet Air Conditions During Koh Run 6. $L = 0.0889$ m, $T_{in} = 82.2^{\circ}\text{C}$, $W_{in} = 0.01421$, $T_o = 26.7^{\circ}\text{C}$, $X_o = 2575$, $Ga = 0.0844$ kg/m²s, $ICORR = 3$, $Le = 9$.

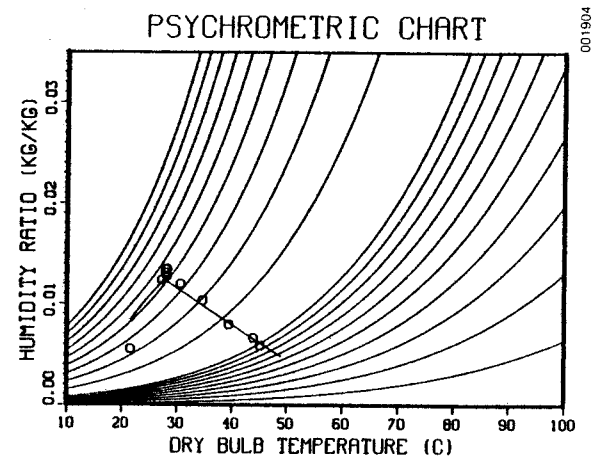
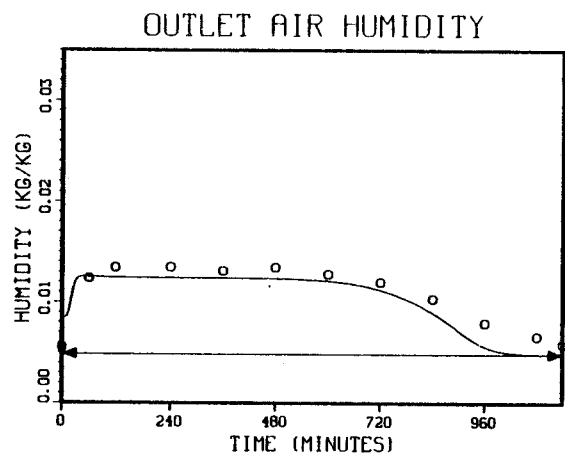
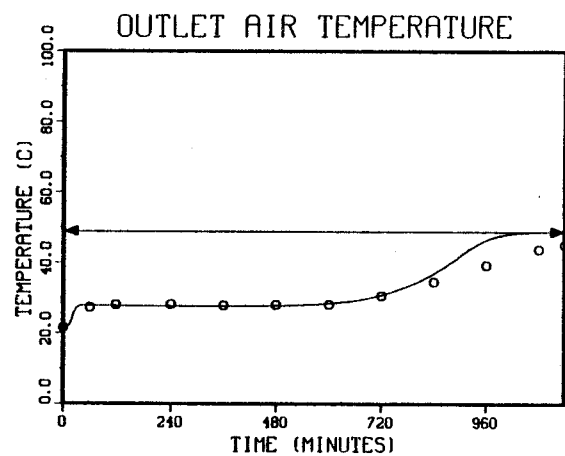


Fig. 4-22. Measured and Predicted Outlet Air Conditions During Koh Run 8. $L = 0.178$ m, $T_{in} = 48.9^{\circ}\text{C}$, $W_{in} = 0.00487$, $T_o = 21.7^{\circ}\text{C}$, $x_o = 2652$, $G_a = 0.0780$ kg/m²s, $ICORR = 1$, $Le = 9$.

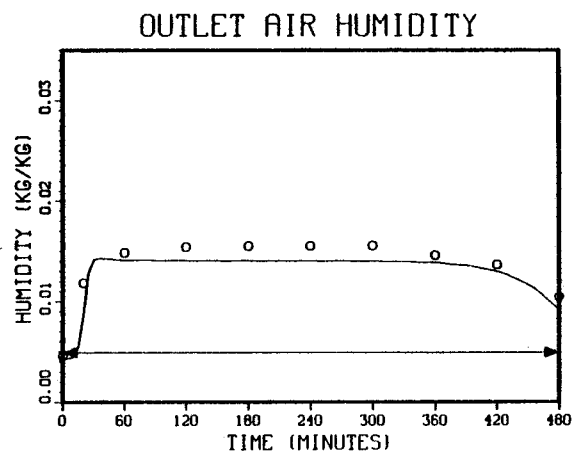
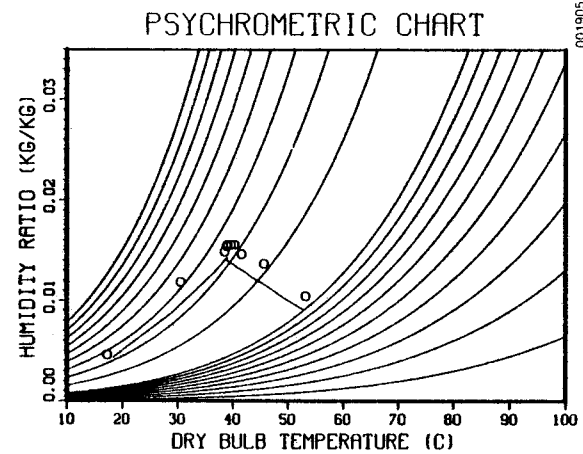
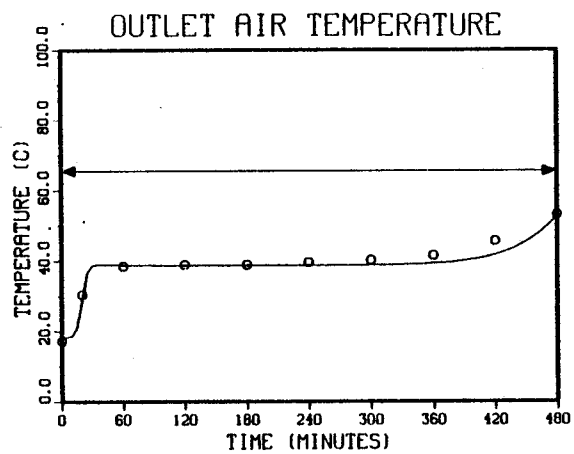


Fig. 4-23. Measured and Predicted Outlet Air Conditions During Koh Run 9. $L = 0.178$ m, $T_{in} = 65.6^{\circ}\text{C}$, $W_{in} = 0.00493$, $T_o = 18.3^{\circ}\text{C}$, $X_o = 1681$, $Ga = 0.0774$ $\text{kg/m}^2\text{s}$, $ICORR = 1$, $Le = 9$.

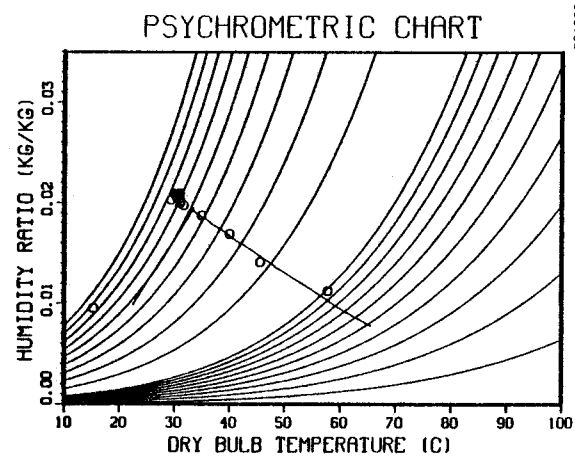
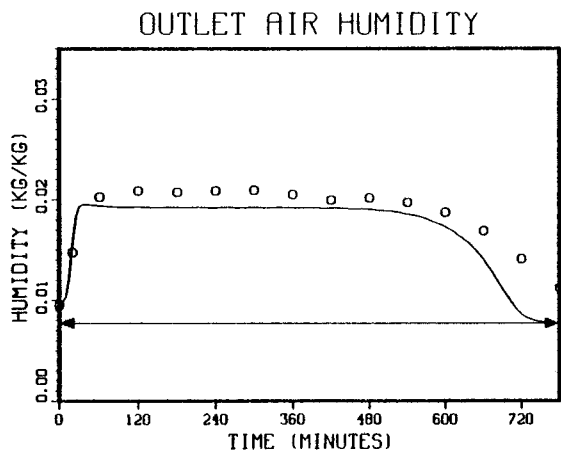
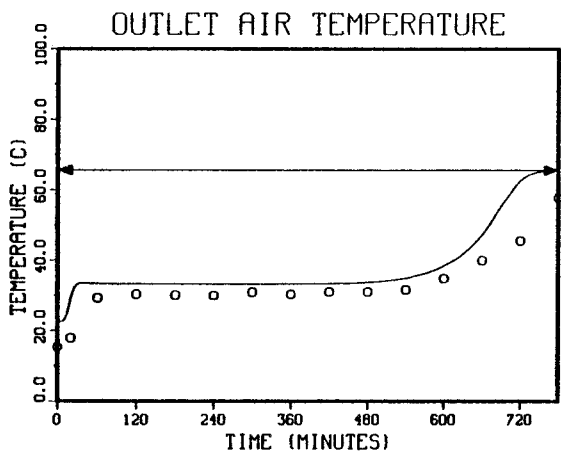


Fig. 4-24. Measured and Predicted Outlet Air Conditions During Koh Run 10. $L = 0.178$ m, $T_{in} = 65.6^{\circ}\text{C}$, $W_{in} = 0.00775$, $T_o = 22.5^{\circ}\text{C}$, $X_o = 2867$, $G_a = 0.0765$ kg/m²s, $ICORR = 1$, $Le = 9$.

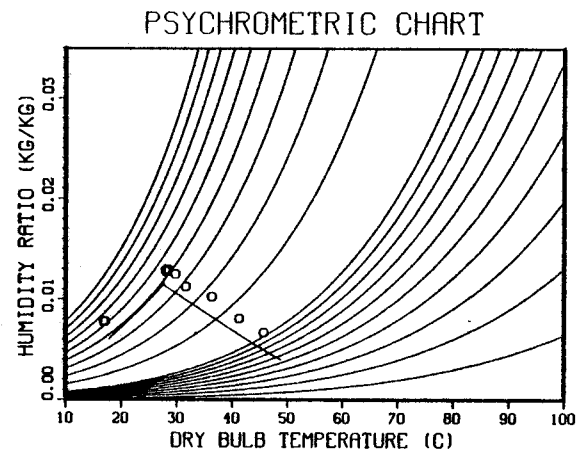
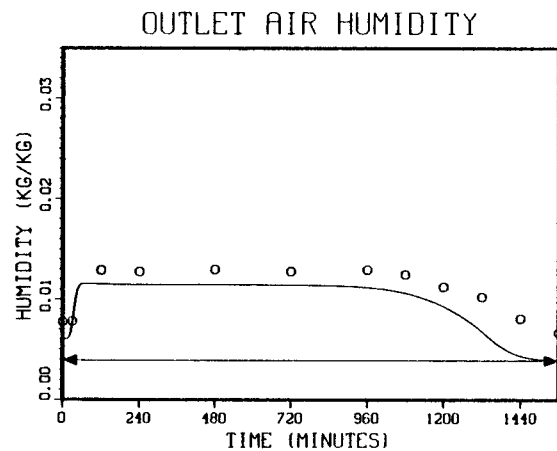
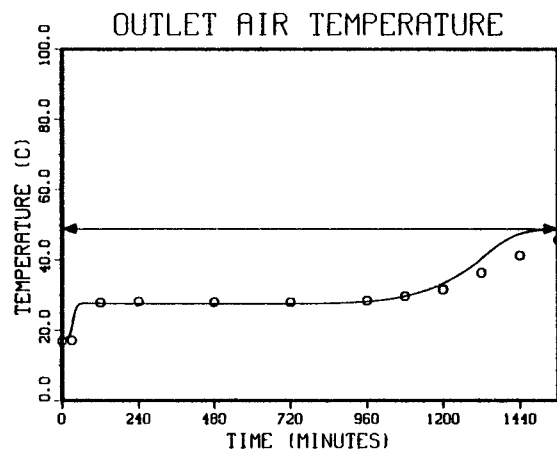


Fig 4-25. Measured and Predicted Outlet Air Conditions During Koh Run 15. $L = 0.267$ m, $T_{in} = 48.9^{\circ}\text{C}$, $W_{in} = 0.00392$, $T_o = 17.8^{\circ}\text{C}$, $X_o = 2484$, $Ga = 0.0741$ kg/m²s, $ICORR = 1$, $Le = 9$.

SERIO 

SECTION 5.0

DESICCANT COOLING SYSTEM SIMULATION

5.1 SYSTEM CONFIGURATION

A single cooling system configuration was chosen for this study. This system consists of an adiabatic dehumidifier, a sensible heat exchanger, two evaporative coolers, and a solar heater. Two modes of operation were considered; the ventilation mode and the recirculation mode. The ventilation mode is illustrated in Fig. 5-1. On the conditioning side of the system, ambient air is dehumidified, sensibly cooled, evaporatively cooled, then delivered to the building. On the regeneration side of the system, indoor air is evaporatively cooled to provide a cold sink for the cycle, heated first in the sensible heat exchanger, then in the solar heater, then used to regenerate or redry the desiccant, and finally exhausted to the atmosphere.

In the recirculation mode, illustrated in Fig. 5-2, the same processes are carried out, except that indoor air is conditioned and delivered back to the building, while outdoor air is used for regeneration, then exhausted back to the atmosphere. In both modes, flow rates on the two sides of the system were assumed to be balanced, and no purge sections such as those used by IGT and AiResearch were included. Thus, the system considered in this study is the simplest possible desiccant cooling system.

5.2 METHOD OF ANALYSIS

The dehumidifier is the heart of a desiccant cooling system. It is the most difficult component to characterize and the most interesting component in terms of research, since the state of the technology in coupled heat and mass transfer is much less advanced than in heat transfer alone. Therefore, the dehumidifier is simulated in detail using the pseudo-steady-state model, while the evaporative cooler and sensible heat exchanger are analyzed simply by specifying an effectiveness and applying the appropriate energy and mass balances.

The inlet air states on both sides of the dehumidifier must be known before the pseudo-steady-state model can be applied. Therefore, the thermodynamic analysis of the cooling cycle operating in either mode proceeds as follows:

- The outlet conditions from evaporative cooler 1 (state 2) are determined by calculating the wet bulb temperature at state 1, calculating the saturation humidity at this wet bulb temperature, and using a specified saturation effectiveness.
- The humidity ratio at state 4 is assumed to be the same as that at state 2, and the temperature at state 4 (the regeneration temperature) is specified.
- The pseudo-steady-state model is used to determine the average outlet states from both sides of the humidifier (states 5 and 7).

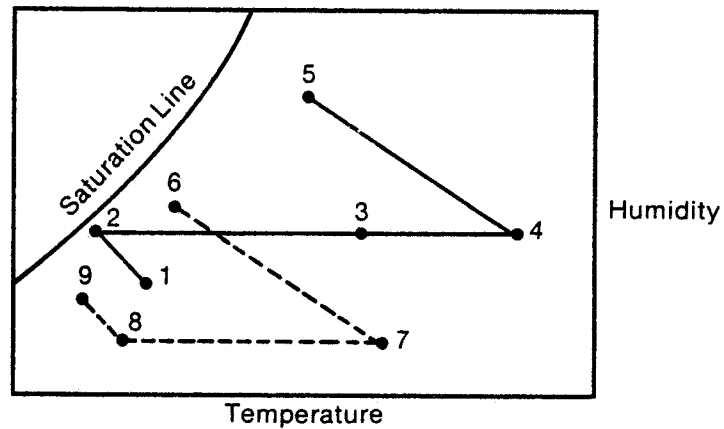
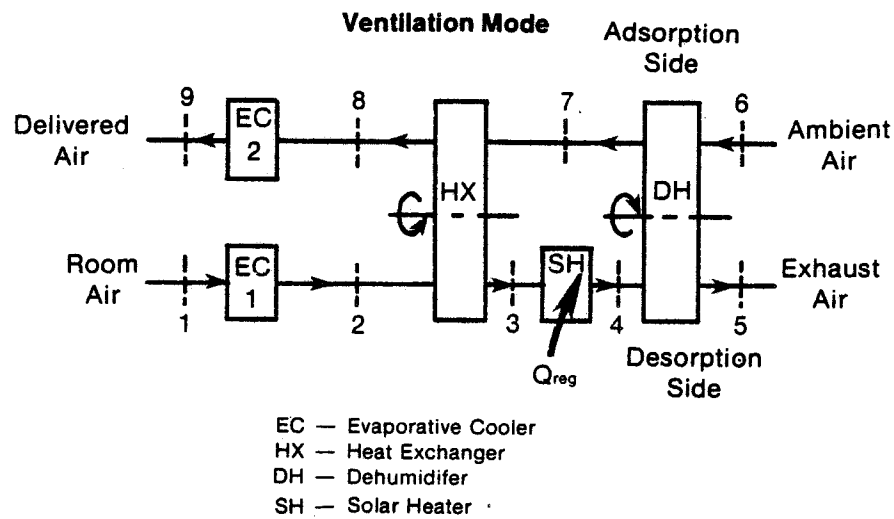


Fig. 5-1. System Schematic and Typical Psychrometric Cycle Diagram for the Ventilation Mode

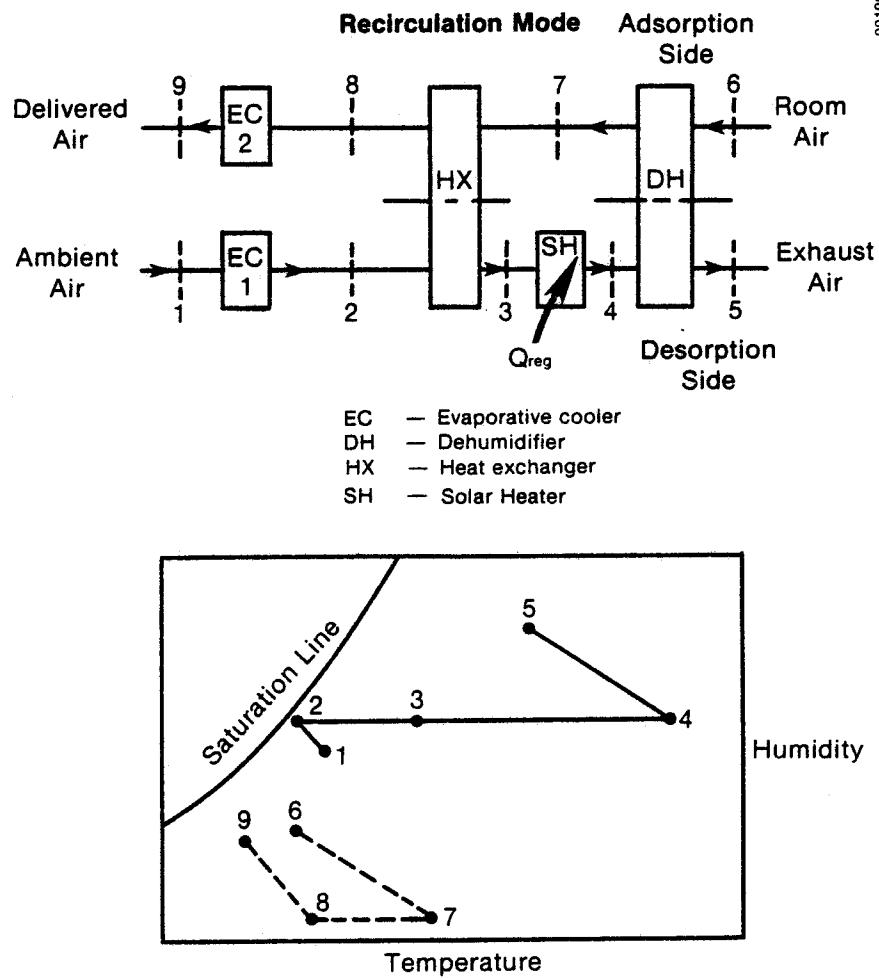


Fig. 5-2. System Schematic and Typical Psychrometric Cycle Diagram for the Recirculation Mode

- Outlet states from the sensible heat exchanger (states 3 and 8) are calculated based on a specified heat exchanger effectiveness.
- The outlet state from evaporative cooler 2 (state 9) is determined in the same manner as for evaporative cooler 1. (I.e., wet bulb temperature is at state 8, etc.)
- The COP and cooling capacity of the system are calculated from air enthalpies determined in the above manner using Eq. 3-21.

The methods of analysis, assumptions, and equations for each component are discussed in greater detail in the following sections. Throughout the analysis, it is assumed that the states of the air streams between each component are uniform and that there is no leakage of air.

5.3 COMPONENT ANALYSIS AND EQUATIONS

The psychrometric process line for evaporative cooling is assumed to be a line of constant wet bulb temperature. It is also assumed that the performance of the evaporative cooler can be characterized by a saturation effectiveness, such that state 2 is given by

$$T_2 = T_1 + E_{cl}(T_1^* - T_1) \quad (5-1a)$$

$$w_2 = w_1 + E_{cl}(w_1^* - w_1) \quad (5-1b)$$

where T_1^* is the wet bulb temperature at state 1 and w_1^* in the saturation humidity of that temperature. This wet bulb temperature is calculated using the iterative equations given by ASHRAE standards [45]. The procedure used in the computer program is to guess a value of T_1^* based on the enthalpy at state 1 and a polynomial relationship between enthalpy and wet bulb temperature. The humidity ratio based on this guess and the dry bulb temperature at state 1 is then calculated using the following equation in English units:

$$w_{\text{check}} = \frac{(1093 - 0.556T_1)w^* - 0.24(T_2 - T_1^*)}{(1093 + 0.444T - T_1^*)} \quad (5-2)$$

The value of w_{check} is compared to the known w_1 and the bisection method is used in adjusting T_1^* and iterating through Eq. 5-2 until the correct value of T_1^* is found to within a narrow tolerance.

The dehumidifier is analyzed using the pseudo-steady-state model. This model was described in Secs. 3.0 and 4.0 in terms of the simulation of single-blow adsorption or desorption. The model can also be applied to cyclic operation of a fixed bed or to a rotating dehumidifier. To simulate the performance of a dehumidifier wheel, the model is applied to a small element as shown in Fig. 5-3. The advance of time in the simulation corresponds to the progression of this element in a circular arc through either the adsorption or the desorption side of the system. As the element progresses, the outlet air state progresses along the process lines described in Sec. 6. Once the element has completely traversed one side of system and crosses to the other side, the direction of the conveyor belt model is reversed and the inlet air

conditions are changed. The average outlet state on each side of the dehumidifier is of primary interest in this study and is calculated at the end of each half-period. The total amount of water adsorbed or desorbed by the desiccant is also calculated at the end of each half-period. To predict the steady-state performance of the system, the computer model is cycled between adsorption and regeneration until the amount of water adsorbed and desorbed in the two half-cycles balances to within a defined convergence criterion. For this study, the water balance was required to be within 0.1%.

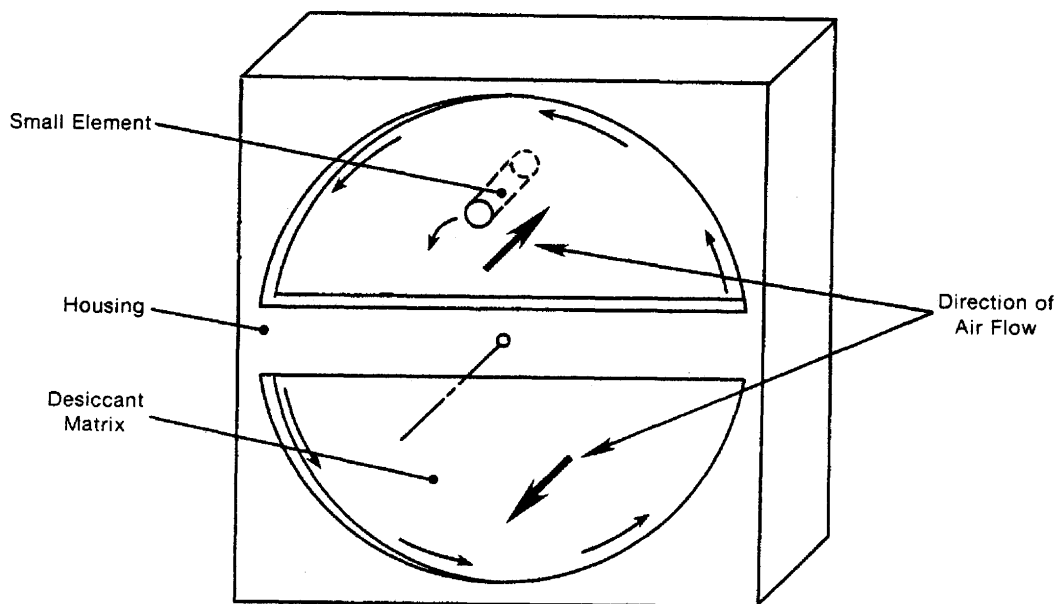


Fig. 5-3. Small Element Used in Simulations of Rotary Dehumidifiers

The sensible heat exchanger is modeled simply by assuming an overall heat transfer effectiveness. It is also assumed that no moisture is transferred between air streams. The capacity rates of the air streams are calculated as

$$C_{ads} = \dot{m}_{ads} c_p [T(7), W(7)] \quad (5-3)$$

$$C_{reg} = \dot{m}_{reg} c_p [T(2), W(2)] \quad , \quad (5-4)$$

where flow rates \dot{m}_{ads} and \dot{m}_{reg} refer to dry air. Specific heats are calculated from Eq. 3-23. The total energy transfer is

$$\dot{Q}_{hx} = E_{hx} C_{min} [T(7) - T(2)] \quad . \quad (5-5)$$

Thus, enthalpies at states 3 and 8 are

$$h(3) = h(2) + \dot{Q}_{hx} / \dot{m}_{reg} \quad (5-6)$$

$$h(8) = h(7) + \dot{Q}_{hx} / \dot{m}_{ads} \quad (5-7)$$

Temperatures at states 3 and 8 are calculated from Eq. 3-22. Note that, in this study, balanced flow is assumed, so \dot{m}_{ads} and \dot{m}_{reg} are equal.

The solar or auxiliary heater is assumed to supply just enough energy to raise the regeneration stream to the specified temperature.

$$\dot{Q}_{reg} = \dot{m}_{reg} [h(4) - h(3)] \quad (5-8)$$

The cooling capacity of the system is based on the enthalpy difference between the room air supplied to the system and the conditioned air delivered to the room.

For the balanced-flow case, we have

$$\dot{Q}_{cool} = \dot{m}_{ads} [h_{room} - h(9)] \quad (5-9)$$

The thermal COP of the system is the ratio of the total cooling capacity to the total thermal energy added for regeneration:

$$COP = \frac{\dot{Q}_{cool}}{\dot{Q}_{reg}} \quad (5-10)$$

No estimates of parasitic power have been included in this study. Experimental data on pressure drop in the packed silica gel bed used in SERI's adsorption test is included in Ref. [48].

SECTION 6.0

THE PHYSICAL BEHAVIOR OF DESICCANT BEDS

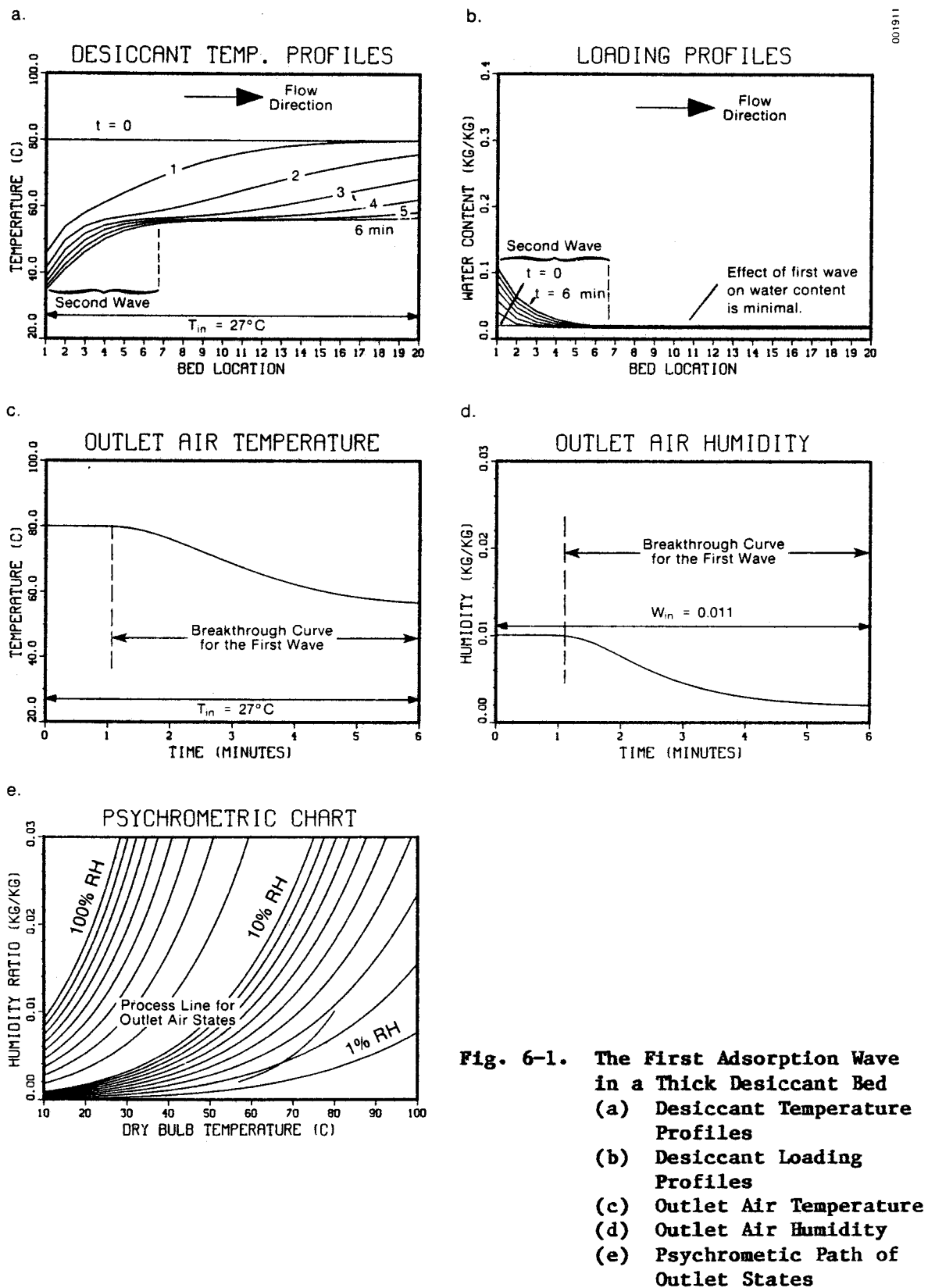
This section presents a detailed discussion of the way silica gel beds behave during adiabatic adsorption and desorption, and how this behavior within the desiccant bed affects the outlet states of the process air leaving the bed. This detailed discussion is included because an understanding of the behavior of desiccant beds seems critical to achieving an understanding of desiccant cooling systems and to directing future research toward improving desiccant systems.

This discussion relies heavily on graphics. All graphs were generated using the DESSIM computer programs, the DISSPLA graphics software package, and a CALCOMP plotter. In the plots of temperature and loading profiles, bed location refers to the 20 evenly divided bed sections used in the simulations and is, in effect, a nondimensional distance through the bed.

6.1 BEHAVIOR OF THICK BEDS DURING ADIABATIC ADSORPTION

The adiabatic adsorption process involves the propagation of two waves through a desiccant bed. Heat transfer and mass transfer occur simultaneously during the passing of each wave, and both are coupled thermal and moisture waves. However, the first wave has a primarily thermal effect within the bed. That is, the temperature of the desiccant may change significantly with the passing of the first wave, but the moisture content of the bed changes only slightly. The second wave is what is usually referred to as the moisture wave, but the temperature and moisture content of the desiccant change simultaneously with the passing of this wave.

The first wave travels much faster than the second wave in silica gel. Therefore, two time scales are used in the two sets of figures illustrating this process. Figure 6-1 illustrates single-blow adsorption with a flow rate of $0.5 \text{ kg/m}^2\text{s}$ in a 0.5-m-thick bed of 8-10 mesh silica gel. The time scale used in these graphs corresponds to the time it takes for the first wave to pass completely through the bed. Figures 6-1(a) and (b) show temperature and moisture profiles within the bed at one-minute intervals. Figure 6-1(a) shows that the first wave passes through the bed in about six minutes, and that a significant change in bed temperature accompanies its passing. Figure 6-1(b) demonstrates that the moisture content of the bed changes very little with the passing of this wave. Both figures show that the second wave has only begun its progression into the bed during this time. Figures 6-1(c) and (d) show the outlet air temperature and humidity as a function of time during the passing of the first wave. Both quantities change, and it is important to note that the air humidity changes significantly with the passing of the first wave, even though the first wave acts somewhat like a pure thermal wave within the bed. Figure 6-1(e) demonstrates that this change occurs along a psychrometric process line that is similar to, but steeper than, a line of constant relative humidity.



The same adsorption process is illustrated on a much longer time scale in Fig. 6-2. Temperature and loading profiles are shown at 30-minute intervals in Figs. 6-2(a) and (b). The second wave becomes very spread out during adsorption and has not left the bed even after 180 minutes, whereas a square wave involving the same change in conditions would pass through the bed in less than 90 minutes. Figures 6-2(b) and (c) show outlet air states as a function of time. Here, the breakthrough curve for the first wave is compressed to the far left portion of each graph. This is followed by a dwell period during which the outlet air remains at a constant state. After about 25 minutes, the outlet air state begins to move slowly toward the inlet state as the second wave begins to pass the outlet end of the bed.

Figure 6-2(e), the psychrometric chart, shows the two distinctly different process lines followed by the outlet air states as the two waves pass through the bed. With this relatively thick bed there is a sharp elbow at the intersection that corresponds to the dwell state. The trajectories of the two process lines are determined primarily by the physical and equilibrium properties of the desiccant. Close and Banks [27] have presented a detailed analysis of these lines, which will not be repeated here. However, the process lines can be described in the following approximate manner. For pure, regular-density silica gel, the equilibrium water content can be described reasonably well as a function of the relative humidity of the surrounding air, and lines of constant relative humidity on the psychrometric chart can be translated roughly to lines of constant gel moisture content. As the first wave passes, the water content of the bed changes only slightly. Thus, the first process line is not far from a line of constant relative humidity. The passing of the second wave involves the adiabatic addition or removal of water from the air stream. Thus, the second process line is similar to an adiabatic saturation process line, which is a line of constant wet bulb temperature. The second process line differs from an adiabatic saturation line roughly by the difference between the heat of adsorption and the heat of vaporization of water. The heat capacity of the desiccant bed also affects the slopes of both process lines. As the heat capacity of the bed increases, the first process line becomes more vertical and the second process line becomes more horizontal.

6.2 BEHAVIOR OF THICK BEDS DURING ADIABATIC DESORPTION

As was demonstrated by the experimental data from the SERI Desiccant Test Lab, the behavior of desiccant beds during desorption is somewhat different from that during adsorption. The outlet air states followed the same type of psychrometric lines, but the breakthrough curve for the second wave was always steeper than that observed during adsorption. Figures 6-3 and 6-4 show the predicted behavior of an 0.5-m silica gel₂ bed as described above during desorption with the same flow rate, 0.5 kg/m²s. The time scales are the same as for the adsorption case; Fig. 6-3 illustrates the first wave and Fig. 6-4 illustrates the second. From Figs. 6-4(a) and (b) it is again clear that the passing of the first wave has only a slight effect on the water content of the silica gel and that this wave is primarily a thermal wave within the bed. The most notable difference between desorption and adsorption in relatively thick beds is demonstrated by comparing Fig. 6-4 with Fig. 6-2. The temperature and loading profiles of Figs. 6-4(a) and (b) show that the second wave in desorp-

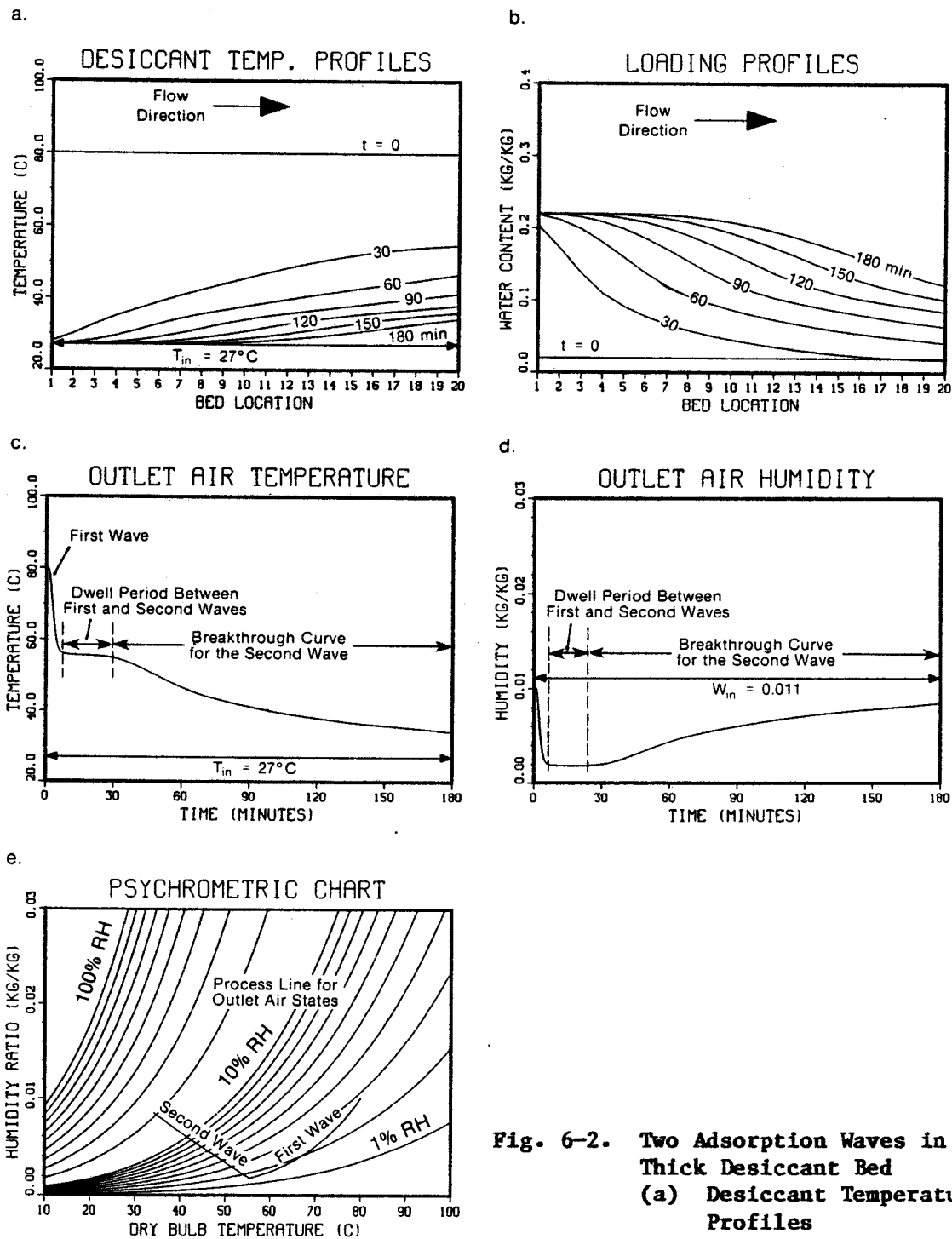
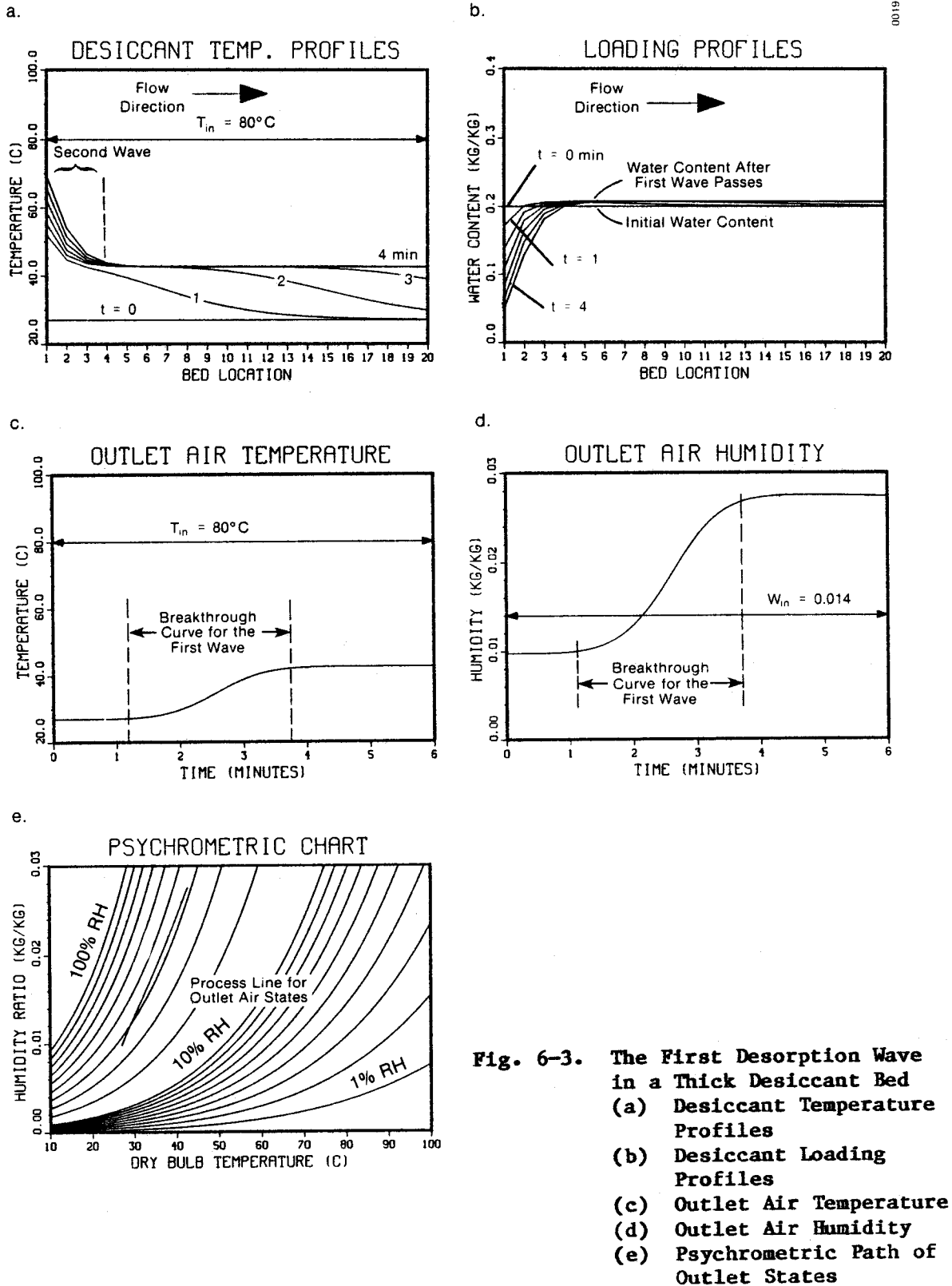


Fig. 6-2. Two Adsorption Waves in a Thick Desiccant Bed
 (a) Desiccant Temperature Profiles
 (b) Desiccant Loading Profiles
 (c) Outlet Air Temperature
 (d) Outlet Air Humidity
 (e) Psychrometric Path of Outlet States



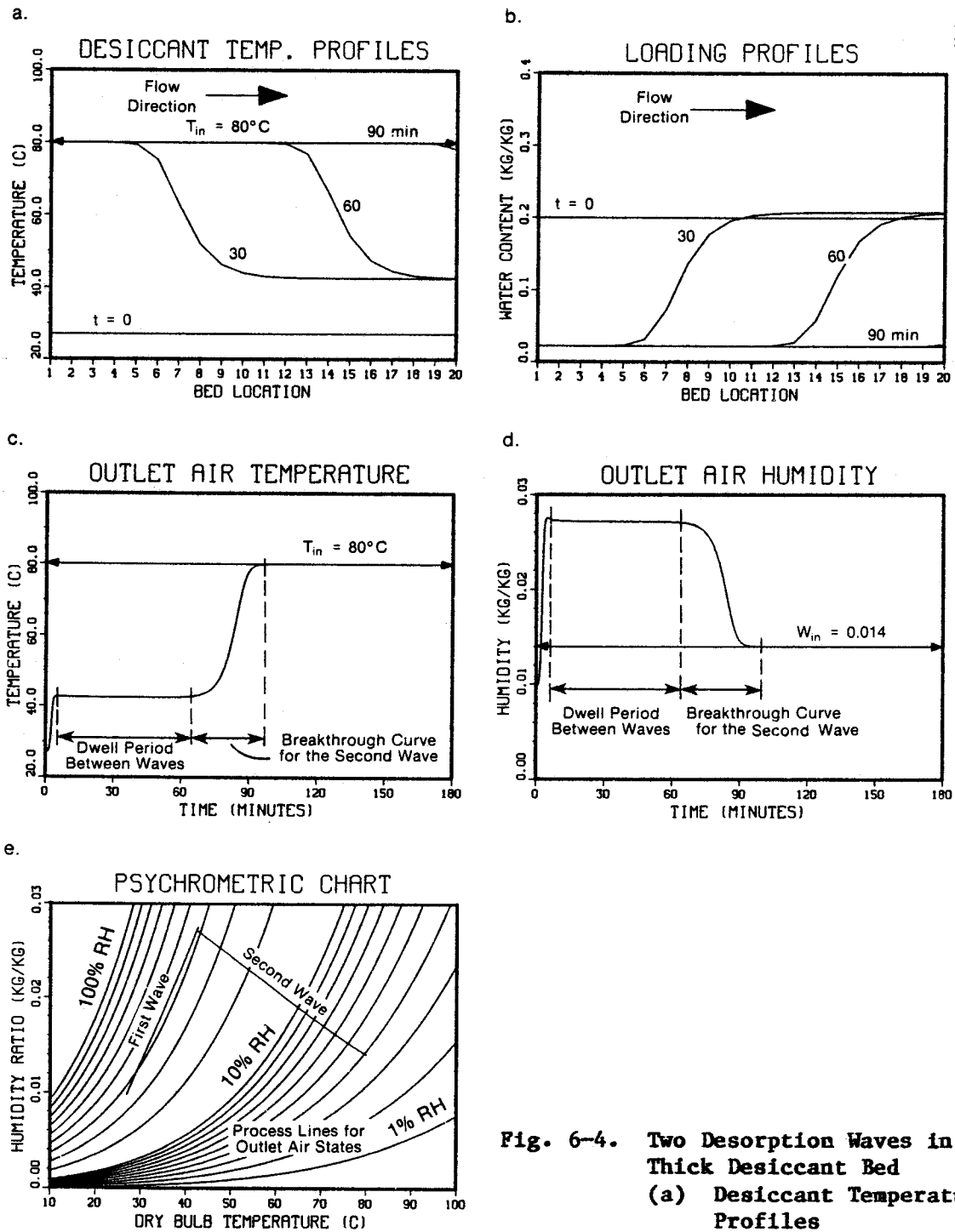


Fig. 6-4. Two Desorption Waves in a Thick Desiccant Bed
 (a) Desiccant Temperature Profiles
 (b) Desiccant Loading Profiles
 (c) Outlet Air Temperature
 (d) Outlet Air Humidity
 (e) Psychrometric Path of Outlet States

tion develops a constant shape that is much steeper than the second wave front in adsorption. This results in a longer dwell period and a steeper breakthrough curve, as illustrated in Figs. 6-4(b) and (c).

In general, the second wave is a dispersive wave during adsorption, but a self-sharpening wave during desorption. This is due to the coupling of heat and mass transfer processes and to the fact that, as the wave passes, the properties of the air/water/silica gel system change. The properties determine wave speed, so the local wave speed changes as the wave itself passes. Specifically, local wave speed is affected by the local value of the partial derivative ($\partial Y/\partial m_g$), taken along the path of the psychrometric process line. This is analogous to the specific capacity ratio for heat transfer alone. (Note that $\partial Y/\partial m_g$ taken in the direction of the second psychrometric process path is similar to γ_2 in the analogy method [26].) Local wave speed decreases as this derivative increases. As the second wave progresses through the bed during adsorption, air states at a given location move to lower temperatures and higher humidities along a process path such as that in Fig. 6-2(e). The derivative ($\partial Y/\partial m_g$) taken along that path increases as the second wave passes, causing the local wave speed to decrease. This causes spreading of the second wave during adsorption. During desorption, local air states move in the opposite direction. This derivative decreases, causing local wave speed to tend to increase as the second wave passes. The constant shape of the wave front shown in Figs. 6-4(a) and (b) is reached through a balance between this self-sharpening effect and the spreading effect of finite transfer coefficients.

6.3 BEHAVIOR OF THIN BEDS

The examples above illustrate a desiccant bed many times thicker than those used in cooling systems. Relatively thin beds must be used in desiccant cooling, because of restrictions of pressure drop and parasitic power. With thin beds the two waves are not completely distinct. The first wave does not have time to pull away from the second wave, and the effects of the two are superimposed to some extent. Figures 6-5 and 6-6 show the predicted behavior of a 0.04-m packed bed of 8-10 mesh silica gel during adsorption. Again the flow rate is 0.5 kg/m²s, and two time scales are used to focus on the two waves.

Figures 6-5(a) and (b) show that the second wave is already well into the bed by the time the first wave leaves. In fact, the leading edge of the second wave always overlaps the tail of the first wave. This is demonstrated by the fact that there is no dwell period in the graphs of outlet air states [Figs. 6-6(b) and (c)]. This superposition of wave effects is also demonstrated by the psychrometric process paths for the outlet air states [Fig. 6-6(e)]. Here there is no longer a sharp elbow at the intersection of two equilibrium process lines as in Fig. 6-2(e). Rather, the path of outlet states cuts the corner near this intersection point. This intersection point or dwell point is the driest state achievable during adsorption. Therefore, the inability of a thin desiccant bed to reach and maintain that state reduces cooling system performance from its maximum potential.

Figures 6-7 and 6-8 illustrate the behavior of the same thin bed during desorption. Because of the self-sharpening nature of the waves during desorp-

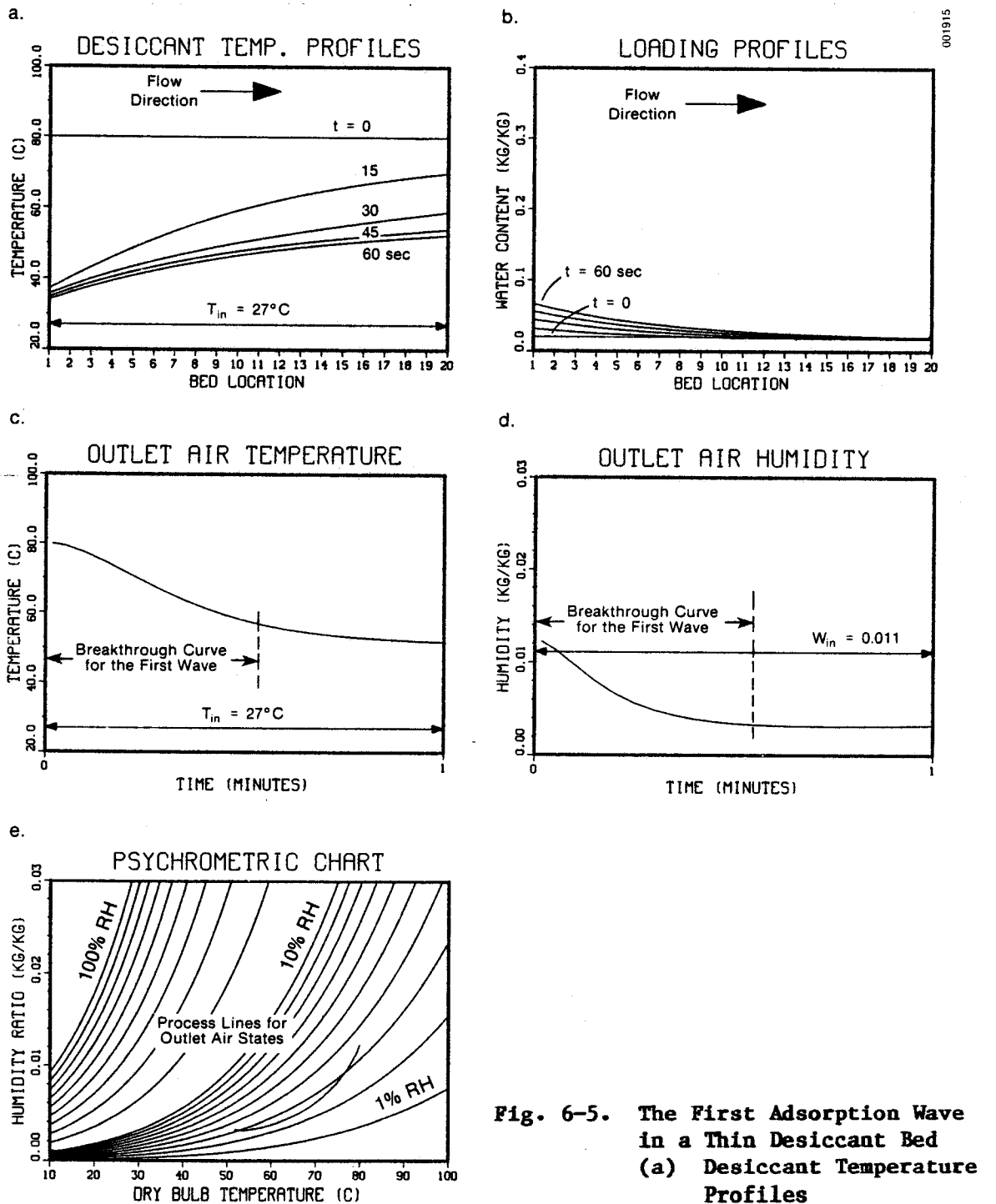


Fig. 6-5. The First Adsorption Wave in a Thin Desiccant Bed
 (a) Desiccant Temperature Profiles
 (b) Desiccant Loading Profiles
 (c) Outlet Air Temperature
 (d) Outlet Air Humidity
 (e) Psychrometric Path of Outlet States

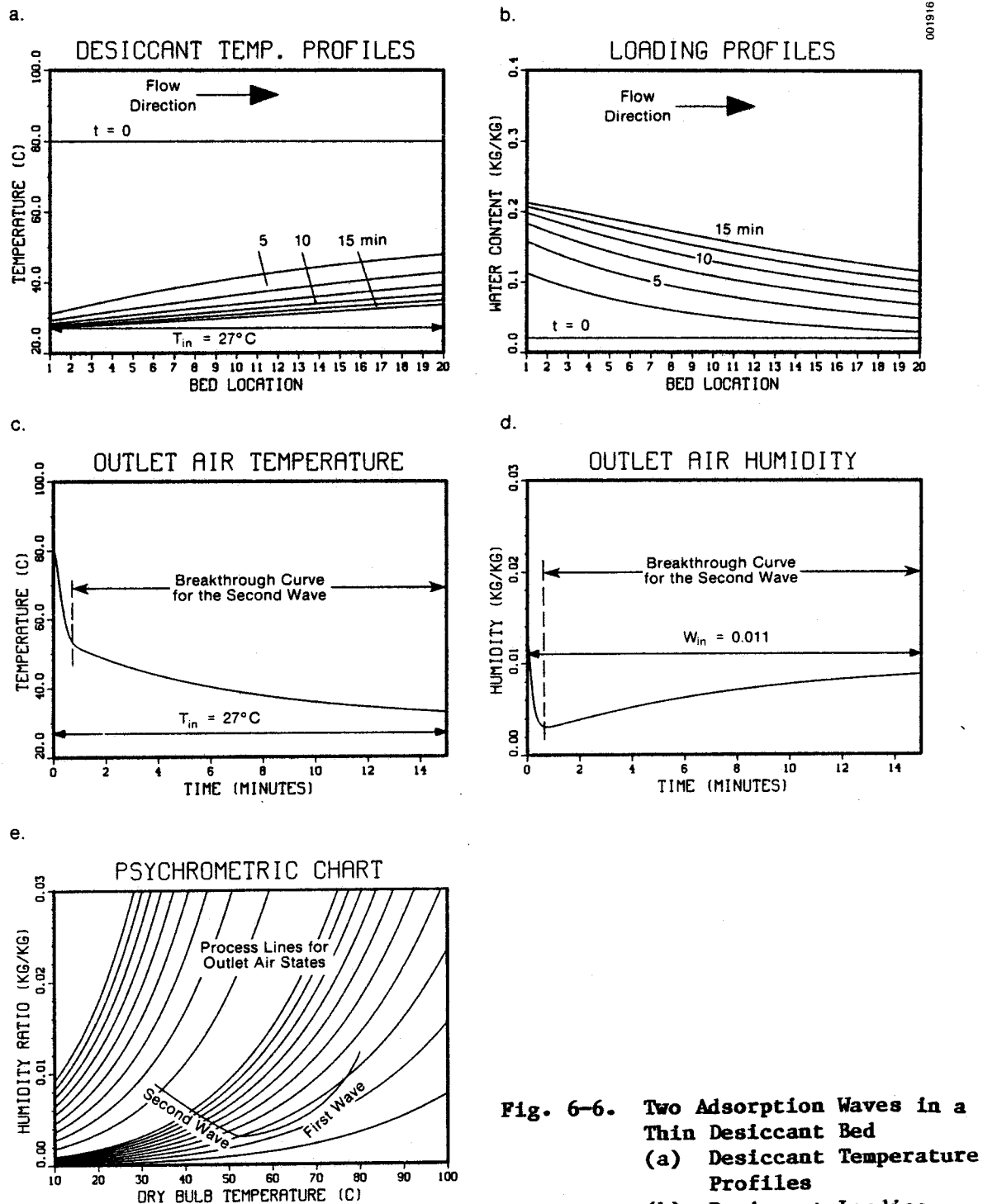


Fig. 6-6. Two Adsorption Waves in a Thin Desiccant Bed
 (a) Desiccant Temperature Profiles
 (b) Desiccant Loading Profiles
 (c) Outlet Air Temperature
 (d) Outlet Air Humidity
 (e) Psychrometric Path of Outlet States

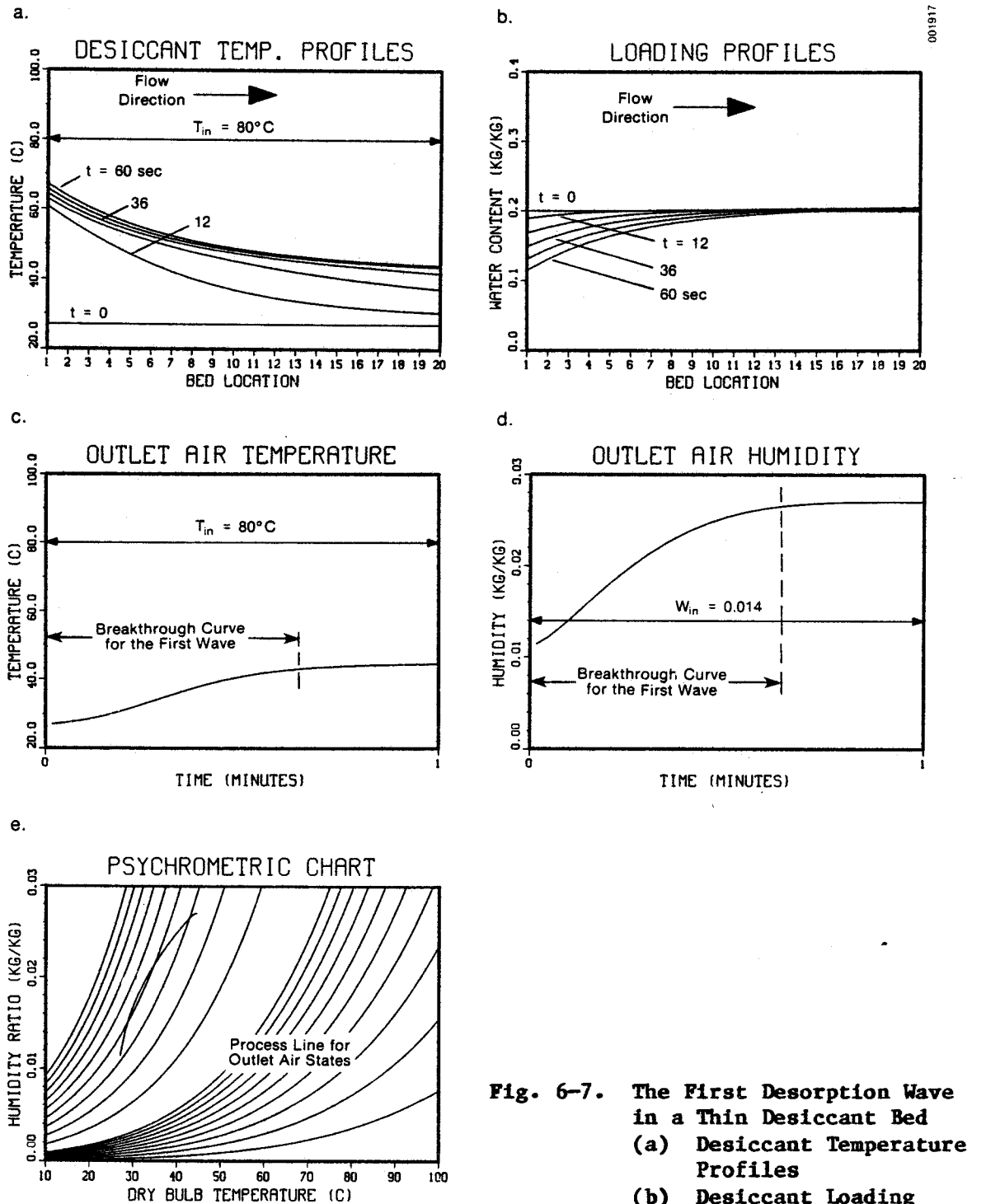
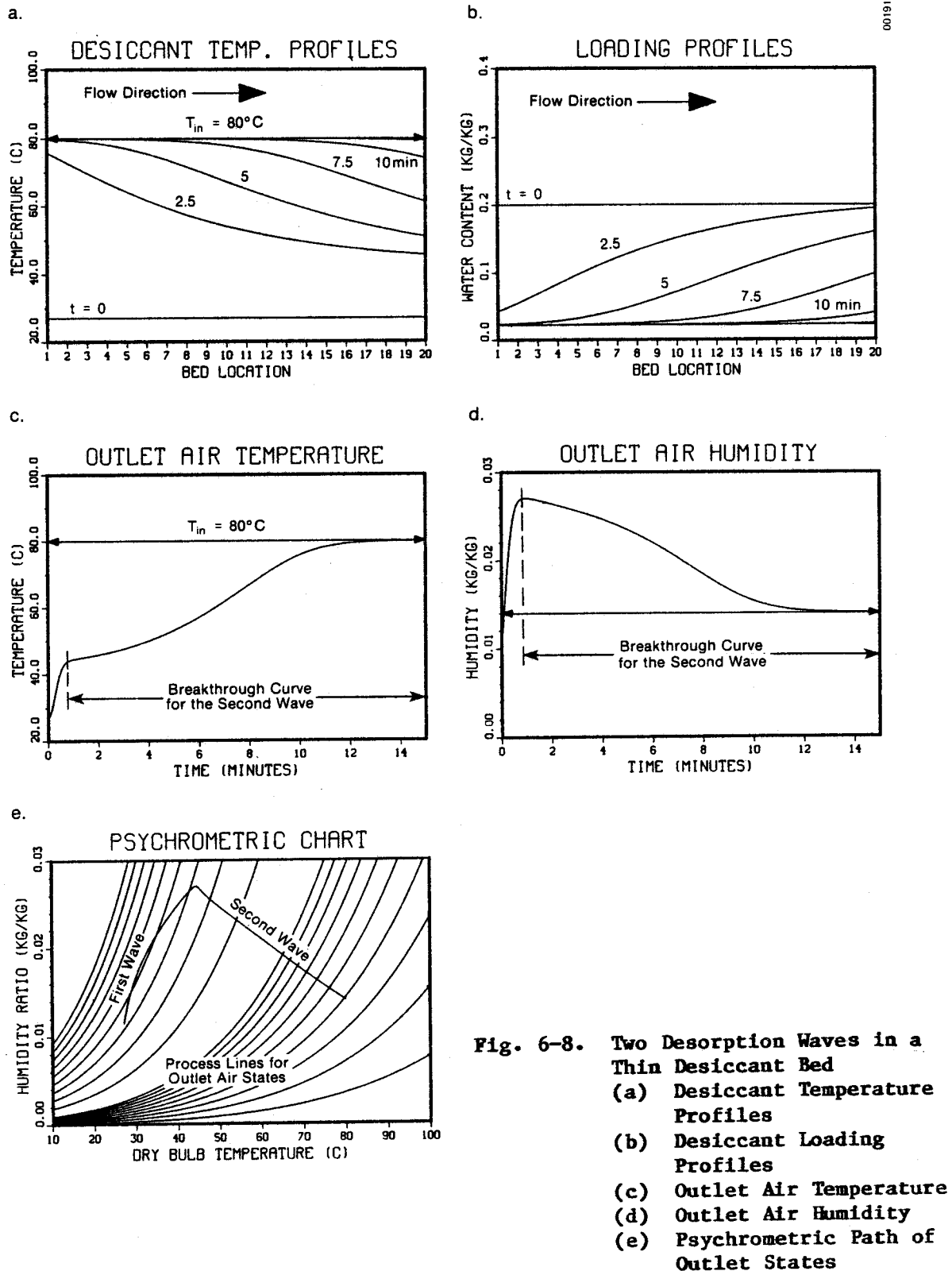


Fig. 6-7. The First Desorption Wave in a Thin Desiccant Bed
 (a) Desiccant Temperature Profiles
 (b) Desiccant Loading Profiles
 (c) Outlet Air Temperature
 (d) Outlet Air Humidity
 (e) Psychrometric Path of Outlet States



tion, slightly less overlapping of the two waves occurs [Figs. 6-7(a) and (b)]. The balance between the self-sharpening effect and the dispersive effect of finite transfer coefficients again leads to the formation of a constant pattern second desorption wave. This is shown in Figs. 6-8(a) and (b), although the effect is not as distinct as with the thicker bed. Figures 6-8(c) and (d) demonstrate that there is still no identifiable dwell period in the outlet air state, and the psychrometric process path in Fig. 6-8(e) does not quite reach the intersection point obtained in Fig. 6-4(e) with the thicker bed.

Note that during both adsorption and desorption in the thin desiccant bed, the temperature and loading profiles for both waves are relatively flat. That is, neither the first nor the second wave is at any time contained completely within the desiccant bed. This is what makes the behavior of the type of beds used in desiccant cooling very different from that of the type of beds used in most industrial adsorption applications.

6.4 BEHAVIOR DURING CYCLE OPERATION

The examples above were for single-blow adsorption or desorption where the desiccant bed exhibited uniform initial conditions of temperature and moisture content. In a cooling system, a thin bed is continuously cycled between adsorption and desorption. The behavior of a thin desiccant bed in cyclic operation is illustrated in Fig. 6-9. Here, the DESSIM system simulation program was used to model a cooling system operating in the ventilation mode between ARI standard indoor and outdoor conditions. The bed thickness and air flow rates were again taken to be 0.04 m and 0.5 kg/m²s, respectively. The overall cycle time for the desiccant wheel was set at 10 minutes. Thus, recalling Fig. 5.3, a small axial dehumidifier element spends five minutes in each stream. In cyclic operation, the best performance is obtained with counterflow operation. Thus, flow directions during absorption and desorption are opposite.

Figures 6-9(a) and (b) and 6-9(e) and (f) show the temperature and loading profiles in the desiccant at one-minute intervals during adsorption and regeneration, respectively. In each case, we see that the first wave passes completely through the bed in slightly over one minute, causing a large change in bed temperature but only a slight corresponding change in silica gel moisture content. From Figs. 6-9(b) and (f) it is clear that the average cycled capacity of the desiccant is only about 3% by weight. This is a consequence of the thinness of the bed in comparison to the second wave front. Only a part of the second wave is contained within the bed, and the front is pushed back and forth relatively little as the bed cycles between desorption and adsorption.

A significant consequence of the differences between the adsorption and desorption processes is that the second wave is not centered within the bed. Rather, it is skewed toward the adsorption inlet side. Thus, during regeneration, the desiccant near the regeneration inlet is typically dried to equilibrium with the regeneration air, but the desiccant near the adsorption inlet is still far from equilibrium with the inlet air at the end of the adsorption half-cycle. The effects of this on the outlet air states on both sides of the

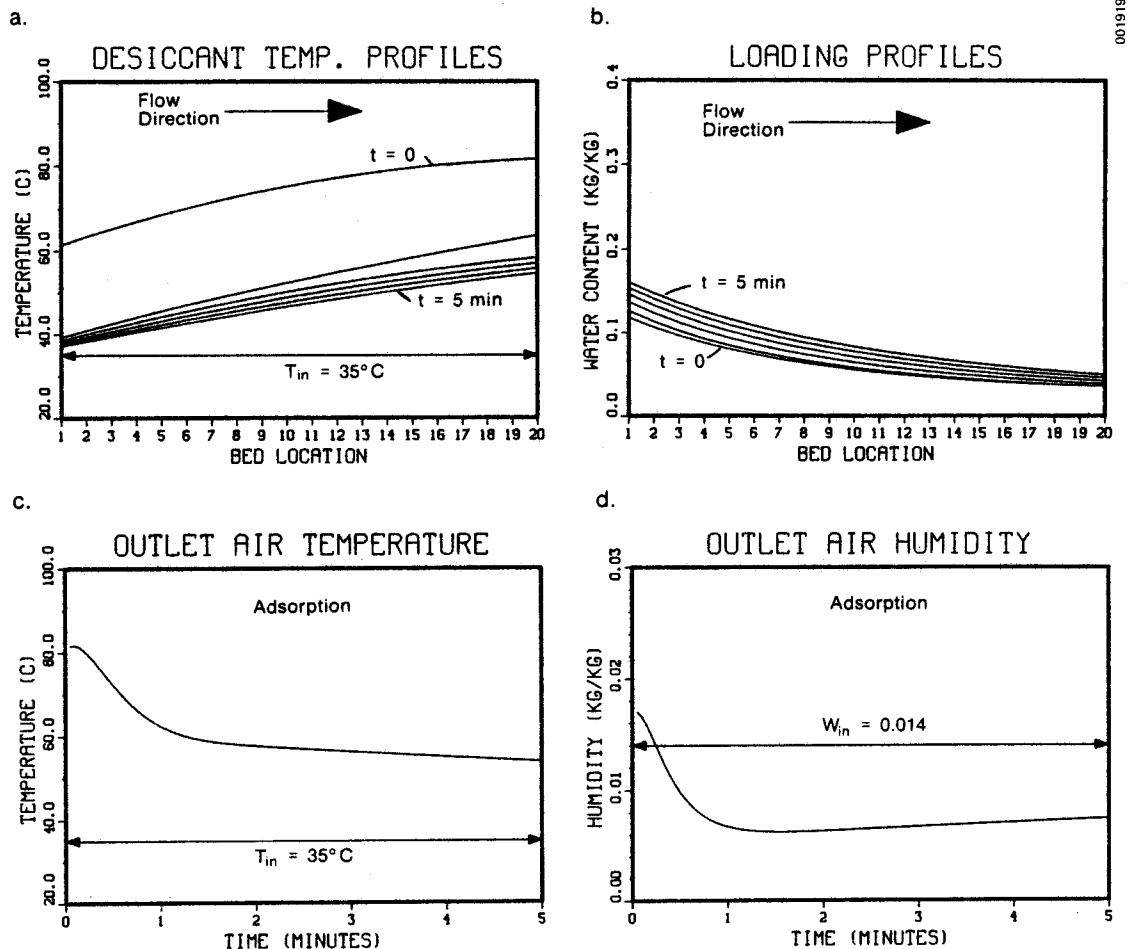


Fig. 6-9. Behavior of a Thin Desiccant Bed During Cyclic Operation

- (a) Temperature Profiles During Adsorption
- (b) Loading Profiles During Adsorption
- (c) Outlet Air Temperature During Adsorption
- (d) Outlet Air Humidity During Adsorption
- (e) Temperature Profiles During Desorption
- (f) Loading Profiles During Desorption
- (g) Outlet Air Temperature During Desorption
- (h) Outlet Air Humidity During Desorption
- (i) Psychrometric Paths of Outlet States

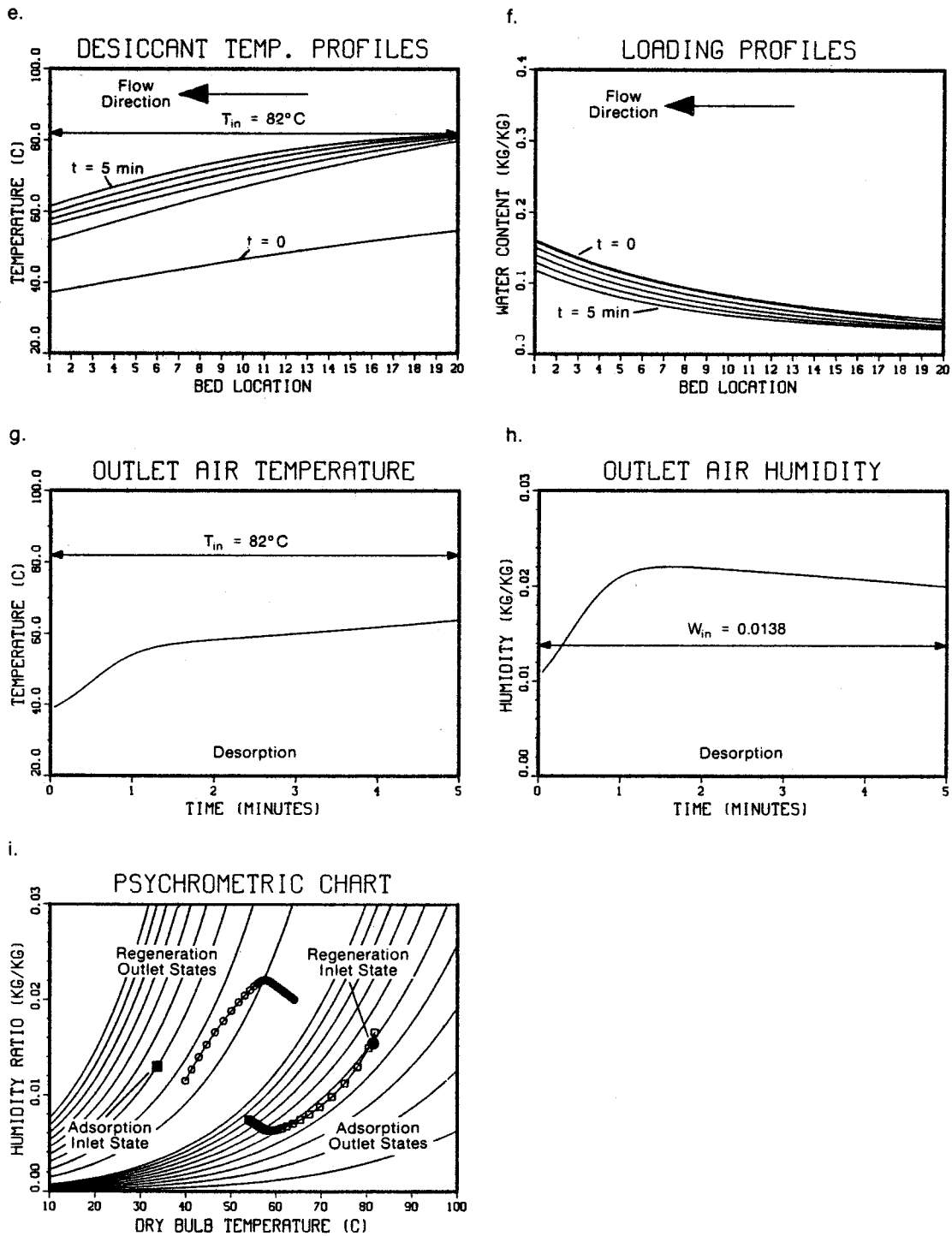


Fig. 6-9. (Concluded). Behavior of a Thin Desiccant Bed During Cyclic Operation

dehumidifier are shown in Fig. 6-9(i), the psychrometric chart. The process paths for the outlet air states during both adsorption and regeneration have been enhanced with symbols spaced at 6-second intervals. Each symbol corresponds to the steady-state outlet air state at a fixed circumferential position downstream of the dehumidifier. The inlet states for adsorption and regeneration are also shown. During adsorption the first leg of the process path begins at the regeneration inlet state because that end of the bed reached equilibrium with the inlet air during regeneration. However, during regeneration the first leg of the process path does not pass through the adsorption inlet state. Instead, it begins at a point along the trajectory of the adsorption process path that corresponds to the wettest condition reached by the desiccant during adsorption.

It is the average outlet air state during adsorption that is of greatest concern in desiccant cooling. The closer this average outlet state can be brought toward the type of intersection point or dwell state shown in Fig. 6-2(c)-(e), the higher the thermal performance of the system will be.



SECTION 7.0

PARAMETRIC STUDIES OF DESICCANT COOLING SYSTEMS

A series of parametric runs as carried out using the system simulation version of the DESSIM computer model. These parametric studies have two objectives. The first is to characterize the effect on performance of various operating parameters, including dehumidifier wheel speed, outdoor conditions, indoor conditions, and regeneration temperature. The second is to provide information for an initial assessment of the potential benefits in system performance that could be achieved through development of advanced components with higher effectivenesses than have been measured to date in desiccant cooling prototypes. Performance is measured by the thermal COP as defined by Eq. 5-10 and the cooling capacity per unit mass of conditioned air, which is equal to the enthalpy difference between the room air and the conditioned air.

7.1 EFFECT OF SIMULATION PARAMETERS IN THE DEHUMIDIFIER MODEL

With any finite-difference computational method, the choice of time and space increments is important and often represents a compromise between accuracy and computational efficiency. Figure 7-1 shows the effect of changing the simulation time step on the thermal COP of the base case system described in Sec. 7.2, operating in the ventilation mode. The spacial increment is also varied as a parameter. The predicted COP decreases as the time increment is decreased for a given number of bed sections. However, the predicted COP increases as the spatial increment is decreased (number of sections is increased) for a given time step. This conveniently allows us to use moderate time and space increments and still obtain predicted results quite close to the value that the method would converge to with very small time and space increments. Based on this result, all the remaining parametric studies were performed using 10 bed sections and a time step of two seconds.

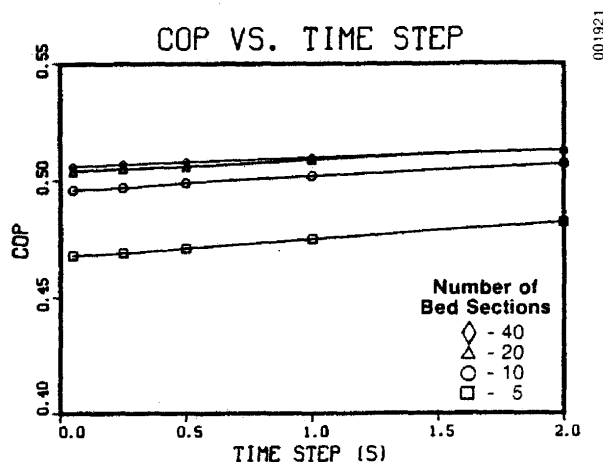


Fig. 7-1. Predicted COP vs. Simulation Time Step

The effects on predicted performance of using different equilibrium correlations and different values for the effective Lewis number for regeneration are also of interest. Figures 7-2(a) and (b) show the effect of regeneration Lewis number on system COP and capacity, respectively. Both quantities drop as the regeneration Lewis number increases, but not as quickly as one might expect with this large change in the mass transfer coefficient. Each is only decreased by about 12% as the mass transfer coefficient during regeneration decreases by a factor of three. Because there is still some uncertainty as to the applicability of a high desorption Lewis number to the case of a rapidly cycling dehumidifier, a Lewis number of 3 is used in these parametric studies. This is consistent with the recommendations of van Leersum [47].

In Fig. 7-2, ICORR indicates which of the three equilibrium correlations described in Sec. 3.7 was used in the simulation. There is little difference between predictions using the Bullock and Threlkeld correlation (ICORR = 1) and the Close and Banks modified correlation (ICORR = 2). This is to be expected, since both correlations are based on the same data. The correlation based on the Rojas data (ICORR = 3) leads to somewhat poorer predicted performance. COP is lower by about 8% and capacity is lower by about 4%. Given that the first two correlations represent an available silica gel and that the modified Close and Banks correlation is simpler, the Close and Banks correlation was used in the remaining studies.

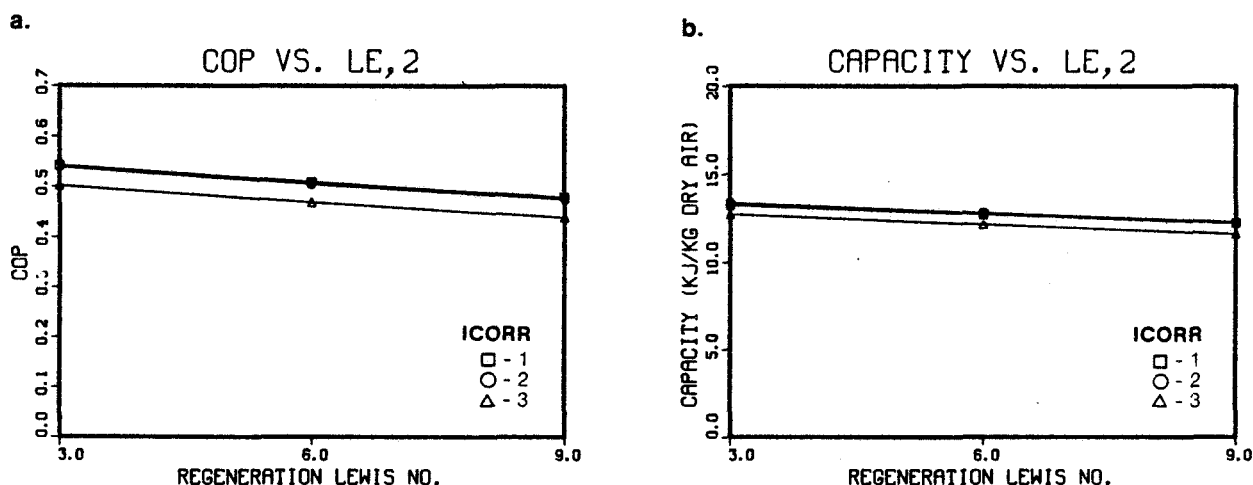


Fig. 7-2 (a) COP vs. Regeneration Lewis Number
(b) Capacity vs. Regeneration Lewis Number

7.2 SYSTEM SPECIFICATIONS

The general system configuration that the DESSIM program models was described in Sec. 5.1. For these parametric studies, two specific systems were considered. The first contains components that are representative of those found in existing prototype systems, and this system performs similarly to the tested prototypes. The second is a higher performance system containing components with performance levels that have not yet been obtained in desiccant cooling prototypes. Simulation of this system gives an indication of the potential gains in thermal performance that could be achieved through improved component design. The second system is not an optimized design, and there is no special significance to its component specifications other than that they have a higher effectiveness. In particular, the dehumidifier is assumed to be a packed bed, whereas it is probable that laminar-flow, parallel-passage designs will prove to be more appropriate for high effectiveness dehumidifiers.

An important parameter that must be optimized for each system is the rotation speed of the desiccant wheel. Figures 7-3(a) and (b) show COP and capacity versus half-cycle time for desiccant beds 3 cm to 7 cm thick in a ventilation system having 90% effective evaporative coolers and heat exchanger and operating at ARI standard conditions with an 80°C regeneration temperature. Each curve displays a broad optimum. Optimum COP and capacity increase as the thickness of the bed increases. The optimum half-cycle time also increases with bed thickness. For a given bed thickness, the half-cycle time giving the highest capacity is longer than that giving the highest COP. For example, with the 4 cm bed, COP peaks between 4 and 5 minutes, while capacity peaks between 5 and 6 minutes.

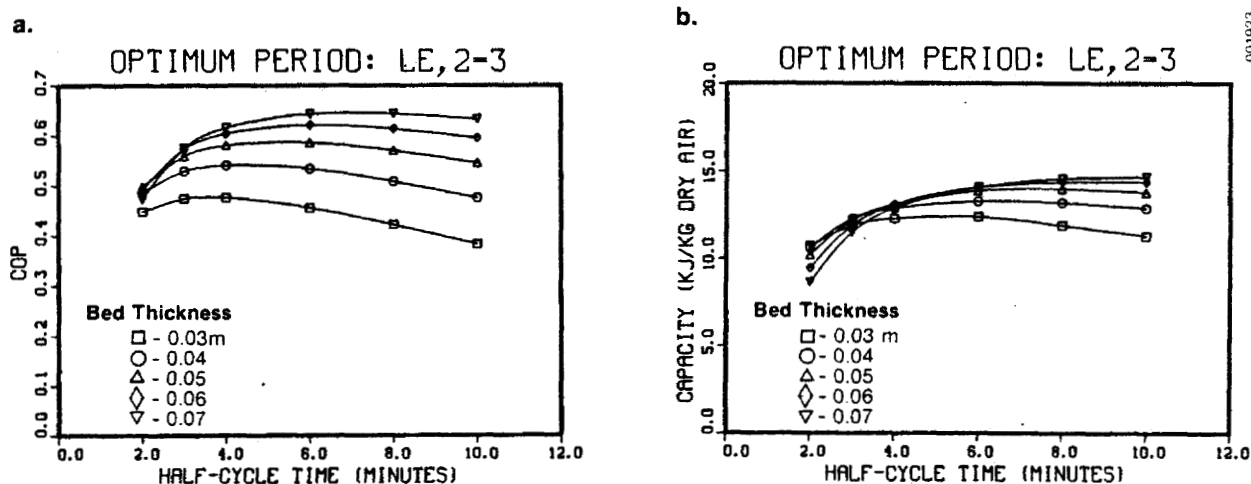


Fig. 7-3 (a) COP vs. Half-Cycle Time
(b) Capacity vs. Half-Cycle Time

The specifications of the base system and the high-performance system are summarized in Table 7-1, and nominal operating conditions are given in Table 7-2. The sections that follow present results of parametric studies of these systems. These studies cover the effects on performance of outdoor conditions, indoor conditions, regeneration temperature, heat exchanger effectiveness, and evaporative cooler effectiveness.

7.3 EFFECT OF OUTDOOR CONDITIONS

Characterization of the performance of a desiccant cooling system is complicated by the fact that performance is sensitive to operating conditions of humidity as well as temperature. In this parametric study, the outdoor conditions were varied while other conditions were held constant. Outdoor temperatures from 27.5°C to 40°C (81.5°F to 104°F) and outdoor humidity ratios from

Table 7-1. System Specifications for Parametric Studies

	Base System	High-Performance System
Dehumidifier wheel (Packed silica gel):		
Thickness	0.04 m	0.10 m
Particle diameter	0.00193 m	0.00193 m
Bed density	740 kg/m ³	740 kg/m ³
Specific heat	921 J/kg°C	921 J/kg°C
Surface area	1335 m ² /m ³	1335 m ² /m ³
Air flow rate	0.5 kg/m ² s	0.5 kg/m ² s
Half-cycle time	5 min	10 min
Lewis number	3	3
Heat exchanger effectiveness	0.9	0.95
Effectiveness of evaporative cooler 1	0.9	0.95

Table 7-2. Nominal Operating Environment for Parametric Studies

	Temperature	Humidity Ratio (kg/kg)
Indoor conditions (ARI standard):	26.7°C (80°F)	0.0111
Outdoor conditions (ARI standard):	35.0°C (95°F)	0.014
Regeneration:	80°C (176°F)	

0.008 kg/kg to 0.017 kg/kg were used. Each system was operated in both ventilation and recirculation modes. Figures 7-4(a),(b),(c), and (d) show the effect of outdoor conditions on the performance of the base-case system. Figures 7-4(b) and (d) demonstrate that in the recirculation mode, both COP and capacity are linearly dependent on outdoor temperature and nearly linearly dependent on outdoor humidity. In the recirculation mode, COP and capacity decrease as outdoor temperature and humidity increase. Figures 7-4(a) and (c) demonstrate that in the ventilation mode the ambient temperature dependence of system performance is again nearly linear. However, particularly with COP, the slope of the line changes with the humidity ratio, so that at low humidities, COP increases slightly with increases in temperature. Figure 7-4(c) also demonstrates that the base-case system is much more sensitive to outdoor humidity in the ventilation mode than in the recirculation mode.

Figure 7-5 shows the effect of outdoor conditions on the high performance system. As one would expect, performance levels, particularly COP, are higher than for the base system. The most interesting result is that, with high effectiveness components, the ventilation mode exhibits better performance than the recirculation mode. The opposite is often true with the base system. In particular, the COP of the high-performance system in the ventilation mode is relatively insensitive to both outdoor temperature and humidity. Capacity in the ventilation mode also becomes less sensitive to outdoor conditions when the component effectivenesses are increased.

7.4 EFFECT OF INDOOR CONDITIONS

In this study, indoor conditions were varied while other conditions were held constant. Indoor temperatures from 23°C to 29°C (73°F to 84°F) and indoor humidities from 0.008 to 0.012 were used. Each system was again simulated in ventilation and recirculation modes. Figure 7-6 shows the effect of indoor conditions on the performance of the base system. All four graphs in Figure 7-6 demonstrate a linear dependence of COP and capacity on indoor temperature and humidity, with both quantities increasing with increasing indoor temperature and humidity. With the base system, performance in the ventilation mode is slightly more sensitive to changes in indoor conditions than performance in the recirculation mode. Under the specified operating conditions, COPs are higher in the ventilation mode but capacities are higher in the recirculation mode.

Figure 7-7 shows the effect of indoor conditions on COP and on the capacity of the high-performance system. Again, both COP and capacity are linearly dependent on indoor temperature and humidity. As one would expect, increasing component effectiveness has the effect of moving all the performance curves up. However, as was observed in the parametric study on the effect of outdoor conditions, the ventilation mode benefits more from increased component effectiveness than does the recirculation mode. Figures 7-7(a) and (b) demonstrate that, under the other nominal operating conditions listed in Table 7-2, the COPs in the ventilation mode are considerably higher than those in the recirculation mode. Figures 7-7(c) and (b) demonstrate that capacities are also higher in the ventilation mode.

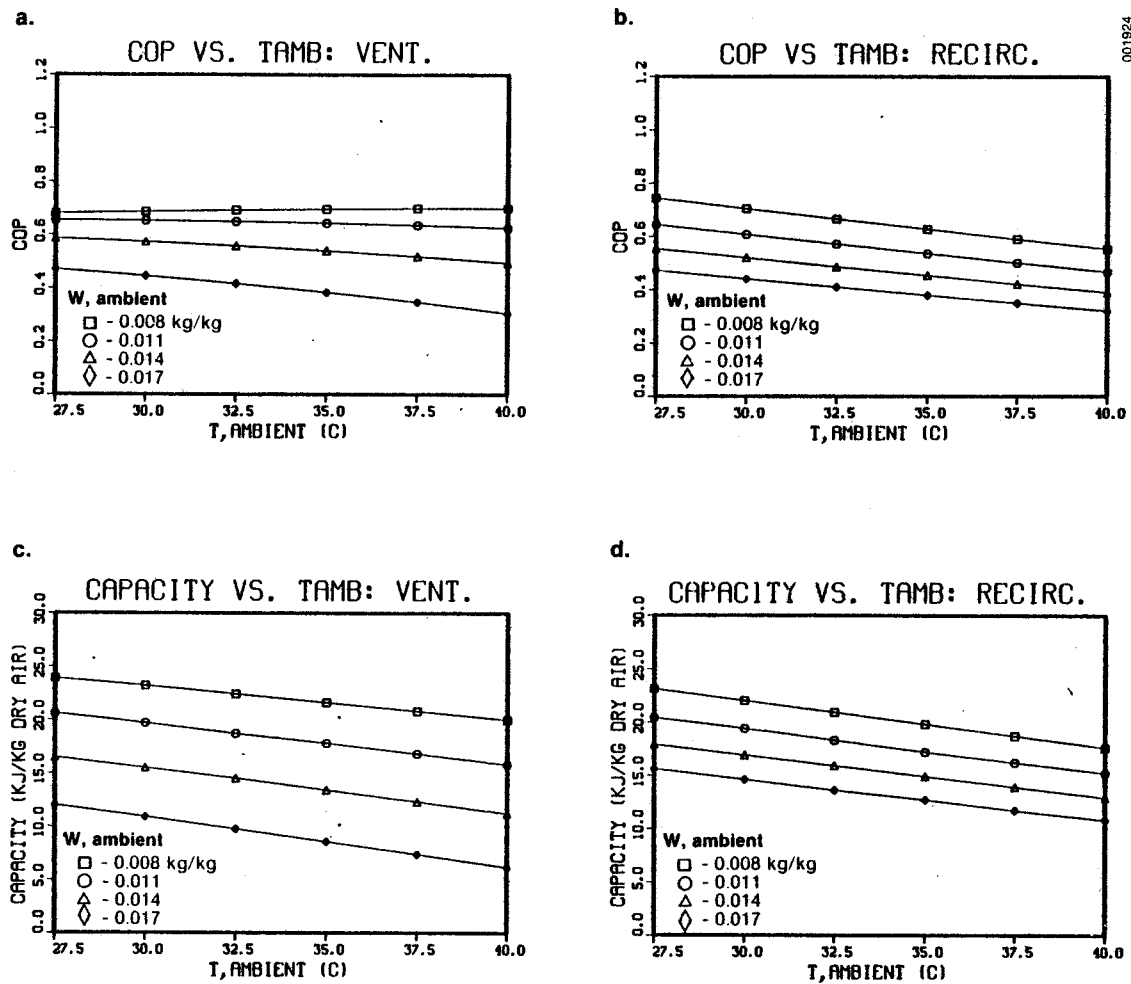


Fig. 7-4. Effect of Outdoor Conditions on Performance of the Base System: (a) COP vs T_{ambient} in Ventilation Mode. (b) COP vs. T_{ambient} in Recirculation Mode. (c) Capacity vs. T_{ambient} in Ventilation mode. (d) Capacity vs. T_{ambient} in Recirculation Mode.

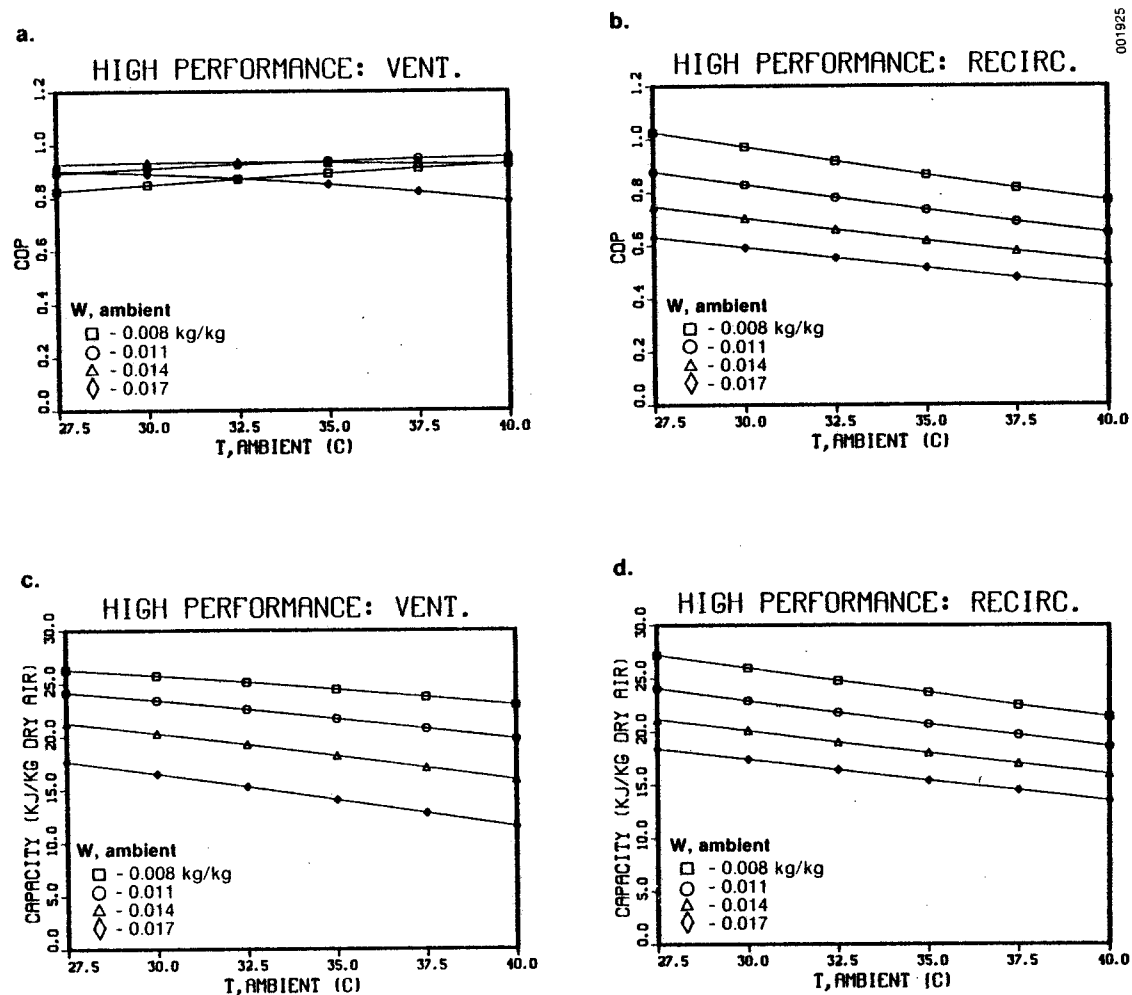


Fig. 7-5. Effect of Outdoor Conditions on Performance of the High Performance System: (a) COP vs. T_{ambient} in Ventilation Mode. (b) COP vs. T_{ambient} in Recirculation Mode. (c) Capacity vs. T_{ambient} in Ventilation Mode. (d) Capacity vs. T_{ambient} in Recirculation Mode.

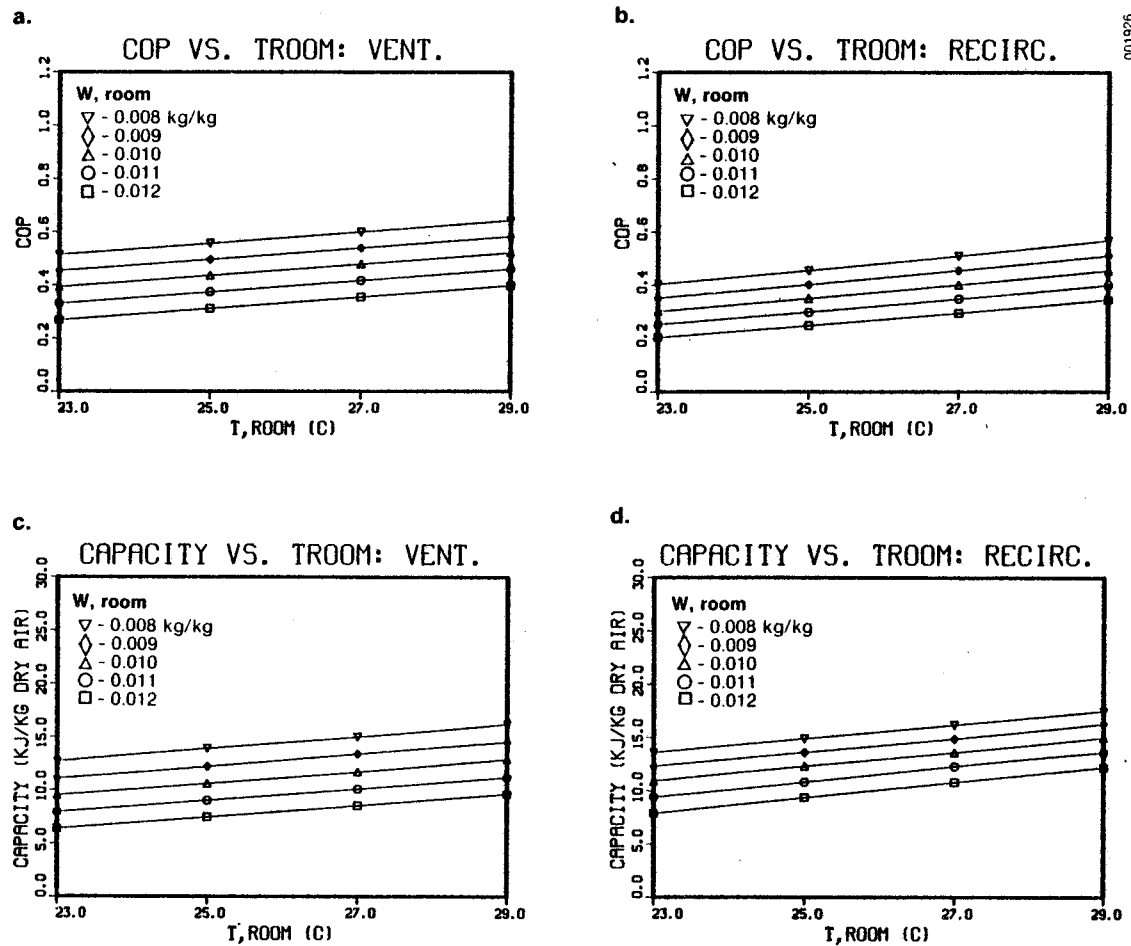


Fig. 7-6. Effect of Indoor Conditions on Performance of the Base System: (a) COP vs. T_{room} in Ventilation Mode. (b) COP vs. T_{room} in Recirculation Mode. (c) Capacity vs. T_{room} in Ventilation Mode. (d) Capacity vs. T_{room} in Recirculation Mode.

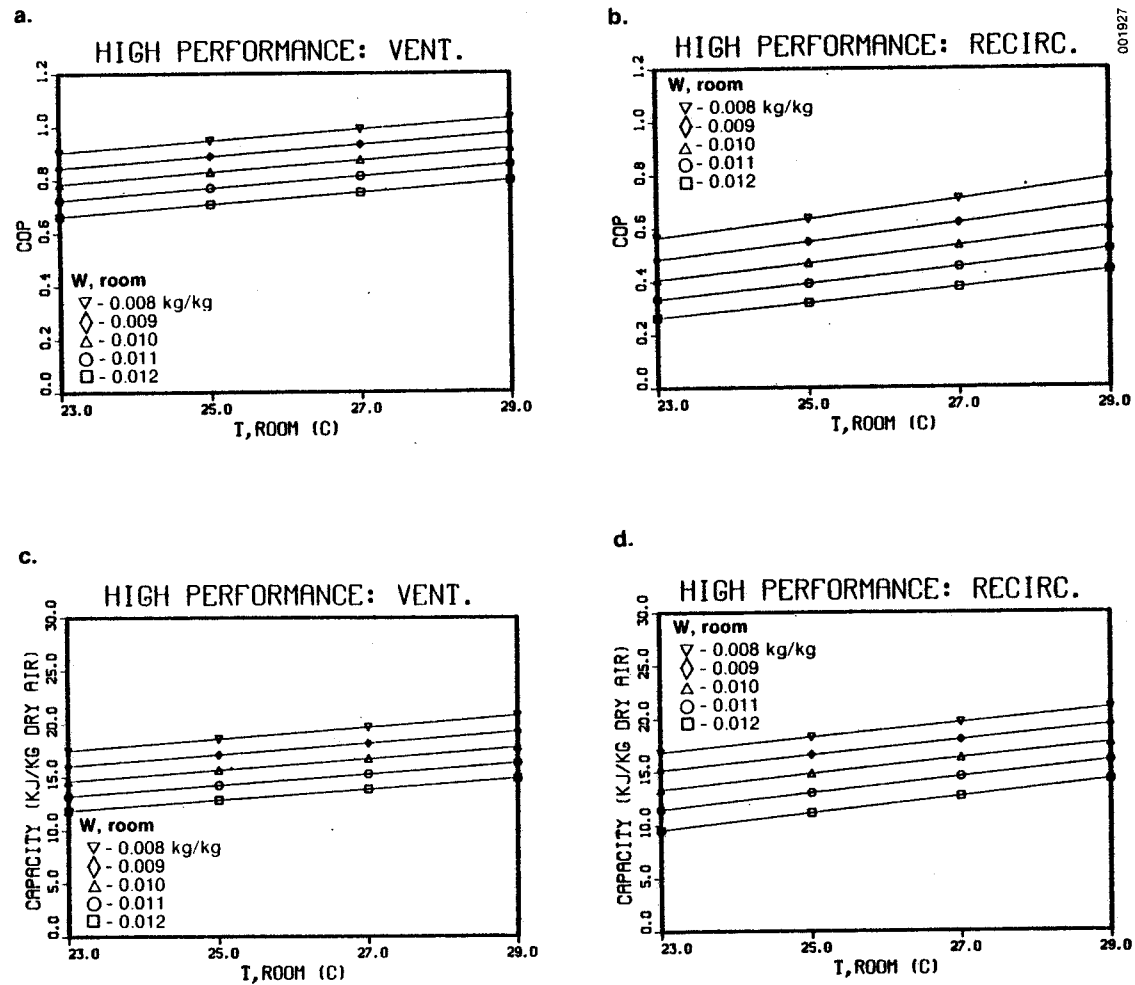


Fig. 7-7. Effect of Indoor Conditions on Performance of the High Performance System: (a) COP vs. T_{room} in Ventilation Mode. (b) COP vs. T_{room} in Recirculation Mode. (c) Capacity vs. T_{room} in Ventilation Mode. (d) Capacity vs. T_{room} in Recirculation Mode.

7.5 EFFECT OF REGENERATION TEMPERATURE

Figures 7-8(a) and (b) show the effect of regeneration temperature on COP and capacity, respectively, for both systems operating in both modes. With the base system, COP reaches a broad maxima between regeneration temperatures of 70°C and 80°C. With the high-performance system, this maxima shifts toward lower regeneration temperatures, which offers the potential benefit of allowing solar collectors to operate at lower, more efficient temperatures. As an example of the magnitude of potential performance gains, compare performance in the ventilation mode of the base system operating at an 80°C regeneration temperature with that of the high-performance system operating at a 60°C regeneration temperature. The cooling capacities are similar, but the COP is roughly doubled through the use of high-effectiveness components. With both systems, capacity increases monotonically with increases in regeneration temperature. Again, both figures demonstrate that the ventilation mode benefits more from increased component effectiveness than does the recirculation mode.

7.6 EFFECT OF HEAT EXCHANGER EFFECTIVENESS

Measured heat exchanger effectivenesses reported by the developers of desiccant cooling prototype systems range from 0.89 to 0.93, and values up to 0.95 have been proposed. Figures 7-9(a) and (b) show the effect of heat exchanger effectiveness on COP and capacity, respectively, for both systems operating in both modes. As one would expect, performance increases monotonically with increasing heat exchanger effectiveness. Again, it is clear that the ventilation mode benefits more than the recirculation mode from increased component effectiveness.

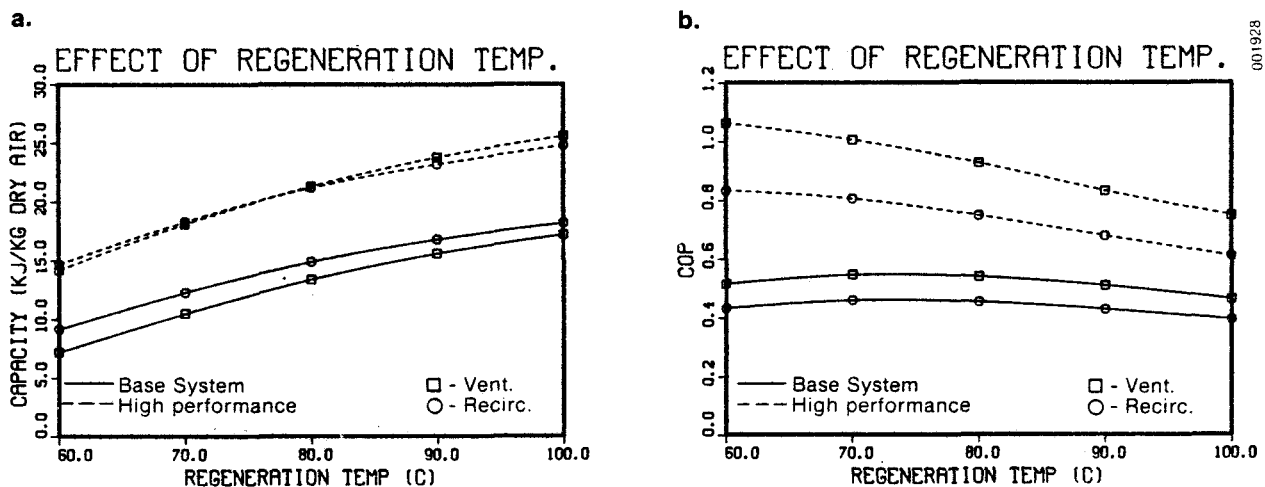


Fig. 7-8. (a) Effect of Regeneration Temperature on COP
(b) Effect of Regeneration Temperature on Capacity

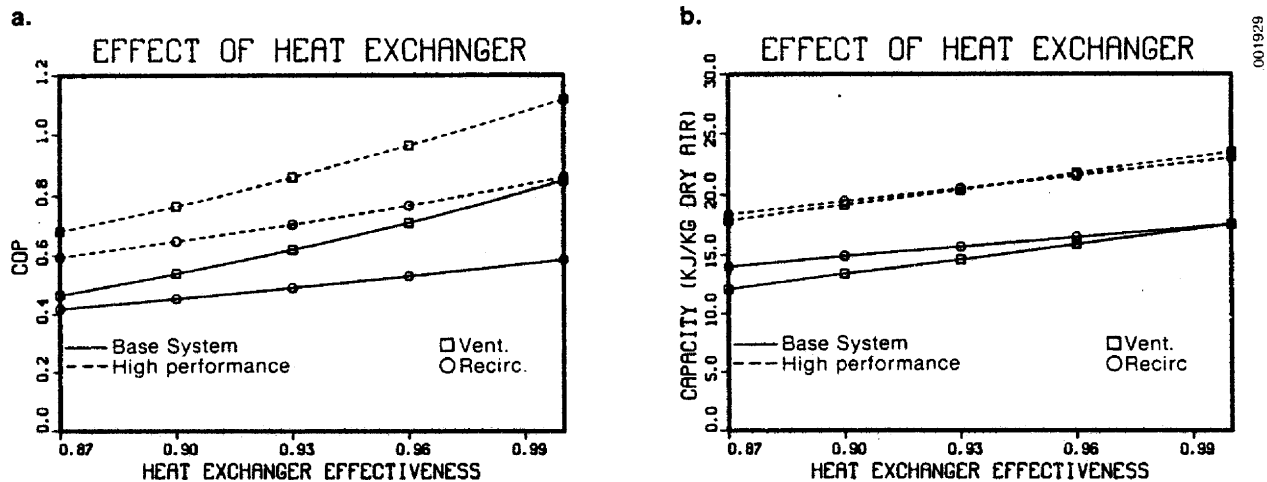


Fig. 7-9. (a) Effect of Heat Exchanger Effectiveness on COP
(b) Effect of Heat Exchanger Effectiveness on Capacity

7.7 EFFECT OF EVAPORATIVE COOLER 1

The evaporative cooler at the inlet of the regeneration side of the system provides a cold sink for the cooling cycle which defines the coldest temperature that can be achieved by the conditioned air leaving the heat exchanger. One would expect the performance of the system to improve as this cold sink temperature decreases. Thus, one would expect increasing performance with increasing effectiveness of evaporative cooler 1. Figure 7-10 shows the effect of the effectiveness of this evaporative cooler on the performance of the base system. Both COP and capacity increase as effectiveness increases. However, the magnitude of these increases is small. Evaporative coolers in the prototype system already operate in the 0.8 to 0.9 effectiveness range, and little improvement in system performance would be gained by improving this component.

7.8 SUMMARY OF PARAMETRIC STUDIES

This set of parametric studies had two objectives: to investigate the behavior of desiccant systems under various operating conditions, and to study the effect of improving individual components on overall system performance. A part of this second objective was to provide information for an initial assessment of the potential for improving desiccant system performance through developing advanced, high-effectiveness components.

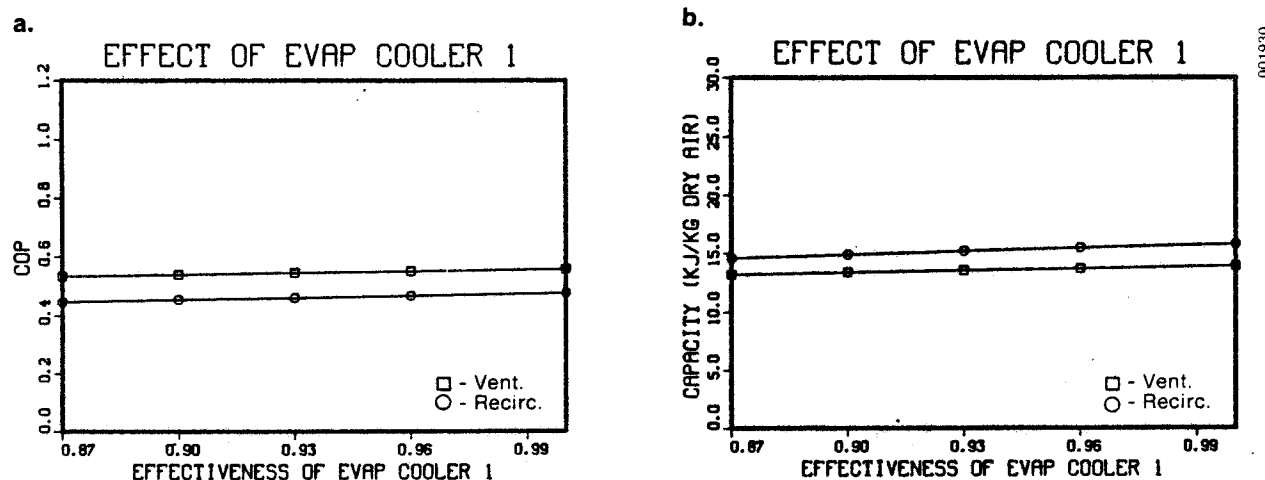


Fig. 7-10. Effect of the Effectiveness of Evaporative Cooler 1 on Performance of the Base System
 (a) COP
 (b) Capacity

With regard to the general operating behavior of the desiccant systems modeled here, COP and capacity both decrease as the temperature and humidity differences between indoor and outdoor conditions increase, as we might expect. An interesting result is that in most cases there is a linear dependence between performance and the indoor or outdoor conditions. This simplifies the process of developing equations describing performance maps that can be used in seasonal simulations of desiccant system performance.

With regard to the benefits of developing high-performance components, several important results have come from the parametric studies. First, the major components in terms of performance are the heat exchanger and the dehumidifier. The effectiveness of both these components must be high to achieve high system performance. The studies indicate, however, that there is more to be gained by increasing dehumidifier performance from levels typical of existing prototypes. Referring to Fig. 7-9, an increase in heat exchanger effectiveness from 0.9 to 0.95, which is probably the reasonable upper limit, does not produce as large an increase in performance as using a thicker, more effective desiccant bed. This underscores the importance of research into high-performance, low-pressure-drop dehumidifier concepts.

The second important result is that the ventilation mode is clearly superior to the recirculation mode when high-effectiveness components are used. The ventilation mode is more compatible with low-infiltration construction and energy conservation methods.

The third result is that using high-effectiveness components allows the system to be operated at lower regeneration temperatures. This in turn permits the solar collector system to operate at lower, more efficient temperatures.



SECTION 8.0

CONCLUSIONS AND RECOMMENDATIONS

8.1 CONCLUSIONS REGARDING THE PSEUDO-STEADY-STATE MODEL

- A computer model for the simulation of coupled heat and mass transfer in adiabatic desiccant beds has been developed.
- This computer model uses a new approach in that simple effectiveness equations for steady-state heat and mass exchangers are used within a finite difference procedure. This simplifies the mathematics of the adsorption analysis, making the model easy to adapt to investigate a variety of adsorption problems.
- The model has been validated through comparison with experimental data for packed beds of silica gel from SERI's Desiccant Test Laboratory and from other sources.
- Agreement between measured and predicted results during adiabatic adsorption is well within the uncertainty in measured values. This demonstrates that the use of a lumped, gas-side resistance to mass transfer is adequate for adsorption modeling. The lumped gas-side mass transfer coefficient can be obtained from heat transfer correlations and an effective Lewis number that can be estimated on the basis of theory or determined experimentally for a given dehumidifier geometry. For typical packed-bed adsorption situations, an effective Lewis number of about 3.0 is appropriate.
- In cases of single-blow desorption, agreement between measured and predicted results is not obtained unless the effective Lewis number is increased substantially (by a factor of 3) from that used in adsorption. This discrepancy cannot be explained in terms of a simple diffusion model within the desiccant particles. It appears to be caused by a dynamic hysteresis in the adsorption/desorption characteristics of silica gel.
- Effective mass transfer coefficients for desorption can be determined through experiments, but further work would be necessary to determine a general method of predicting useful desorption coefficients for packed beds, particularly for rapid cycling situations.
- Three correlations for the equilibrium properties of silica gel and two correlations for the heat of adsorption were compared. Relatively small differences in predictions using the different correlations were observed. Of these three, the Close and Banks correlation, as simplified in this report (ICORR = 2), is recommended for future studies on regular-density silica gel.
- The pseudo-steady-state model was used to generate a series of graphs that illustrate the physical behavior of desiccant beds in single-blow cases and in cyclic operation. This series of graphs facilitates a clearer understanding of the adsorption process and the desiccant cooling cycle.

8.2 CONCLUSIONS REGARDING COOLING SYSTEM PERFORMANCE

- The pseudo-steady-state adsorption/desorption model was incorporated into a computer program simulating a complete desiccant cooling system.
- Parametric studies were carried out to characterize the effects of operating environment on system COP and cooling capacity, and to provide information for an initial assessment of the potential benefits of advanced, high-effectiveness components.
- These studies demonstrate that the thermal performance of desiccant cooling systems can be significantly increased from levels obtained by existing prototypes. A doubling of performance to the target of 1.0 to 1.2 COP is technically feasible. The practicality of such an increase considering the restrictions on equipment size and parasitic power remains to be assessed.
- The ventilation mode benefits more from increases in component effectiveness than does the recirculation mode, and the ventilation mode is clearly superior to the recirculation mode in a high-performance system.
- The dehumidifier and the sensible heat exchanger are the two components that are critical to thermal performance. Heat exchangers with an effectiveness ranging from 0.93 to 0.95 should be considered. The state of technology in dehumidifiers is not as advanced as that in sensible heat exchangers, and the greatest potential for improving system performance appears to be in the development of advanced, high-effectiveness, low-pressure-drop dehumidifiers.
- The thermal performance of a desiccant cooling system varies with indoor and outdoor temperature and humidity. Generally, performance degrades as the difference between indoor and outdoor conditions becomes greater. A significant exception to this is that the thermal COP of a high-performance system in the ventilation mode is relatively insensitive to outdoor conditions.
- The parasitic power consumption of various systems was not considered in this report, because it is anticipated that packed desiccant beds will not be appropriate for high-effectiveness dehumidifiers. Although not addressed in this report, parallel-passage dehumidifiers based on existing heat exchanger technology are expected to demonstrate superiority over packed-bed designs for a given pressure drop.

8.3 RECOMMENDATIONS

The pseudo-steady-state model should be used to evaluate the potential performance of spiral-wound, parallel-passage dehumidifiers based on Australian heat exchanger technology. Other low-pressure-drop geometries that seem promising can also be assessed. Work at UCLA has indicated that, with the small particles that would be used in parallel passages, the solid-side resistance to mass transfer is small. Thus, a Lewis number near one would be appropriate for both adsorption and desorption. This would eliminate the uncertainty regarding appropriate transfer coefficients for desorption in packed beds.

Future evaluations of advanced dehumidifiers should include detailed considerations of parasitic power and system size. This work has been proposed for completion at SERI during FY 1982.

The pseudo-steady-state model can be applied to a variety of adsorption problems. In particular, it can be used to assess concepts for dehumidification of passively cooled buildings.



REFERENCES

1. Löf, G. O. G. "House Heating and Cooling with Solar Energy." Solar Energy Research. Madison: University of Wisconsin Press. 1955.
2. Dunkle, R. V. "A Method of Solar Air Conditioning." Inst. Engr. Aust. Mech. and Chem. Trans. MCI 1; 1965.
3. Lunde, P. J. Preliminary Design of a Solar-Powered Desiccant Air Conditioning for USERDA. Hartford, CT: The Center for the Environment and Man. 1976.
4. Nelson, J. S. "An Investigation of Solar-Powered Open Cycle Air Conditioners." M. S. Thesis. Madison: University of Wisconsin. 1976.
5. Wurm, Kinast, Rush, Zawacki, Macriss. Solar-MEC® Development Program--Annual Progress Report. Institute of Gas Technology COO-4495-15. 1979 (October).
6. Rousseau, J. Development of a Solar Desiccant Dehumidifier: Phase II Technical Progress Report. AiResearch Manufacturing Co. 81-17773. 1981 (March).
7. Lavan, Z.; Worek, V.; Monnier, J. "Cooled Bed Solar-Powered Air Conditioning." 16th IECEC. Atlanta, GA. 1981 (August).
8. Booz-Allen & Hamilton. Evaluation of Residential and Commercial Solar/Gas Heating and Cooling Technologies. Gas Research Institute GRI-79/0105. 1981.
9. Hougen, O. A.; Marshall, W. R. "Adsorption from a Fluid Stream Flowing Through a Stationary Granular Bed." Chemical Engineering Progress. Vol. 43 (No. 4); pp. 197-208. 1947 (April).
10. Ahlberg, J. E. "Rates of Water Vapor Adsorption from Air by Silica Gel." Industrial and Engineering Chemistry. Vol. 31 (No. 8); pp. 988-992. 1939 (August).
11. Rosen, J. B. "Kinetics of a Fixed Bed System for Solid Diffusion into Spherical Particles." Journal of Chemical Physics. Vol. 20 (No. 3); pp. 387-394. 1952 (March).
12. Rosen, J. B. "General Numerical Solution for Solid Diffusion in Fixed Beds." Industrial and Engineering Chemistry. Vol. 46 (No. 8); pp. 1590-94. 1954 (August).
13. Eagleton, L. C.; Bliss, H. "Drying of Air in Fixed Beds." Chemical Engineering Progress. Vol. 49 (No. 10); pp. 543-548. 1953 (October).
14. Antonson, C. R.; Dranoff, J. S. "The Kinetics of Ethane Adsorption on Molecular Sieves." Physical Adsorption Processes and Principles. Chemical Engineering Progress Symposium, Series. Vol. 63; pp. 61-67. 1967.

15. Carter, J. W. "Adsorption Drying of Gases: Part I." British Chemical Engineering. 1960 (July); pp. 472-476.
16. Carter, J. W. "Adsorption Drying of Gases: Part II." British Chemical Engineering. 1960 (August); pp. 552-555.
17. Carter, J. W. "Adsorption Drying of Gases: Part III." British Chemical Engineering. 1960 (Sept.); pp. 615-631.
18. Carter, J. W. "A Numerical Method for Prediction of Adiabatic Adsorption in Fixed Beds." Trans. Instu. Chem. Engrs. Vol. 44; pp. T253-T259. 1966.
19. Carter, J. W. "Isothermal and Adiabatic Adsorption in Fixed Beds." Trans. Instu. Chem. Engrs. Vol 46; pp. T213-221. 1968.
20. Meyer, O. A.; Weber, T. W. "Nonisothermal Adsorption in Fixed Beds." AIChE Journal. Vol. 13 (No. 3); pp. 457-465. 1967 (May).
21. Bullock, C. E.; Threlkeld, J. L. "Dehumidification of Moist Air by Adiabatic Adsorption." Trans. of ASHRAE. Vol. 72; 301-313. 1966.
22. Hubbard, S. S. "Equilibrium Data for Silica Gel and Water Vapor." Ind. and Eng. Chem. Vol. 46; pp. 356-358. 1954.
23. Chi, C. W.; Wasan, D. T. "Fixed Bed Adsorption Drying." AIChE Journal. Vol. 16 (No. 1); pp. 23-31. 1970 (January).
24. Koh, H. K. "Study on the Use of Solar Energy for the Regeneration of Silica Gel Used for Grain Drying." Ph. D. Thesis. Kansas State University. University Microfilms International Order No. 7802410. 1978.
25. MacLaine-cross, I. L.; Banks, P. J. "Coupled Heat and Mass Transfer in Regenerators--Prediction Using an Analogy with Heat Transfer." Int. J. Heat Mass Transfer. Vol. 15; pp. 1225-1242. 1972.
26. Banks, P. J. "Coupled Equilibrium Heat and Single Adsorbate Transfer in Fluid Flow through a Porous Medium--I, Characteristic Potentials and Specific Capacity Ratios." Chemical Engineering Science. Vol. 27; pp. 1143-1155. 1972.
27. Close, D. J.; Banks, P. J. "Coupled Equilibrium Heat and Single Adsorbate Transfer in Fluid Flow through a Porous Medium--II, Predictions for a Silica-Gel Air-Drier Using Characteristic Charts." Chemical Engineering Science. Vol. 27; pp. 1157-1169. 1974.
28. Banks, P. J. "Prediction of Heat and Water Vapor Exchanger Performance from that of a Similar Heat Exchanger." Compact Heat Exchangers--History, Technological Advancement and Mechanical Design Problems. ASME HTD. Vol. 10; pp. 57-64. 1980.
29. Pla-Barby, F. E.; Vliet, G. C.; Panton, R. L. "Performance of Rotary Bed Silica Gel Solid Desiccant Dryers." ASME 78-H-36. 1978 (May).

30. Holmberg, R. B. "Combined Heat and Mass Transfer in Regenerators with Hygroscopic Materials." Journal of Heat Transfer. Vol. 101; pp. 205-210. 1979 (May).
31. Barker, J. M.; Kettleborough, C. F. "The Adiabatic Adsorption--Desorption Characteristics of Silica Gel Beds--Part 1: Theory." ASME 80-WA/Sol-30. Also M.S. Thesis. Texas A & M University, 1979.
32. Mathiprakasam, B.; Lavan, Z. "Performance Predictions for Adiabatic Desiccant Dehumidifiers Using Linear Solutions." Journal of Solar Energy Engineering. Vol. 102; pp. 73-79. 1980 (February).
33. Mathiprakasam, B. "Performance Prediction of Silica Gel Desiccant Cooling System." Ph.D. Thesis. Illinois Institute of Technology. 1979 (December).
34. Nienberg, J. W. "Modeling of Desiccant Performance for Solar-Desiccant-Evaporative Cooling Systems." M.S. Thesis. University of California, Los Angeles. 1977.
35. Handley, D.; Heggs, P. J. "Momentum and Heat Transfer Mechanisms in Regularly Shaped Packings." Trans. Inst. Chem. Engr. Vol. 46; pp. 251-264. 1968.
36. Pesaran, A. A. "Air Dehumidification in Packed Silica Gel Beds." M.S. Thesis. University of California, Los Angeles. UCLA-ENG-8038. 1980 (June).
37. MacLaine-cross, I. L. "A Theory of Combined Heat and Mass Transfer in Regenerators." Ph. D. Thesis. Monash University, Australia. 1974.
38. Holman, J. P. Heat Transfer. McGraw-Hill Book Company. New York. 1972.
39. Lunde, P. J.; Kester, F. L. "Chemical and Physical Gas Adsorption in Finite Multimolecular Layer." Chem. Eng. Science. Vol. 30; pp. 1497-1505. 1975.
40. Rojas, F. "Pure Vapor Adsorption of Water on Silica Gels of Different Porosity." M. S. Thesis 2342. Colorado School of Mines. 1980.
41. Jury, S. H.; Edwards, H. R. "The Silica Gel Water Vapor Sorption Therm." Canadian J. Chem. Engr. Vol. 49; pp. 663-666. Oct. 1979.
42. Beecher, B. K. "Drying Agents" Encyclopedia of Chemical Technology. Vol. 7; pp. 378-398. 1975.
43. Davison Silica Gels. W. R. Grace and Co. Baltimore, MD.
44. Close, D. J. "Prediction of the Behavior of Packed Adsorbent Beds." Australian National Chemical Engineering Conference. 1974. pp. 241-253.

45. ASHRAE Handbook 1977 Fundamentals. American Society of Heating, Refrigeration, and Air-Conditioning Engineers.
46. Edwards, D. K.; Denny, V. E.; Mills, A. F. 1973. Transfer Processes. Holt, Rinehart and Winston, Inc., New York.
47. Van Leersum. Personal communication. 1981 (Oct).
48. Kutscher, C.; Barlow, R. S. "Dynamic Performance of a Packed Bed Dehumidifier: Experimental Results from the SERI Desiccant Test Loop." SERI TR/253-1429. 1981.
49. Barlow, R.; Collier, K. "Optimizing the Performance of Desiccant Beds for Solar Regenerated Cooling." SERI/TP-631-1157. Presented at the AS/ISES Annual Conference, 26-30 May 1981, Philadelphia, PA.

APPENDIX A

USER'S GUIDE TO COMPUTER PROGRAMS

A-1. OVERVIEW OF COMPUTER PROGRAMS

Three computer programs were used in this study: DESSIM, for simulation of single-blow cases; DESSIM 2, for simulation of steady-state performance of desiccant cooling systems; and DESSIM 4, for parametric studies of cooling systems. The core of the adsorption/desorption analysis is identical in all three programs. All programs are written in standard FORTRAN 4, and complete listings are included in Appendix B. These programs were run on the Control Data Corporation Cyber 720/76 computer at SERI. The first line in each program is specific to the CDC system and should be removed if the program is to be run on other systems. Also, all graphics are based on the DISSPLA* graphics software package. Sections of the programs that involve graphics have been identified to allow for alteration or deletion if the programs are to be run on a system that does not support the DISSPLA package.

The logic and equations used in the pseudo-steady-state model and the system analysis were described in Secs. 3.0 and 5.0, and the program listings are thoroughly documented. Therefore, no further discussion of program logic will be included in this section.

For most simulations in cooling or dehumidification applications, 10 bed sections should be sufficient. This can be increased to 15 or 20 if improved resolution in graphing temperature and loading profiles is desired. Also, it may be advisable to use more bed sections when simulating thick desiccant beds. Once NBED is specified, the time step should be chosen so as to give $RMASS \approx 0.3$ ($0.1 < RMASS < 0.5$ is reasonable). RMASS is the dry mass ratio of the air chunk to the bed section.

$$RMASS = \frac{FLOW * DT * NBED}{AFRONT * HEIGHT * BDENS}$$

Computation time depends on the parameters of the simulation. On the Cyber 720/76, typical single-blow simulations using DESSIM required less than two seconds of central processor time. Typical system simulations using DESSIM 2 required about 8 to 10 seconds. In parametric studies using DESSIM 4, the computation time per steady-state point can be reduced to about 5 to 6 seconds, because the temperature and loading profiles are retained between successive simulations.

*Display Integrated Software System and Plotting Language by Integrated Software Systems Corporation (ISSCO).

A-2. JOB CONTROL FILES AND INPUT DATA

Each of the three programs has a job control file or submit file associated with it that initiates the job and contains input data for the specific simulation. The commands in these files are somewhat specific to the CDC system at SERI, and will not be outlined in detail. However, the three files are listed below and the input variables and their units are identified. The units of each variable are listed in the index of FORTRAN variables in Section A-3. Lines of input data in the submit file must correspond to the READ lines in the programs. Note that some of the input variables are one- or two-dimensional arrays.

Table A-1. Submit File for DESSIM

```

/JOB
STAGE, STSBD, T50.
ACCOUNT
ATTACH, HEADING.
HEADING.  BARLOW
HEADING.  DESSIM
HEADING.
HEADING.
HEADING.
FILE(DESSIM, RT=Z)
GETPF, DESSIM, TY=G, ST=CNS, UN=SE1174,          PN=113100, CH=252.
ATTACH, DISSPLA.
ATTACH, DISSPLB.
LIBRARY, DISSPLA, DISSPLB.
FTN, I=DESSIM, GO.
SAVEPF, PLFILE, UN=SE1174,          CH=252, PN=113100, TY=R, ST=CNS.
EXIT.
SAVEPF, PLFILE, UN=SE1174,          CH=252, PN=113100, TY=R, ST=CNS.
/NOSEQ
/EOR
.412 .035 .00193 1335. 1. 850. 921.
40. .0184 60. .0167
.208 70. .5 70. 1. 10
82800. 3.0 2
50
/READ, DAT85A

```

```

AFRONT, HEIGHT, DIAM, ARATIO, FRAC, BDENS, CBED
TIN, WIN, TBØ, XBØ
FLOW, TRUN, TPRINT, TGRAPH, DT, NBED
PATM, RLEWIS, ICORR
IDATA
Name of file containing experimental data

```

Table A-2. Submit File for DESSIM2

```

/JOB
DESSIM2,STSD,T100.
ACCOUNT,DUM1234.
HEADING.  BARLOW
HEADING.  DESSIM2
HEADING.
HEADING.
HEADING.
FILE(DESSIM2,RT=Z)
GETPF,DESSIM2,TY=G,ST=CNS,UN=SE1174,          PN=113100,CH=252.
ATTACH,DISSPLA.
ATTACH,DISSPLB.
LIBRARY,DISSPLA,DISSPLB.
FTN,I=DESSIM2,GO.
SAVEPF,PLFILE,UN=SE1174,          CH=252,PN=113100,TY=R,ST=CNS.
EXIT.
SAVEPF,PLFILE,UN=SE1174,          CH=252,PN=113100,TY=R,ST=CNS.
/NOSEQ
/EOR
1.0 .04 .00193 1335. 1. 740. 921.
26.7 .0111 35. .014 80.
.5 5. 0.1 1. 1. 55. .07 10
.9 .93 .9 1 3. 3. 1 3

AFRONT, HEIGHT, DIAM, ARATIO, FRAC, BDENS, CBED
TROOM, WROOM, TAMB, WAMB, TREG
FLOW, TRUN, TPRINT, TGRAPH, DT, TBØ, XBØ, NBED
EC1, EHX, EC2, MODE, RLEWIS(1), RLEWIS(2), IPLOT, ICORR

```

Table A-3. Submit File for DESSIM4

```

/JOB
DESSIM4,STSD,T100.
ACCOUNT,DUM1234.
HEADING.  BARLOW
HEADING.  PARAMETRIC
HEADING.
HEADING.
HEADING.
FILE(DESSIM4,RT=Z)
GETPF,DESSIM4,TY=G,ST=CNS,UN=SE1174,UP=BARLOW,PN=113100,CH=252.
FTN,I=DESSIM4,GO.
EXIT.
/NOSEQ
/EOR
1.0 .04 .00193 1335. 1.0 740. 921.
26.7 .0111 35.0 .014 80.
.5 5. 1. 55. .07 10
.9 .9 .9 1 3. 3. 2
27.5 30. 32.5 35. 37.5 40.
.008 .011 .014 .017

AFRONT, HEIGHT, DIAM, ARATIO, FRAC, BDENS, CBED
TROOM, WROOM, TAMB, WAMB, TREG
FLOW, TRUN, DT, TBØ, XBØ, NBED
EC1, EHX, EC2, MODE, RLEWIS(1), RLEWIS(2), ICORR
PARAM1 (Array)
PARAM2 (Array)

```

A-3. A PARTIAL LISTING OF FORTRAN VARIABLES

Real variables and important integer variables are listed below in alphabetical order with definitions. Corresponding text variables, if used, are also given. Some variables do not appear in all three programs. Integer variables that are used only as counters or indices are not included, nor are variables that are used only for graphics. None of the graphics procedures are documented here and the reader is referred to the DISSPLA manual for further information.

FORTRAN VARIABLE	DEFINITION
ADFRAC	Ratio of total mass of water adsorbed or desorbed to the total mass of dry desiccant.
ADS	Total mass of water adsorbed or desorbed (kg).
ADSERR	Error tolerance for absorbed water (fractional).
ADSOLD	Mass of water adsorbed or desorbed in the previous half-cycle (kg).
AFRONT	Exposed face area of desiccant bed on each side of the system (m^2).
AMASS	Mass of air chunk (kg). Text: M_a .
ARATIO	Surface area per unit volume in the desiccant bed (m^2/m^3).
BDENS	Density of bed material (kg/m^3). Text: ρ_b .
BMASS	Mass of single bed section (kg). Text: M_b .
CA	Air capacity rate used in exchanger calculations ($W/^\circ C$ or kg/s). Text: C_{air} .
CADS	Heat capacity rate of the adsorption air stream ($W/^\circ C$).
CAIR	Specific heat of air ($J/kg^\circ C$). Text - c_p .
CAP	Cooling capacity of system (kJ/kg dry air).
CB	Capacity rate of bed or desiccant material ($W/^\circ C$ or kg/s). Text: C_{bed} .
CBED	Specific heat of the bed ($J/kg^\circ C$). Text: c_b .
CC	Ratio of CMIN/CMAX. Text: CC.
CMAX	Larger of the capacity rates CA,CB.
CMIN	Smaller of CA,CB.
COP	Thermal coefficient of performance of the system.
CREG	Heat capacity rate of regeneration air stream ($W/^\circ C$).
CWATER	Specific heat of liquid water ($J/kg^\circ C$). Text: C_w .
C1,C2,C3	Constants from Eq. 3-40.
DAREA	Surface area within one bed section (m^2). Text: A_s .

DAT	Two-dimensional input array containing experimental data for graphics.
DELH	Enthalpy change of air passing through the dehumidifier (kJ/kg dry air).
DHCOOL	Enthalpy difference between room air and delivered air (kJ/kg dry air).
DHDT	In-line function for the specific heat of moist air (J/kg ^o C).
DHREG	Enthalpy increase of regeneration air due to solar heat input (kJ/kg dry air).
DPVDX	Derivative of equilibrium vapor pressure with respect to desiccant loading fraction. Text: $\frac{\partial P_{ve}}{\partial X_T}$.
DYDMS	Derivative of mass fraction in desiccant with respect to mass fraction in air. Text: $\partial Y / \partial m_{sT}$.
DT	Time step (s). Text: Δt .
DIAM	Particle diameter (m). Text: D_p .
D1	Array for experimental data. Contains time (minutes).
D2	Array for experimental data. Contains temperature (^o C).
D3	Array for experimental data. Contains humidity ratio (kg/kg).
EFF	Effectiveness of exchange process.
EC1	Effectiveness of evaporative cooler 1. Text: E_{c1} .
EHX	Effectiveness of heat exchanger. Text: E_{hx} .
EC2	Effectiveness of evaporative cooler 2. Text: E_{c2} .
ENTH	In-line function for the enthalpy of moist air (J/kg). Text: h_a .
FLOW	Total flow rate of dry air in each process stream (kg/s).
FRAC	Mass fraction of desiccant in bed. (Equals 1.0 for packed bed.)
G	Mass transfer coefficient (kg/m ² s). Text: g .
GA	Mass flow rate of dry air per unit face area (kg/m ² s). Text: G_a .
GRAPH	Three-dimensional array for storage of temperature and loading profiles in the bed.
GTIME	Elapse time clock. Reset each time that temperature and loading profiles are stored.
H	Heat transfer coefficient (W/m ² ^o C). Text: H .
HAVE	Average enthalpy of outlet air (kJ/kg dry air).
HEAT	Thermal energy transferred to air chunk in heat transfer process (J). Text: Q .

HEIGHT	Total thickness of desiccant bed (m). Text: L.
HROOM	Enthalpy of room air (kJ/kg dry air).
HSEC	Thickness of one bed section (m).
HSHV	Ratio of heat of adsorption to heat of vaporization. Text: h_{ads}/h_{vap} .
HSUM	Sum used to calculate HAVE.
HVAP	Heat of vaporization of water (J/kg). Text: h_{vap} .
ICORR	Correlation number.
IDATA	Number of experimental data points to be plotted.
IPLLOT	1 - Plotter on. 0 - Plotter off.
NBED	Number of bed sections.
NCYCLE	Number of half-cycles.
NPASS	Number of air chunks to be sent through the bed. Same as total number of time steps.
OUT1	Array of outlet conditions. Time (minutes).
OUT2	Array of outlet conditions. Temperature ($^{\circ}\text{C}$).
OUT3	Array of outlet conditions. Humidity ratio (kg/kg).
OUT4	Array of outlet conditions. Relative humidity.
OUT5	Array of outlet conditions. Enthalpy (kJ/kg).
PARAM1	Array for parametric studies.
PARAM2	Array for parametric studies.
PATM	Ambient pressure (N/m^2). Text: P_{atm} .
PS	In-line function for saturation pressure.
PSAT	Saturation vapor pressure of water in air (N/m^2). Text: P_{sat} .
PTIME	Elapse time clock. Reset each time outlet air conditions are stored for printing or graphics.
PVE	Equilibrium vapor pressure (N/m^2). Text: P_{ve} .
QEXCH	Heat transfer rate in system heat exchanger. Text: \dot{Q}_{hx} .
QREGEN	Rate of heat addition from solar. Text: \dot{Q}_{reg} .
RH	Relative humidity. Text: RH.
RK	Thermal conductivity of air ($\text{W/m}^{\circ}\text{C}$). Text: k.
RLEWIS	Effective Lewis number. Text: Le.
RMASS	Ratio of mass of air chunk to mass of bed section. Gives indication of appropriate match of time and space increments. ($0.1 \leq \text{RMASS} \leq 0.5$ is advised.)
RMA1	Mass fraction of water vapor in air before mass transfer calculation. Text: m_{a1} .

RMA2	Mass fraction of water vapor in air after mass transfer calculation. Text: m_{a2} .
RMS	Mass Fraction of water vapor in air in equilibrium with the desiccant surface. Text: m_s .
RMU	Dynamic viscosity of air (kg/ms). Text: μ .
RNTU	Number of transfer units. Text: Ntu.
TAMB	Ambient temperature ($^{\circ}\text{C}$).
TAVE	Average outlet temperature ($^{\circ}\text{C}$).
TA1	Temperature of air chunk before heat transfer calculation ($^{\circ}\text{C}$).
TA2	Temperature of air chunk after heat transfer calculation ($^{\circ}\text{C}$).
TBED	Array of bed section temperatures.
TBINT	Bed section temperature after the energy balance ($^{\circ}\text{C}$). Text: T_b .
TBO	Initial temperature of bed ($^{\circ}\text{C}$).
TB1	Temperature of bed section before energy balance ($^{\circ}\text{C}$). Text: T_{b1} .
TB2	Temperature of bed section after heat transfer calculation ($^{\circ}\text{C}$). Text: T_{b2} .
TGRAPH	Time interval at which temperature and loading profiles in the bed are stored for printing/graphing (minutes).
TIME	Elapse time clock for complete adsorption or desorption process (seconds).
TIN	Temperature of inlet air ($^{\circ}\text{C}$).
TPRINT	Time interval at which outlet air states are stored for printing/graphics (minutes).
TREG	Regeneration temperature for cooling system ($^{\circ}\text{C}$).
TROOM	Room temperature ($^{\circ}\text{C}$).
TRUN	Total time for adsorption or desorption (minutes).
TWB	Wet bulb temperature ($^{\circ}\text{C}$). Text: T^* .
WATER	Mass of water transferred from air chunk to bed section (kg). Text: M_w .
WAMB	Ambient temperature ($^{\circ}\text{C}$).
WAVE	Average outlet humidity from dehumidifier wheel (kg/kg).
WA1	Humidity ratio of air chunk before mass transfer calculation (kg/kg). Text: w_{a1} .
WA2	Humidity ratio of air chunk after mass transfer calculation (kg/kg). Text: w_{a2} .
WIN	Humidity ratio of inlet air (kg/kg).

WROOM	Room humidity (kg/kg).
WSTAR	Room ratio humidity for a given wet bulb temperature (kg/kg).
WSUM	Sum used to calculate WAVE.
XBED	Array of moisture ratios in bed section (kg/kg).
XBO	Initial moisture ratio of the desiccant (kg/kg).
XB1	Moisture ratio of desiccant section before mass transfer calculation (kg/kg). Text: X_{b1} .
XB2	Moisture ratio of desiccant section after mass transfer calculation (kg/kg). Text: X_{b2} .

APPENDIX B

PROGRAM LISTINGS

```

      PROGRAM DESSIM(INPUT,OUTPUT,TAPES=INPUT,TAPES6=OUTPUT,PLFILE)
C
C *****
C *
C *   DESSIM: SIMULATION OF SILICA GEL BEDS
C *   R. BARLOW, SERI, DECEMBER 1980
C *
C *****
C
C
C THIS VERSION OF THE DESSIM PROGRAM IS DESIGNED TO
C SIMULATE SINGLE BLOW ADSORPTION OR DESORPTION IN A SILICA
C GEL PACKED BED WITH UNIFORM INITIAL CONDITIONS OF MOISTURE
C CONTENT AND TEMPERATURE, AND CONSTANT INLET AIR CONDITIONS.
C
      DIMENSION TBED(50),XBED(50),GRAPH(50,20,2),
      2OUT1(500),OUT2(500),OUT3(500),OUT4(500),OUT5(500),
      3X(101),Y(101),DAT(4,50),D1(50),D2(50),D3(50)
C
C INITIALIZE DISSPLA GRAPHICS
      CALL COMPRS
C
C DEFINE CONSTANTS IN SI UNITS
      CAIR=1006.
      CWATER=4181.
C
C READ DATA. NOTE THAT DAT IS A TWO DIMENSIONAL DATA ARRAY.
      READ(5,*) AFRONT,HEIGHT,DIAM,ARATIO,FRAC,BDENS,CBED
      READ(5,*) TIN,WIN,TBO,XBO
      READ(5,*) FLOW,TRUN,TPRINT,TGRAPH,DT,NBED
      READ(5,*) PATM,RLEWIS,ICORR
      READ(5,*) IDATA
      READ(5,*) DAT
C
C SET UP ARRAYS FOR GRAPHING EXPERIMENTAL DATA
      IF (IDATA.EQ.0) GO TO 11
      DO 10 J=1,IDATA
      D1(J)=DAT(2,J)
      D2(J)=DAT(3,J)
      D3(J)=DAT(4,J)
10    CONTINUE
C
C SET UP PARAMETERS FOR SIMULATION
11    HSEC=HEIGHT/FLOAT(NBED)
      BMASS=HSEC*AFRONT*BDENS
      DAREA=HSEC*AFRONT*ARATIO
      AMASS=FLOW*DT
      NPASS=INT(TRUN*60./DT)
      TIME=0.
      PTIME=0.
      GTIME=0.
      ADS=0.
      KK=0
      NN=1
      RMASS=AMASS/BMASS
C
C INITIALIZE TEMPERATURE AND WATER CONTENT IN THE BED
      DO 12 I=1,NBED
      TBED(I)=TBO
12    XBED(I)=XBO
      IF (TIME.EQ.0.) GO TO 41
C

```

```

C HEAT TRANSFER COEFFICIENT FROM HADLEY AND HEGGS CORRELATION.
C MASS TRANSFER COEFFICIENT IS CALCULATED USING AN EFFECTIVE
C VALUE FOR THE LEWIS NUMBER THAT ACCOUNTS FOR THE RESISTANCE
C TO DIFFUSION OF WATER WITHIN THE SOLID DESICCANT.
15  GA=FLOW/AFRONT
    RK=.02624+7.58E-5*(TIN-27.)
    RMU=1.859E-5+4.32E-8*(TIN-27.)
    H=.58*RK*(DIAM*GA/RMU)**.67/DIAM
    G=H/(RLEWIS*CAIR)

C
C MAIN CALCULATION LOOP BEGINS. NPASS IS THE NUMBER OF TIME
C STEPS IN THE COMPLETE PROCESS AND THE NUMBER OF AIR CHUNKS
C THAT MUST BE SENT THROUGH THE BED. TO SIMULATE VARIABLE INLET
C AIR CONDITIONS, TIN AND WIN CAN BE MADE FUNCTIONS OF TIME.
DO 46 N=1,NPASS
  WA1=WIN
  TA1=TIN

C
C ONE CHUNK OF AIR IS PASSED COMPLETELY THRU THE BED.
C AS THE AIR IS EXPOSED TO EACH BED SECTION, CALCULATIONS ARE
C CARRIED OUT AS FOLLOWS: 1) MASS TRANSFER CALCULATION,
C 2) ENERGY BALANCE TO ACCOUNT FOR THE HEAT OF ADSORPTION
C 3) HEAT TRANSFER CALCULATION BETWEEN THE BED AND THE AIR.
DO 40 I=1,NBED
  TB1=TBED(I)
  XB1=XBED(I)

C
C MASS TRANSFER CALCULATION: COUNTER-FLOW EXCHANGER METHOD.
C THE AMOUNT OF WATER TRANSFERED IN A SINGLE TIME STEP IS
C CALCULATED USING EQUATIONS ANALOGOUS TO THOSE FOR A
C STEADY STATE COUNTER-FLOW HEAT EXCHANGER. THE QUANTITY
C "DYDMS" IS THE PARTIAL DERIVATIVE OF THE DESICCANT LOADING
C FRACTION WITH RESPECT TO THE EQUILIBRIUM MASS FRACTION
C OF WATER IN THE AIR AT THE INTERFACE. THIS IS ANALOGOUS TO
C THE SPECIFIC HEAT IN THE HEAT TRANSFER PROBLEM AND REPLACES
C THE INVERSE OF HENRY CONSTANT USED IN GAS-LIQUID MASS EXCHANGE
C PROBLEMS.
  PSAT=PS(TB1)
  CALL PROPS(ICORR,XB1,TB1,PSAT,PVE,HSHV)
  RMS=.622*PVE/(PATM-.378*PVE)
  RMA1=WA1/(1.+WA1)
  CA=AMASS*(1.+WA1)/DT
  CALL DERIV(ICORR,XB1,TB1,RMS,HSHV,PATM,PSAT,DYDMS)
  CB=FRAC*BMASS*(1+XB1)*DYDMS/DT
  CMIN=AMIN1(CA,CB)
  CMAX=AMAX1(CA,CB)
  CC=CMIN/CMAX
  RNTU=G*DAREA/CMIN
  EFF=(1.-EXP(-RNTU*(1.-CC)))/(1.-CC*EXP(-RNTU*(1.-CC)))
  RMA2=RMA1-EFF*(RMA1-RMS)
  WA2=RMA2/(1.-RMA2)
  WATER=AMASS*(WA1-WA2)
  XB2=(XB1*FRAC*BMASS+WATER)/(FRAC*BMASS)

C
C ENERGY BALANCE
C AN INTERMEDIATE TEMPERATURE IS CALCULATED FOR THE BED SECTION WHILE THE
C AIR IS ASSUMED TO REMAIN AT ITS INITIAL TEMPERATURE. THE DIFFERENCE
C BETWEEN THE HEAT OF ADSORPTION AND THE HEAT OF VAPORIZATION IS
C ACCOUNTED FOR. HSHV IS THE RATIO OF THE HEAT OF ADSORPTION TO
C THE HEAT OF VAPORIZATION AND IS RETURNED BY SUBROUTINE PROPS.
  HVAP=2358500.-2460.*(TB1-60.)
  TBINT=(TB1*BMASS*(CBED+FRAC*XB1*CWATER)
    1  +AMASS*(ENTH(TA1,WA1)-ENTH(TA1,WA2))+WATER*HVAP*
    2  (HSHV-1.))/(BMASS*(CBED+FRAC*XB2*CWATER))

C
C HEAT TRANSFER CALCULATION:
C THE MODEL ASSUMES THAT THE FINAL TEMPERATURES OF THE AIR CHUNK
C AND THE BED SECTION AT THE END OF THE TIME STEP ARE THE SAME AS
C THE STEADY STATE OUTLET TEMPERATURES FROM A SIMPLE COUNTER FLOW
C HEAT EXCHANGER THAT HAS STEADY FLOWS OF AIR AND DESICCANT MATERIAL
C WITH INLET CONDITIONS EQUAL TO THE INITIAL CONDITIONS OF THE AIR
C CHUNK AND THE BED SECTION. THE EFFECTIVENESS OF THIS HEAT
C EXCHANGE PROCESS IS DETERMINED BY THE HEAT TRANSFER COEFFICIENT,
C THE TOTAL SURFACE AREA IN THE BED SECTION, AND THE HEAT CAPACITY
C RATES OF THE AIR AND BED MATERIAL.

```

```

CA=AMASS*DHDT(TA1,WA2)/DT
CB=BMASS*(CBED+XB2*FRAC*CWATER)/DT
CMIN=AMIN1(CA,CB)
CMAX=AMAX1(CA,CB)
CC=CMIN/CMAX
RNTU=H*DAREA/CMIN
EFF=(1.-EXP(-RNTU*(1.-CC)))/(1.-CC*EXP(-RNTU*(1.-CC)))
HEAT=EFF*CMIN*(TB2-TA1)*DT
TA2=TA1+HEAT/(DHDT(TA1,WA2)*AMASS)
TB2=TBINT-HEAT/(BMASS*(CBED+FRAC*XB2*CWATER))
ADS=ADS+WATER
TBED(I)=TB2
XBED(I)=XB2
WA1=WA2
TA1=TA2
40  CONTINUE
C AN AIR CHUNK LEAVES THE BED AT THIS POINT.  THIS CORRESPONDS TO
C ONE TIME STEP IN THE OVERALL SIMULATION.
C
C ADVANCE THE CLOCKS.
TIME=TIME+DT
PTIME=PTIME+DT
GTIME=GTIME+DT
IF (N.EQ.1) GO TO 45
C
C OUTLET CONDITIONS ARE STORED AT PTIME TIME INCREMENTS.
IF (ABS(PTIME/60.-TPRINT).LT.1.E-6) GO TO 43
GO TO 44
43  NN=NN+1
PTIME=0.
45  PSAT=PS(TA2)
OUT1(NN)=TIME/60.
OUT2(NN)=TA2
OUT3(NN)=WA2
OUT4(NN)=PATM*WA2/((.622+WA2)*PSAT)
OUT5(NN)=ENTH(TA2,WA2)/1000.
C
C TEMPERATURE AND LOADING PROFILES IN THE BED ARE STORED AT
C GTIME TIME INCREMENTS.
44  IF (ABS(GTIME/60.-TGRAPH).LT.1.E-6) GO TO 41
GO TO 46
41  KK=KK+1
GTIME=0.
DO 42 I=1,NBED
GRAPH(I,KK,1)=TBED(I)
42  GRAPH(I,KK,2)=XBED(I)
IF (TIME.EQ.0.) GO TO 13
46  CONTINUE
C THE MAIN CALCULATION LOOPS BACK FROM HERE TO SEND ANOTHER AIR
C CHUNK THROUGH THE BED.
C
ADFRAC=ADS/(FRAC*BMASS*FLOAT(NBED))
C
C PRINT RESULTS
WRITE(6,100) AFRONT,HEIGHT,DIAM,ARATIO,FRAC,SDENS,CBED,
1TIN,WIN,TB0,XB0,FLOW,TRUN,DT,NBED,PATM,RLEWIS,RMASS,ICORR
WRITE(6,101) ADS,ADFRAC
DO 51 I=1,NN
51  WRITE(6,102) OUT1(I),OUT2(I),OUT3(I),OUT4(I),OUT5(I)
WRITE(6,103)
DO 52 L=1,KK
TG=TGRAPH*FLOAT(L-1)
WRITE(6,104) TG
DO 52 I=1,NBED
52  WRITE(6,105) I,GRAPH(I,L,1),GRAPH(I,L,2)
C
C BEGIN PLOTTING ROUTINES USING DISSPLA
STEP=1.
IF (TRUN.GE.10.) STEP=2.
IF (TRUN.GE.20.) STEP=10.
IF (TRUN.GT.120.) STEP=30.
IF (TRUN.GT.300.) STEP=60.
IF (TRUN.GT.600.) STEP=120.
IF (TRUN.GT.900.) STEP=240.
CALL TITLE("OUTLET AIR TEMPERATURE (C)",-22,
1 "TIME (MINUTES)",14,"TEMPERATURE (C)",15,5.,3.5)

```

```

CALL XINTAX
CALL YTICKS(2)
CALL GRAF(0.,STEP,TRUN,20.,20.,100.)
CALL CURVE(OUT1,OUT2,NN,0)
IF (IDATA.GT.0) CALL CURVE(D1,D2,IDATA,-1)
CALL FRAME
CALL RLVEC(0.,TIN,TRUN,TIN,1202)
CALL ENOPL(0)
CALL TITLE("OUTLET AIR HUMIDITY",-19,"TIME (MINUTES)",14,
1 "HUMIDITY (KG/KG)",16,5.,3.5)
CALL YTICKS(5)
CALL GRAF(0.,STEP,TRUN,0.,.01,.03)
CALL CURVE(OUT1,OUT3,NN,0)
IF (IDATA.GT.0) CALL CURVE(D1,D3,IDATA,-1)
CALL FRAME
CALL RLVEC(0.,WIN,TRUN,WIN,1202)
CALL ENOPL(0)
CALL TITLE("DESICCANT TEMP. PROFILES",-24,
1 "BED LOCATION",12,"TEMPERATURE (C)",15,5.,3.56)
CALL YTICKS(2)
RNBED=FLOAT(NBED)
CALL GRAF(1.,1.,RNBED,20.,20.,100.)
CALL FRAME
DO 56 I=1,KK
DO 55 K=1,NBED
Y(K)=GRAPH(K,I,1)
55 X(K)=FLOAT(K)
56 CALL CURVE(X,Y,NBED,0)
CALL RLVEC(1.,TIN,RNBED,TIN,1202)
START=FLOAT(NBED/2-NBED/10)
FINISH=FLOAT(NBED/2+NBED/10)
CALL RLVEC(START,93.,FINISH,93.,1501)
CALL ENOPL(0)
CALL TITLE("LOADING PROFILES",-16,
1 "BED LOCATION",12,"WATER CONTENT (KG/KG)",21,5.,3.56)
CALL YTICKS(1)
CALL GRAF(1.,1.,RNBED,0.,.1,.4)
CALL FRAME
DO 58 I=1,KK
DO 57 K=1,NBED
Y(K)=GRAPH(K,I,2)
57 X(K)=FLOAT(K)
58 CALL CURVE(X,Y,NBED,0)
CALL RLVEC(START,.35,FINISH,.35,1501)
CALL ENOPL(0)
CALL TITLE("PSYCHROMETRIC CHART",-19,
1 "DRY BULB TEMPERATURE (C)",24,
2 "HUMIDITY RATIO (KG/KG)",22,5.,3.5)
CALL XTICKS(1)
CALL YTICKS(5)
CALL GRAF(10.,10.,100.,0.,.01,.03)
CALL BLNK1(0.,5.,3.5,5.,0)
CALL FRAME
CALL CURVE(OUT2,OUT3,NN,0)
IF (IDATA.GT.0) CALL CURVE(D2,D3,IDATA,-1)
DO 71 I=1,10
RH=.01*FLOAT(I)
NP=0
DO 70 IT=10,100
NP=NP+1
X(NP)=FLOAT(IT)
TDB=X(NP)+273.
PSAT=EXP(23.28199-3780.82/TDB-225805./TDB**2)
Y(NP)=.622*RH*PSAT/(PATM-RH*PSAT)
70 IF (Y(NP).GT..040) Y(NP)=.03
CALL CURVE(X,Y,NP,0)
71 CONTINUE
DO 73 I=2,10
RH=FLOAT(I)*.1
NP=0
DO 72 IT=10,65
NP=NP+1
X(NP)=FLOAT(IT)
TDB=FLOAT(IT)+273.
PSAT=EXP(23.28199-3780.82/TDB-225805./TDB**2)
Y(NP)=.622*RH*PSAT/(PATM-RH*PSAT)

```

```

72 IF ((Y(NP).GE..035).OR.(Y(NP).LT.0.)) Y(NP)=.03
   CALL CURVE(X,Y,NP,0)
73 CONTINUE
   CALL ENDPL(0)
   CALL DONEPL
   STOP
100 FORMAT("1",////,1X,15HBED PARAMETERS:,10X,
122HFRONTAL AREA (M2)      =,F6.4,
1/,26X,22HBED THICKNESS (M)    =,F6.4,
2/,26X,22HPARTICLE DIAMETER (M)=,F7.5,
2/,26X,22HSURFACE AREA (M2/M3) =,F6.0,
3/,26X,22HDESICCANT FRACTION   =,F5.3,
4/,26X,22HBED DENSITY (KG/M3)  =,F5.0,
5/,26X,22HSPECIFIC HEAT (J/KG) =,F6.0,
6//,1X,19HCONDITIONS FOR RUN:,6X,22HINLET AIR TEMP. (C) =,F5.1,
7/,26X,22HINLET HUMIDITY(KG/KG)=,F6.5,
8/,26X,22HINITIAL BED TEMP. (C)=,F5.1,
9/,26X,22HINITIAL BED LOADING  =,F5.3,
1/,26X,22HFLOW RATE (KG/S)     =,F5.3,
2/,26X,22HLENGTH OF RUN (MIN)  =,F4.0,
3/,26X,22HTIME STEP (S)        =,F3.0,
4/,26X,22HNO. OF BED SECTIONS  =,I3,
5//,26X,22HAMBIENT PRESSURE     =,F7.0,
6/,26X,22HLEWIS NUMBER         =,F5.3,
7/,26X,22HAM, AIR/M, BED       =,F5.3,
8/,26X,22HSILICA GEL CORR. NO. =,I2)
101 FORMAT(////,1X,18HWATER CYCLED (KG)=,F8.5,
25X,23HFRACTION OF BED CYCLED=,F6.4,
4 ////,1X,18HOUTLET CONDITIONS:,2X,
5 10HTIME (MIN),10X,8HTOUT (C),9X,12HWOUT (KG/KG),11X,4HROUT,
6 6X,"ENTHALPY (KJ/KG)",/)
102 FORMAT(20X,F10.3,10X,F8.2,10X,F10.6,10X,F7.4,10X,F8.4)
103 FORMAT("1",////,1X,36HTEMPERATURE AND LOADING PROFILES AT ,
123HTGRAPH TIME INCREMENTS:,,/)
104 FORMAT(//,1X,5HTIME=,F8.1,1X,5H MIN.,//,11X,4HNBED,13X,
110HTEMP (C) ,9X,7HLOADING,/)
105 FORMAT(12X,I2,10X,F10.2,10X,F10.5)
END

```

```

C
C FUNCTION FOR SATURATION PRESSURE AS A FUNCTION OF TEMPERATURE
C CORRELATION FROM MACLAINE-CROSS THESIS
FUNCTION PS(T)
  TK=T+273.
  PS=EXP(23.28199-3780.82/TK-225805./TK**2)
  RETURN
END

```

```

C
C FUNCTION FOR ENTHALPY FROM TEMPERATURE AND HUMIDITY
C FROM MACLAINE-CROSS THESIS
FUNCTION ENTH(T,W)
  ENTH=(1005.22+.02615*T)*T+W*(2500800.+1868.*T)
  RETURN
END

```

```

C
C FUNCTION FOR THE SPECIFIC HEAT OF AIR
FUNCTION DHDT(T,W)
  DHDT=1005.22+.0523*T+1868.*W
  RETURN
END

```

```

C
C
C SUBROUTINE FOR THE EQUILIBRIUM PROPERTIES OF REGULAR DENSITY
C SILICA GEL. CORRELATIONS BASED ON EXPERIMENTAL DATA ARE USED
C TO CALCULATE THE EQUILIBRIUM VAPOR PRESSURE AT THE DESICCANT
C SURFACE AND TO CALCULATE THE RATIO OF THE HEAT OF ADSORPTION
C TO THE HEAT OF VAPORIZATION. THREE CORRELATIONS ARE INCLUDED,
C AND THE PASSED INTEGER "ICORR" DETERMINES WHICH ONE IS USED.
C
C      ICORR=1      BULLOCK AND THRELKELD FIT TO HUBARD'S DATA
C                  AND CLOSE AND BANKS EQNS FOR HADS/HVAP.
C
C      ICORR=2      CLOSE AND BANKS FIT TO HUBARD'S DATA.
C                  F(X)=2.009*X AND LINEAR EQNS FOR HADS/HVAP ARE USED.
C
C      ICORR=3      FIT TO DATA OF F. ROJAS FOR DAVISON PA-40
C                  SILICA GEL. LINEAR EQNS FOR HADS/HVAP.
C

```

```

C      SUBROUTINE PROPS(ICORR,X,TC,PSAT,PVE,HSHV)
C      GO TO (10,30,40) ICORR
C
C ICORR=1
C
10  T=TC*1.8+32.
    IF(X.GT..05) GO TO 11
    PVE=((((4.02263E-4*X+1.186214E-5)*T-8.938272E-2*
1X-3.267901E-3)*T+7.068827*X+.322929)*T-182.1523*X-
210.41436)*X
    GO TO 17
11  IF (X.GT..1) GO TO 12
    PVE=((((-7.808642E-6*X+1.989198E-6)*T+4.312037E-3*X-
1 6.024537E-4)*T-.484787*X+.058058)*T+17.20448*X-1.836323
    GO TO 17
12  IF (X.GT..15) GO TO 13
    PVE=((((2.083333E-5*X-8.75E-7)*T-3.825E-3*X+2.1125E-4)*T
1+.255417*X-.015963)*T-4.6825*X+.352375
    GO TO 17
13  IF (X.GT..2) GO TO 14
    PVE=((((5.333333E-5*X-5.75E-6)*T-1.38E-2*X+1.7075E-3)
1*T+1.264667*X-.16735)*T-38.*X+5.35
    GO TO 17
14  IF (X.GT..25) GO TO 15
    PVE=((((-8.166667E-5*X+2.125E-5)*T+2.135E-2*X-5.3225E-3)
1*T-1.752333*X+.43605)*T+47.6*X-11.77
    GO TO 17
15  IF (X.GT..3) GO TO 16
    PVE=((((4.E-5*X-9.16667E-6)*T-8.1E-3*X+2.04E-3)
1*T+.599*X-.151783)*T-14.1*X+3.655
    GO TO 17
16  PVE=((((2.E-5*X-3.166667E-6)*T-3.7E-3*X+7.2E-4)
1*T+.291*X-.059383)*T-6.9*X+1.495
17  PVE=PVE*101325./29.92
    IF (X.GT..04) GO TO 21
    HSHV=8533.*X**3-542.*X*X+11.79*X+1.1557
    GO TO 50
21  IF (X.GT..1) GO TO 22
    HSHV=45.4*X*X-8.97*X+1.5922
    GO TO 50
22  HSHV=-9.1553*X**3+7.048*X*X-1.8966*X+1.2789
    GO TO 50
C
C ICORR=2
C
30  IF (X.GT..1) GO TO 31
    HSHV=1.3-1.75*X
    GO TO 32
31  HSHV=1.14-.15*X
32  PVE=(101325./29.91)*(29.91*2.009*X*PSAT/101325.)*HSHV
    GO TO 50
C
C ICORR=3
C
40  IF (X.GT..1) GO TO 41
    HSHV=1.3-1.75*X
    GO TO 42
41  HSHV=1.14-.15*X
42  R=(.616238*X+16.7916*X*X-74.34228*X**3+116.6834*X**4)
1/(1.-(TC-40.)/300.)
    PVE=R*PSAT
50  RETURN
    END
C
C
C
C SUBROUTINE FOR CALCULATING THE PARTIAL DERIVATIVE OF THE MASS
C FRACTION OF WATER IN THE DESICCANT WITH RESPECT TO THE MASS

```



```

C FRACTION OF WATER IN THE AIR AT EQUILIBRIUM. THREE CORRELATIONS
C ARE INCLUDED, AND THE PASSED INTEGER "ICORR" DETERMINES WHICH
C CORRELATION IS USED.
C DERIVATIVES OF THE EQUATIONS GIVEN IN SUBROUTINE PROPS ARE USED.
C
      SUBROUTINE DERIV(ICORR,X,TC,RMS,HSHV,PATM,PSAT,DYDMS)
      GO TO (10,20,30) ICORR
C
C ICORR=1
C
10  T=TC+1.8+32.
      IF (X.GT..05) GO TO 11
      DPVDX=((8.0453E-4*X+11.862E-6)*T-.17876*X+32.679E-4)*T
1  +14.138*X+.32293)*T-364.34*X-10.414
      GO TO 50
11  IF (X.GT..1) GO TO 12
      DPVDX=(-7.8086E-6*T+43.12E-4)*T-.48479)*T+17.204
      GO TO 50
12  IF (X.GT..15) GO TO 13
      DPVDX=((20.833E-6*T-38.25E-4)*T+2.5542)*T-4.6825
      GO TO 50
13  IF (X.GT..2) GO TO 14
      DPVDX=((53.333E-6*T-.0138)*T+1.2647)*T-38.
      GO TO 50
14  IF (X.GT..25) GO TO 15
      DPVDX=(-81.667E-6*T+.02135)*T-1.7523)*T+47.6
      GO TO 50
15  IF (X.GT..3) GO TO 16
      DPVDX=((4.E-5*T-81.E-4)*T+.599)*T-14.1
      GO TO 50
16  DPVDX=((2.E-5*T-37.E-4)*T+.291)*T-6.9
      GO TO 50
C
C ICORR=2
C
20  C1=3388.
      C2=5.93E-4*PSAT
      C3=-1.75
      IF (X.GT..1) C3=-.15
      DPVDX=C1*(C2*HSHV*(C2*X)**(HSHV-1.))+C3*(C2*X)**HSHV*ALOG(C2*X))
      GO TO 50
C
C ICORR=3
C
30  DPVDX=PSAT*(.616238+33.5832*X-223.027*X*X+466.734*X**3)
1  /(1.-(TC-40.)/300.)
50  DYDMS=.622*PATM/((1.+X)**2*(.622+.378*RMS)**2*DPVDX)
      RETURN
      END

```

```

      PROGRAM DESSIM2(INPUT,OUTPUT,TAPES=INPUT,TAPE6=OUTPUT,PLFILE)
C
C *****
C *
C * DESSIM2: SIMULATION OF SILICA GEL COOLING SYSTEMS *
C * R. BARLOW, SERI, DECEMBER 1980 *
C *
C *****
C
C THIS VERSION OF THE DESSIM PROGRAM SIMULATES THE STEADY
C STATE PERFORMANCE OF A COMPLETE DESICCANT COOLING SYSTEM
C COMPOSED OF A ROTARY DEHUMIDIFIER, A REGENERATIVE SENSIBLE
C HEAT EXCHANGER, AND TWO EVAPORATIVE COOLERS. PROPERTIES OF
C MEDIUM DENSITY SILICA GEL ARE USED. OPERATION OF THE
C DEHUMIDIFIER IS ASSUMED TO BE ADIABATIC. THE HEAT AND MASS
C TRANSFER PROCESSES IN THE DEHUMIDIFIER ARE MODELED BY USING
C PSUEDO-STEADY-STATE CALCULATIONS BASED ON THE EFFECTIVENESS-
C NTU METHOD FOR COUNTER-FLOW HEAT OR MASS EXCHANGERS.
C THIS VERSION OF THE DESSIM PROGRAM INCLUDES EXTENSIVE GRAPHICS
C CAPABILITY THAT USES THE "DISSPLA" GRAPHICS SOFTWARE PACKAGE.
C
C
C      DIMENSION TBED(50),XBED(50),TIN(2),WIN(2),RLEWIS(2),
C      2OUT1(500),OUT2(500),OUT3(500),OUT4(500),OUT5(500),GRAPH(50,20,2),
C      3X(101),Y(101),TPA(500),WPA(500),TPR(500),WPR(500),T(9),W(9),HS(9)
C      LOGICAL FLAG
C
C INITIALIZE DISSPLA GRAPHICS PACKAGE
C      CALL COMPRS
C
C DEFINE CONSTANTS IN SI UNITS
C      PATM=101325.
C      CAIR=1006.
C      CWATER=4181.
C      ADSOLD=0.
C      NCYCLE=1
C      M=1
C      ADSERR=.001
C      FLAG=.FALSE.
C
C READ DATA. NOTE THAT SOME OF THE INPUT VARIABLES ARE ARRAYS.
C      READ(5,*) AFRONT,HEIGHT,DIAM,ARATIO,FRAC,BDENS,CBED
C      READ(5,*) TROOM,WROOM,TAMB,WAMB,TREG
C      READ(5,*) FLOW,TRUN,TPRINT,TGRAPH,DT,TB0,XB0,NBED
C      READ(5,*) EC1,EHX,EC2,MODE,RLEWIS,IPL0T,ICORR
C
C INITIALIZE TEMPERATURE AND WATER CONTENT OF DESICCANT BED.
C      DO 1 I=1,NBED
C      TBED(I)=TB0
C 1    XBED(I)=XB0
C
C DEFINE KNOWN STATE POINTS FOR SYSTEM.
C MODE 1=VENTILATION. MODE 2=RECIRCULATION
C      IF (MODE.EQ.2) GO TO 2
C      T(1)=TROOM
C      W(1)=WROOM
C      T(6)=TAMB
C      W(6)=WAMB
C      GO TO 3
C 2    T(1)=TAMB
C      W(1)=WAMB
C      T(6)=TROOM
C
C      W(6)=WROOM
C 3    T(4)=TREG
C      HS(1)=ENTH(T(1),W(1))/1000.
C      HS(6)=ENTH(T(6),W(6))/1000.
C
C DETERMINE OUTLET STATE FOR FIRST EVAP. COOLER.
C      CALL WETBLB(T(1),W(1),HS(1),TWB,PATM)
C      PSAT=PS(TWB)
C      WSTAR=.622*PSAT/(PATM-PSAT)
C      T(2)=T(1)+EC1*(TWB-T(1))
C      W(2)=W(1)+EC1*(WSTAR-W(1))
C      HS(2)=ENTH(T(2),W(2))/1000.

```

```

C
C HUMIDITY RATIOS ARE UNAFFECTED BY THE HEAT EXCHANGE PROCESS.
  W(3)=W(2)
  W(4)=W(3)
C
C SET UP INLET CONDITIONS ON TWO SIDES OF DEHUMIDIFIER.
  TIN(1)=T(6)
  WIN(1)=W(6)
  TIN(2)=T(4)
  WIN(2)=W(4)
C
C SET UP PARAMETERS FOR DESICCANT SIMULATION.
C SIMULATION IS BASED ON A SMALL AXIAL ELEMENT IN THE
C ROTATING DEHUMIDIFIER WHEEL, AND ALL CALCULATIONS
C ARE BASED ON UNIT FACE AREA.
  GA=FLOW/AFRONT
  HSEC=HEIGHT/FLOAT(NBED)
  AMASS=GA*DT
  BMASS=HSEC*BDENS
  RMASS=AMASS/BMASS
  DAREA=HSEC*ARATIO
C
C INITIALIZE COUNTERS FOR ADSORPTION OR REGENERATION HALF CYCLE.
11  NPASS=INT(TRUN*60./DT)
    TIME=0.
    PTIME=0.
    GTIME=0.
    ADS=0.
    TSUM=0.
    WSUM=0.
    HSUM=0.
    KK=0
    NN=0
    IF (TIME.EQ.0.) GO TO 43
C
C TRANSFER COEFFICIENTS FROM HADLEY AND HEGGS CORRELATION.
13  RK=.02624+7.58E-5*(TIN(M)-27.)
    RMU=1.859E-5+4.32E-8*(TIN(M)-27.)
    H=.56*RK*(DIAM*GA/RMU)**.67/DIAM
    G=H/(CAIR*RLEWIS(M))
C
C MAIN CALCULATION LOOP FOR DEHUMIDIFIER SIMULATION.
C NPASS IS THE NUMBER OF TIME STEP TO BE TAKEN IN THE
C COMPLETE RUN AND THE NUMBER OF AIR CHUNKS THAT MUST
C BE PASSED THROUGH THE BED.
C ADSORPTION M=1      REGENERATION M=2
  DO 46 N=1,NPASS
    WA1=WIN(M)
    TA1=TIN(M)
    DO 40 II=1,NBED
      IF (M.EQ.1) I=II
      IF (M.EQ.2) I=NBED+1-II
      TB1=TBED(I)
      XB1=XBED(I)
C
C MASS TRANSFER CALCULATION: COUNTER-FLOW EXCHANGER METHOD.
C THE AMOUNT OF WATER TRANSFERED IN A SINGLE TIME STEP IS
C CALCULATED USING EQUATIONS ANALOGOUS TO THOSE FOR A
C STEADY STATE COUNTER-FLOW HEAT EXCHANGER. THE QUANTITY
C "DYDMS" IS THE PARTIAL DERIVATIVE OF THE DESICCANT LOADING
C FRACTION WITH RESPECT TO THE EQUILIBRIUM MASS FRACTION
C OF WATER IN THE AIR AT THE INTERFACE. THIS IS ANALOGOUS TO
C THE SPECIFIC HEAT IN THE HEAT TRANSFER PROBLEM AND REPLACES
C THE INVERSE OF HENRY CONSTANT USED IN GAS-LIQUID MASS EXCHANGE
C PROBLEMS.
    PSAT=PS(TB1)
    CALL PROPS(ICORR,XB1,TB1,PSAT,PVE,HSHV)
    RMS=.622*PVE/(PATM-.378*PVE)
    RMA1=WA1/(1.+WA1)
    CA=AMASS*(1.+WA1)/DT
    CALL DERIV(ICORR,XB1,TB1,RMS,HSHV,PATM,PSAT,DYDMS)
    CB=FRAC*BMASS*(1+XB1)*DYDMS/DT
    CMIN=AMIN1(CA,CB)
    CMAX=AMAX1(CA,CB)
    CC=CMIN/CMAX
    RNTU=G*DAREA/CMIN

```

```

      TB2=TBINT-HEAT/(BMASS*(CBED+FRAC*XB2*CWATER))
      HA2=ENTH(TA2,WA2)/1000.
      ADS=ADS+WATER
      TBED(I)=TB2
      XBED(I)=XB2
      WA1=WA2
      TA1=TA2
40    CONTINUE
C
C OUTLET CONDITIONS ARE STORED AT THE END OF EACH TIME STEP
      TIME=TIME+DT
      PTIME=PTIME+DT
      GTIME=GTIME+DT
      IF (ABS(PTIME/60.-TPRINT).LT.1.E-6) GO TO 41
      GO TO 42
41    NN=NN+1
      PTIME=0.
      PSAT=PS(TA2)
      OUT1(NN)=TIME/60.
      OUT2(NN)=TA2
      OUT3(NN)=WA2
      OUT4(NN)=PATM*WA2/((.622+WA2)*PSAT)
      OUT5(NN)=HA2
42    IF (ABS(GTIME/60.-TGRAPH).LT.1.E-6) GO TO 43
      GO TO 45
43    KK=KK+1
      GTIME=0.
      DO 44 I=1,NBED
      GRAPH(I,KK,1)=TBED(I)
44    GRAPH(I,KK,2)=XBED(I)
      IF (TIME.EQ.0.) GO TO 13
45    TSUM=TSUM+TA2
      WSUM=WSUM+WA2
      HSUM=HSUM+HA2
46    CONTINUE
C
C AVERAGE OUTLET STATES ARE CALCULATED AT THE END OF
C EACH HALF CYCLE.
      TAVE=TSUM/FLOAT(NPASS)
      WAVE=WSUM/FLOAT(NPASS)
      HIN=ENTH(TIN(M),WIN(M))/1000.
      HAVE=HSUM/FLOAT(NPASS)
      DELH=HAVE-HIN
      ADFRAC=ADS/(FRAC*BMASS*NBED)
      IF (NCYCLE.GT.100) GO TO 47
      IF ((ABS((ADS+ADSOLD)/ADS).LT.ADSERR).AND.(M.EQ.1)) GO TO 47
      IF (FLAG) GO TO 47
      GO TO 54
47    IF (M.EQ.2) GO TO 48
      WRITE(6,98)
      T(7)=TAVE
      W(7)=WAVE
      HS(7)=HAVE
      GO TO 49
48    WRITE(6,99)
      T(5)=TAVE
      W(5)=WAVE
      HS(5)=HAVE
C
C RESULTS ARE PRINTED FOR EACH HALF CYCLE ONCE THE CONVERGENCE
C LIMIT FOR THE BALANCE OF WATER ADSORBED AND DESORBED IS ACHIEVED.
49    WRITE(6,100) AFRONT,HEIGHT,DIAM,ARATIO,FRAC,BDENS,CBED,

```

```

      EFF=(1.-EXP(-RNTU*(1.-CC)))/(1.-CC*EXP(-RNTU*(1.-CC)))
      RMA2=RMA1-EFF*(RMA1-RMS)
      WA2=RMA2/(1.-RMA2)
      WATER=AMASS*(WA1-WA2)
      XB2=(XB1*FRAC*BMASS+WATER)/(FRAC*BMASS)
C
C ENERGY BALANCE
C AN INTERMEDIATE TEMPERATURE IS CALCULATED FOR THE BED SECTION WHILE THE
C AIR IS ASSUMED TO REMAIN AT ITS INITIAL TEMPERATURE. THE DIFFERENCE
C BETWEEN THE HEAT OF ADSORPTION AND THE HEAT OF VAPORIZATION IS
C ACCOUNTED FOR. HSHV IS THE RATIO OF THE HEAT OF ADSORPTION TO
C THE HEAT OF VAPORIZATION AND IS RETURNED BY SUBROUTINE PROPS.
      HVAP=2358500.-2460.*(TB1-60.)
      TBINT=(TB1*BMASS*(CBED+FRAC*XB1*CWATER)
1      +AMASS*(ENTH(TA1,WA1)-ENTH(TA1,WA2))+WATER*HVAP*
2      (HSHV-1.))/(BMASS*(CBED+FRAC*XB2*CWATER))
C
C HEAT TRANSFER CALCULATION:
C THE MODEL ASSUMES THAT THE FINAL TEMPERATURES OF THE AIR CHUNK
C AND THE BED SECTION AT THE END OF THE TIME STEP ARE THE SAME AS
C THE STEADY STATE OUTLET TEMPERATURES FROM A SIMPLE COUNTER FLOW
C HEAT EXCHANGER THAT HAS STEADY FLOWS OF AIR AND DESICCANT MATERIAL
C WITH INLET CONDITIONS EQUAL TO THE INITIAL CONDITIONS OF THE AIR
C CHUNK AND THE BED SECTION. THE EFFECTIVENESS OF THIS HEAT
C EXCHANGE PROCESS IS DETERMINED BY THE HEAT TRANSFER COEFFICIENT,
C THE TOTAL SURFACE AREA IN THE BED SECTION, AND THE HEAT CAPACITY
C RATES OF THE AIR AND BED MATERIAL.
      CA=AMASS*DHD(TA1,WA2)/DT
      CB=BMASS*(CBED+XB2*FRAC*CWATER)/DT
      CMIN=AMIN1(CA,CB)
      CMAX=AMAX1(CA,CB)
      CC=CMIN/CMAX
      RNTU=H*DAREA/CMIN
      EFF=(1.-EXP(-RNTU*(1.-CC)))/(1.-CC*EXP(-RNTU*(1.-CC)))
      HEAT=EFF*CMIN*(TBINT-TA1)*DT
      TA2=TA1+HEAT/(DHD(TA1,WA2)*AMASS)
1  TIN(M),WIN(M),FLOW,TRUN,DT,NBED,RMASS,RLEWIS(M),ICORR
2  ,RMASS
      WRITE(6,101)NCYCLE,TAVE,WAVE,HIN,HAVE,DELH,ADS,ADFRAC
      IF (IPL0T.EQ.0) GO TO 59
      IF (M.EQ.1) NA=NN
      IF (M.EQ.2) NR=NN
      DO 51 I=1,NN
      IF (M.EQ.1) TPA(I)=OUT2(I)
      IF (M.EQ.1) WPA(I)=OUT3(I)
      IF (M.EQ.2) TPR(I)=OUT2(I)
      IF (M.EQ.2) WPR(I)=OUT3(I)
51  WRITE(6,102) OUT1(I),OUT2(I),OUT3(I),OUT4(I),OUT5(I)
      WRITE(6,103)
      DO 52 L=1,KK
      TG=TGRAPH*FLOAT(L-1)
      WRITE(6,104) TG
      DO 52 I=1,NBED
52  WRITE(6,105) I,GRAPH(I,L,1),GRAPH(I,L,2)
C
C BEGIN PLOTTING ROUTINES USING DISSPLA
C
      STEP=1.
      IF (TRUN.GE.14.) STEP=2.
      IF (TRUN.GE.20.) STEP=10.
      CALL TITLE("OUTLET AIR TEMPERATURE (C)",-22,
1      "TIME (MINUTES)",14,"TEMPERATURE (C)&".15,5.,3.5)
      CALL XINTAX
      CALL YTICKS(2)
      CALL GRAF(0.,STEP,TRUN,20.,20.,100.)
      CALL CURVE(OUT1,OUT2,NN,0)
      CALL FRAME
      CALL RLVEC(0.,TIN(M),TRUN,TIN(M),1202)
      CALL ENDPL(0)
      CALL TITLE("OUTLET AIR HUMIDITY",-19,"TIME (MINUTES)",14,
1      "HUMIDITY (KG/KG)",16,5.,3.5)
      CALL YTICKS(5)
      CALL GRAF(0.,STEP,TRUN,0.,.01,.03)
      CALL CURVE(OUT1,OUT3,NN,0)
      CALL FRAME
      CALL RLVEC(0.,WIN(M),TRUN,WIN(M),1202)
      CALL ENDPL(0)

```

```

CALL TITLE("DESICCANT TEMP. PROFILES",-24,
1 "BED LOCATION",12,"TEMPERATURE (C)",15,5.,3.5)
CALL YTICKS(2)
RNBD=FLOAT(NBED)
CALL GRAF(1.,1.,RNBD,20.,20.,100.)
CALL FRAME
DO 56 I=1,KK
DO 55 K=1,NBED
Y(K)=GRAPH(K,I,1)
55 X(K)=FLOAT(K)
56 CALL CURVE(X,Y,NBED,0)
CALL RLVEC(1.,TIN(M),RNBD,TIN(M),1202)
START=FLOAT(NBED/2-3)
FINISH=FLOAT(NBED/2+3)
IF (M.EQ.1) CALL RLVEC(START,93.,FINISH,93.,1501)
IF (M.EQ.2) CALL RLVEC(FINISH,93.,START,93.,1501)
CALL ENDPL(0)
CALL TITLE("LOADING PROFILES",-16,
1 "BED LOCATION",12,"WATER CONTENT (KG/KG)",21,5.,3.5)
CALL YTICKS(1)
CALL GRAF(1.,1.,RNBD,0.,.1.,.4)
CALL FRAME
DO 58 I=1,KK
DO 57 K=1,NBED
Y(K)=GRAPH(K,I,2)
57 X(K)=FLOAT(K)
58 CALL CURVE(X,Y,NBED,0)
IF (M.EQ.1) CALL RLVEC(START,.35,FINISH,.35,1501)
IF (M.EQ.2) CALL RLVEC(FINISH,.35,START,.35,1501)
CALL ENDPL(0)
59 IF (FLAG) GO TO 60
FLAG=.TRUE.
54 IF (M.EQ.1) NEXT=2
IF (M.EQ.2) NEXT=1
M=NEXT
ADSOLD=ADS
NCYCLE=NCYCLE+1
GO TO 11

C
C FINAL SYSTEM PERFORMANCE CALCULATIONS
C
C OUTLET STATES FROM THE SENSIBLE HEAT EXCHANGER
60 CADS=FLOW*DHD(T(7),W(7))
CREG=FLOW*DHD(T(2),W(2))
CMIN=AMIN1(CADS,CREG)/1000.
QEXCH=EHX*CMIN*(T(7)-T(2))
W(8)=W(7)
HS(3)=HS(2)+QEXCH/FLOW
HS(8)=HS(7)-QEXCH/FLOW
T(3)=TH(HS(3),W(3))
T(8)=TH(HS(8),W(8))
HS(4)=ENTH(T(4),W(4))/1000.

C
C SOLAR OR AUXILIARY ENERGY INPUT REQUIRED TO REACH
C THE SPECIFIED REGENERATION TEMPERATURE
DHREG=HS(4)-HS(3)
QREGEN=FLOW*DHREG

C
C OUTLET STATE FROM EVAPORATIVE COOLER 2
CALL WETBLB(T(8),W(8),HS(8),TWB,PATM)
PSAT=PS(TWB)
WSTAR=.622*PSAT/(PATM-PSAT)
T(9)=T(8)+EC2*(TWB-T(8))
W(9)=W(8)+EC2*(WSTAR-W(8))
HS(9)=ENTH(T(9),W(9))/1000.

C
C COOLING CAPACITY AND THERMAL COP
HROOM=ENTH(TROOM,WROOM)/1000.
DHCOOL=HROOM-HS(9)
CAP=DHCOOL*FLOW
COP=CAP/QREGEN

```

```

C
C PRINT SYSTEM RESULTS
  WRITE(6,106)
  IF (MODE.EQ.1) WRITE(6,107) EC1,EHX,EC2
  IF (MODE.EQ.2) WRITE(6,108) EC1,EHX,EC2
  WRITE(6,109)
  DO 80 I=1,9
80  WRITE(6,110) I,T(I),W(I),HS(I)
  WRITE(6,111) DHCOOL,DHREG,QREGEN,CAP,COP
  IF (IPL0T.EQ.0) GO TO 91
C
C PLOT OF DEHUMIDIFIER OUTLET STATES ON THE PSYCH CHART
  CALL TITLE("PSYCHROMETRIC CHART",-19,
1      "DRY BULB TEMPERATURE (C)",24,
2      "HUMIDITY RATIO (KG/KG)",22.5,.3.5)
  CALL XTICKS(1)
  CALL YTICKS(5)
  CALL GRAF(10.,10.,100.,0...01,.03)
  CALL BLNK1(0.,5.,3.5,4.0,0)
  CALL FRAME
  CALL CURVE(TPA,WPA,NA,1)
  CALL CURVE(TPR,WPR,NR,1)
  DO 71 I=1,10
  RH=.01*FLOAT(I)
  NP=0
  DO 70 IT=10,100
  NP=NP+1
  X(NP)=FLOAT(IT)
  TDB=X(NP)+273.
  PSAT=EXP(23.28199-3780.82/TDB-225805./TDB**2)
  Y(NP)=.622*RH*PSAT/(PATM-RH*PSAT)
70  IF (Y(NP).GT..031) Y(NP)=.03
  CALL CURVE(X,Y,NP,0)
71  CONTINUE
  DO 73 I=2,10
  RH=FLOAT(I)*.1
  NP=0
  DO 72 IT=10,65
  NP=NP+1
  X(NP)=FLOAT(IT)
  TDB=FLOAT(IT)+273.
  PSAT=EXP(23.28199-3780.82/TDB-225805./TDB**2)
  Y(NP)=.622*RH*PSAT/(PATM-RH*PSAT)
72  IF ((Y(NP).GE..031).OR.(Y(NP).LT.0.)) Y(NP)=.03
  CALL CURVE(X,Y,NP,0)
73  CONTINUE
  CALL ENDPL(0)
C
C PLOT OF COMPLETE CYCLE ON THE PSYCH CHART
  CALL RESET("BLNK1")
  CALL TITLE("PSYCHROMETRIC CHART",-19,
1      "DRY BULB TEMPERATURE (C)",24,
2      "HUMIDITY RATIO (KG/KG)",22.5,.3.5)
  CALL XTICKS(1)
  CALL YTICKS(5)
  CALL GRAF(10.,10.,100.,0...01,.03)
  CALL BLNK1(0.,5.,3.5,4.0,0)
  CALL FRAME
  DO 83 I=1,10
  RH=.01*FLOAT(I)
  NP=0
  DO 84 IT=10,100
  NP=NP+1
  X(NP)=FLOAT(IT)
  TDB=X(NP)+273.
  PSAT=EXP(23.28199-3780.82/TDB-225805./TDB**2)
  Y(NP)=.622*RH*PSAT/(PATM-RH*PSAT)
84  IF (Y(NP).GT..0318) Y(NP)=.03
  CALL CURVE(X,Y,NP,0)
83  CONTINUE
  DO 86 I=2,10
  RH=FLOAT(I)*.1
  NP=0
  DO 85 IT=10,65

```

```

      NP=NP+1
      X(NP)=FLOAT(IT)
      TDB=FLOAT(IT)+273.
      PSAT=EXP(23.28199-3780.82/TDB-225805./TDB**2)
      Y(NP)=.622*RH*PSAT/(PATM-RH*PSAT)
85  IF ((Y(NP).GE..032).OR.(Y(NP).LT.0.)) Y(NP)=.03
      CALL CURVE(X,Y,NP,0)
86  CONTINUE
      DO 81 I=1,5
        X(I)=T(I)
81  Y(I)=W(I)
        CALL CURVE(X,Y,5,1)
        DO 82 I=1,4
          X(I)=T(I+5)
82  Y(I)=W(I+5)
        CALL CURVE(X,Y,4,1)
        CALL ENDOPL(0)
90  CALL DONEPL
91  CONTINUE
      STOP

```

C

C FORMAT STATEMENTS FOR PRINTED OUTPUT

```

98  FORMAT("1",////,1X,15HADSORPTION MODE)
99  FORMAT("1",////,1X,17HREGENERATION MODE)
100 FORMAT(//,1X,15HBED PARAMETERS:,10X,22HFRONTAL AREA (M2)   =,
      1F6.0,/,26X,22HBED THICKNESS (M)   =,F5.3,
      2/,26X,22HPARTICLE DIAM. (M)   =,F8.6,
      2/,26X,22HSURFACE AREA (M2/M3) =,F6.0,
      3/,26X,22HDESICCANT FRACTION   =,F5.3,
      3/,26X,22HBED DENSITY (KG/M3)  =,F5.0,
      4/,26X,22HSPECIFIC HEAT OF BED =,F5.0,
      5//,1X,19HCONDITIONS FOR RUN:,6X,8HTIN (C)=,F5.1,/,26X,4HWIN=,F6.5,
      6/,26X,17HFLOW RATE (KG/S)=,F8.5,
      7/,26X,13HPERIOD (MIN)=,F8.1,/,26X,
      814HTIME STEP (S)=,F5.0,/,26X,5HNBED=,I2,
      9/,26X,11HMASS RATIO=,F5.3,
      1/,26X,22HLEWIS NUMBER           =,F3.1,
      2/,26X,22HPROPERTY CORRELATION =,I2)
101 FORMAT(//,1X,7HNCYCLE=,I3,10X,5HTAVE=,F5.1,10X,5HWAVE=,F6.5,/,
      121H ENTHALPY IN (KJ/KG)=,F8.4,5X,13HENTHALPY OUT=,F8.4,
      25X,7HCHANGE=,F8.4,/,
      31X,18HWATER CYCLED (KG)=,F10.5,5X,23HFRACTION OF BED CYCLED=,F6.4,
      4 /,"1",////,1X,18HOUTLET CONDITIONS:,2X,
      5 10HTIME (MIN),10X,8HTOUT (C),9X,12HWOUT (KG/KG),11X,4HROUT,
      6 6X,"ENTHALPY (KJ/KG)",/)
102 FORMAT(20X,F10.3,10X,F8.2,10X,F10.6,10X,F7.4,10X,F8.4)
103 FORMAT("1",////,1X,36HTEMPERATURE AND LOADING PROFILES AT ,
      123HTGRAPH TIME INCREMENTS:,//)
104 FORMAT(//,1X,5HTIME=,F8.1,1X,5H MIN.,/,11X,4HNBED,13X,
      110TEMP (C) ,9X,7HLOADING,/)
105 FORMAT(12X,I2,10X,F10.2,10X,F10.5)
106 FORMAT("1",////,1X,34HSYSTEM PERFORMANCE CHARACTERISTICS)
107 FORMAT(/,1X,"VENTILATION MODE: 1-ROOM, 6-AMBIENT,",
      1 " 9-DELIVERED",/,1X,"EFFECTIVITIES: EC1-",F3.2," EHX-",F3.2,
      2 " EC2-",F3.2)
108 FORMAT(/,1X,"RECIRCULATION MODE: 1-AMBIENT, 6-ROOM,",
      1 " 9-DELIVERED",/,1X,"EFFECTIVITIES: EC1-",F3.2," HX-",F3.2,
      2 " EC2-",F3.2)
109 FORMAT(//,1X,"STATE POINTS:",12X,"I",11X,"TEMP (C)",6X,
      1 "HUMIDITY (KG/KG)",3X,"ENTHALPY (KJ/KG)",/)
110 FORMAT(26X,I1,7X,F10.3,9X,F10.5,8X,F10.3)
111 FORMAT(//,26X,"DHCOOL=",F8.3," KJ/KG DRY AIR",/,
      1 26X,"DHREG =",F8.3," KJ/KG DRY AIR",/,
      3 26X,"QREG =",F8.3," KW",/,
      4 26X,"CAP. =",F8.3," KW",/,
      5 26X,"COP =" ,F8.3,/, "1")
      END

```

C

C

C SATURATION VAPOR PRESSURE AS A FUNCTION OF TEMPERATURE.

C CORRELATION FROM MACLAINE-CROSS THESIS.

```

      FUNCTION PS(T)
      TK=T+273.
      PS=EXP(23.28199-3780.82/TK-225805./TK**2)
      RETURN
      END

```



```

C
C
C ENTHALPY OF AIR AS A FUNCTION OF TEMPERATURE AND HUMIDITY
C CORRELATION FROM MACLAINE-CROSS THESIS
  FUNCTION ENTH(T,W)
    ENTH=(1005.22+.02615*T)*T+W*(2500800.+1868.*T)
  RETURN
  END

C
C
C FUNCTION FOR TEMP. FROM ENTHALPY AND HUMIDITY RATIO.
C FROM MACLAINE-CROSS THESIS
  FUNCTION TH(H,W)
    D=(1005.22+1868.*W)/.0523
    TH=-D+SQRT(D*D+(H*1000.-2500800*W)/.02615)
  RETURN
  END

C
C
C FUNCTION FOR THE SPECIFIC HEAT OF AIR
  FUNCTION DHDT(T,W)
    DHDT=1005.22+.0523*T+1868.*W
  RETURN
  END

C
C
C SUBROUTINE FOR WET BULB TEMP. GIVEN DRY BULB TEMP. AND HUMIDITY
C BASED ON EQUATIONS FROM ASHRAE CHAPTER ON PSYCHROMETRICS.
C THE BISECTION METHOD IS USED FOR THIS ITERATIVE SOLUTION.
  SUBROUTINE WETBLB(TDB,W,H,TWB,PATM)
    H0=H+20.1
    TSTART=(-13.9+.5696*H0-.001665*H0**2)
    THI=TSTART+2.
    TLO=TSTART-2.
    DO 5 I=1,15
      TWB=(THI+TLO)/2.
      PSAT=PS(TWB)
      WSTAR=.622*PSAT/(PATM-PSAT)
      TF=TWB*1.8+32.
      TDF=TDB*1.8+32.
      WCHECK=((1093.-.556*TF)*WSTAR-.24*(TDF-TF))/(1093.+ .444*TDF-TF)
      IF (WCHECK.GT.W) THI=TWB
      IF (WCHECK.LT.W) TLO=TWB
    5  CONTINUE
  RETURN
  END

C
C SUBROUTINE FOR THE EQUILIBRIUM PROPERTIES OF REGULAR DENSITY
C SILICA GEL. CORRELATIONS BASED ON EXPERIMENTAL DATA ARE USED
C TO CALCULATE THE EQUILIBRIUM VAPOR PRESSURE AT THE DESICCANT
C SURFACE AND TO CALCULATE THE RATIO OF THE HEAT OF ADSORPTION
C TO THE HEAT OF VAPORIZATION. THREE CORRELATIONS ARE INCLUDED,
C AND THE PASSED INTEGER "ICORR" DETERMINES WHICH ONE IS USED.
C
C      ICORR=1      BULLOCK AND THRELKELD FIT TO HUBARD'S DATA
C                   AND CLOSE AND BANKS EQNS FOR HADS/HVAP.
C
C      ICORR=2      CLOSE AND BANKS FIT TO HUBARD'S DATA.
C                   F(X)=2.009*X AND LINEAR EQNS FOR HADS/HVAP ARE USED.
C
C      ICORR=3      FIT TO DATA OF F. ROJAS FOR DAVISON PA-40
C                   SILICA GEL. LINEAR EQNS FOR HADS/HVAP.
C
C      SUBROUTINE PROPS(ICORR,X,TC,PSAT,PVE,HSHV)
C      GO TO (10,30,40) ICORR

C
C ICORR=1
C
10  T=TC*1.8+32.
    IF(X.GT..05) GO TO 11
    PVE=((((4.02253E-4*X+1.186214E-5)*T-8.938272E-2*
    1X-3.267901E-3)*T+7.068827*X+.322929)*T-182.1523*X-
    210.41436)*X
    GO TO 17

```

```

11 IF (X.GT..1) GO TO 12
   PVE=(((-7.808642E-6*X+1.989198E-6)*T+4.312037E-3*X-
1  6.024537E-4)*T-.484787*X+.058058)*T+17.20448*X-1.836323
   GO TO 17
12 IF (X.GT..15) GO TO 13
   PVE=(( (2.083333E-5*X-8.75E-7)*T-3.825E-3*X+2.1125E-4)*T
1  +.255417*X-.015963)*T-4.6825*X+.352375
   GO TO 17
13 IF (X.GT..2) GO TO 14
   PVE=(( (5.333333E-5*X-5.75E-6)*T-1.38E-2*X+1.7075E-3)
1  *T+1.264667*X-.16735)*T-38.*X+5.35
   GO TO 17
14 IF (X.GT..25) GO TO 15
   PVE=(( (-8.166667E-5*X+2.125E-5)*T+2.135E-2*X-5.3225E-3)
1  *T-1.752333*X+.43605)*T+47.6*X-11.77
   GO TO 17
15 IF (X.GT..3) GO TO 16
   PVE=(( (4.E-5*X-9.16667E-6)*T-8.1E-3*X+2.04E-3)
1  *T+.599*X-.151783)*T-14.1*X+3.655
   GO TO 17
16 PVE=(( (2.E-5*X-3.166667E-6)*T-3.7E-3*X+7.2E-4)
1  *T+.291*X-.059383)*T-6.9*X+1.495
17 PVE=PVE*101325./29.92
   IF (X.GT..04) GO TO 21
   HSHV=8533.*X**3-542.*X*X+11.79*X+1.1557
   GO TO 50
21 IF (X.GT..1) GO TO 22
   HSHV=45.4*X*X-8.97*X+1.5922
   GO TO 50
22 HSHV=-9.1553*X**3+7.048*X*X-1.8966*X+1.2789
   GO TO 50

C
C ICORR=2
C
30 IF (X.GT..1) GO TO 31
   HSHV=1.3-1.75*X
   GO TO 32
31 HSHV=1.14-.15*X
32 PVE=(101325./29.91)*(29.91*2.009*X*PSAT/101325.)*HSHV
   GO TO 50

C
C ICORR=3
C
40 IF (X.GT..1) GO TO 41
   HSHV=1.3-1.75*X
   GO TO 42
41 HSHV=1.14-.15*X
42 R=(.616238*X+16.7916*X*X-74.34228*X**3+116.6834*X**4)
1  /(1.-(TC-40.)/300.)
   PVE=R*PSAT
50 RETURN
   END

C
C
C
C SUBROUTINE FOR CALCULATING THE PARTIAL DERIVATIVE OF THE MASS
C FRACTION OF WATER IN THE DESICCANT WITH RESPECT TO THE MASS
C FRACTION OF WATER IN THE AIR AT EQUILIBRIUM. THREE CORRELATIONS
C ARE INCLUDED, AND THE PASSED INTEGER "ICORR" DETERMINES WHICH
C CORRELATION IS USED.
C DERIVATIVES OF THE EQUATIONS GIVEN IN SUBROUTINE PROPS ARE USED.
C
C SUBROUTINE DERIV(ICORR,X,TC,RMS,HSBV,PATM,PSAT,DYDMS)
C GO TO (10,20,30) ICORR

C
C ICORR=1
C
10 T=TC*1.8+32.
   IF (X.GT..05) GO TO 11
   DPVDX=(( (8.0453E-4*X+11.862E-6)*T-.17876*X+32.679E-4)*T
1  +14.138*X+.32293)*T-364.34*X-10.414
   GO TO 50

```

```

11  IF (X.GT..1) GO TO 12
    DPVDX=(((-7.8086E-6*T+43.12E-4)*T-.48479)*T+17.204
    GO TO 50
12  IF (X.GT..15) GO TO 13
    DPVDX=((20.833E-6*T-38.25E-4)*T+2.5542)*T-4.6825
    GO TO 50
13  IF (X.GT..2) GO TO 14
    DPVDX=((53.333E-6*T-.0138)*T+1.2647)*T-38.
    GO TO 50
14  IF (X.GT..25) GO TO 15
    DPVDX=(((-81.667E-6*T+.02135)*T-1.7523)*T+47.6
    GO TO 50
15  IF (X.GT..3) GO TO 16
    DPVDX=((4.E-5*T-81.E-4)*T+.599)*T-14.1
    GO TO 50
16  DPVDX=((2.E-5*T-37.E-4)*T+.291)*T-6.9
    GO TO 50

C
C ICORR=2
C
20  C1=3388.
    C2=5.93E-4*PSAT
    C3=-1.75
    IF (X.GT..1) C3=-.15
    DPVDX=C1*(C2*HSHV*(C2*X)**(HSHV-1.))+C3*(C2*X)**HSHV*ALOG(C2*X)
    GO TO 50

C
C ICORR=3
C
30  DPVDX=PSAT*(.616238+33.5832*X-223.027*X*X+466.734*X**3)
    1  /((1.-(TC-40.)/300.))
50  DYDMS=.622*PATM/((1.+X)**2*(.622+.378*RMS)**2*DPVDX)
    RETURN
    END

```

```

      PROGRAM DESSIM4(INPUT,OUTPUT,TAPE5=INPUT,TAPE6=OUTPUT)
C
C *****
C *
C * DESSIM4: SIMULATION OF SILICA GEL COOLING SYSTEMS *
C * R. BARLOW, SERI, DECEMBER 1980 *
C *
C *****
C
C THIS VERSION OF THE DESSIM PROGRAM IS DESIGNED TO BE USED
C FOR PARAMETRIC STUDIES ON DESICCANT COOLING SYSTEMS.
C NO GRAPHICS ARE INCLUDED.
C
C
C      DIMENSION TBED(50),XBED(50),TIN(2),WIN(2),RLEWIS(2),
      3T(9),W(9),HS(9),PARAM1(6),PARAM2(5)
      LOGICAL FLAG2
C
C DEFINE CONSTANTS IN SI UNITS
      PATM=101325.
      CAIR=1006.
      CWATER=4181.
C
C READ DATA. NOTE THAT SOME OF THE INPUT VARIABLES ARE ARRAYS.
      READ(5,*) ARATIO,BDENS,FRAC,DIAM,HEIGHT,AFRONT,CBED
      READ(5,*) TROOM,WROOM,TAMB,WAMB,TREG
      READ(5,*) FLOW,TRUN,DT,TB0,XB0,NBED
      READ(5,*) EC1,EHX,EC2,MODE,RLEWIS,ICORR
      READ(5,*) PARAM1
      READ(5,*) PARAM2
C
C INITIALIZE TEMPERATURE AND WATER CONTENT OF DESICCANT BED.
      DO 1 I=1,NBED
        TBED(I)=TB0
      1  XBED(I)=XB0
C
C LOOP FOR PARAMETRIC EVALUATION
C THESE LINES SHOULD BE MODIFIED TO CARRY OUT DIFFERENT PARAMETRIC
C STUDIES. NOTE THAT THE DIMENSIONS OF PARAM1 AND PARAM2 MAY NEED
C TO BE CHANGED.
      DO 91 IP=1,2
        MODE=IP
        DO 91 IP1=1,6
          TAMB=PARAM1(IP1)
          DO 91 IP2=1,5
            WAMB=PARAM2(IP2)
C
C INITIALIZE COUNTERS AND FLAG.
      ADSOLD=0.
      NCYCLE=1
      M=1
      ADSERR=.001
      FLAG2=.FALSE.
C
C INITIAL SYSTEM PERFORMANCE CALCULATIONS
      IF (MODE.EQ.2) GO TO 2
      T(1)=TROOM
      W(1)=WROOM
      T(6)=TAMB
      W(6)=WAMB
      GO TO 3
      2  T(1)=TAMB
        W(1)=WAMB
        T(6)=TROOM
        W(6)=WROOM
      3  T(4)=TREG
        HS(1)=ENTH(T(1),W(1))/1000.
        HS(6)=ENTH(T(6),W(6))/1000.
        CALL WETBLB(T(1),W(1),HS(1),TWB,PATM)
        PSAT=PS(TWB)
        WSTAR=.622*PSAT/(PATM-PSAT)
        T(2)=T(1)+EC1*(TWB-T(1))
        W(2)=W(1)+EC1*(WSTAR-W(1))
        HS(2)=ENTH(T(2),W(2))/1000.

```

```

      W(3)=W(2)
      W(4)=W(3)
      TIN(1)=T(6)
      WIN(1)=W(6)
      TIN(2)=T(4)
      WIN(2)=W(4)
C
C
C SET UP PARAMETERS FOR DESICCANT SIMULATION.
      HSEC=HEIGHT/FLOAT(NBED)
      BMASS=HSEC*AFRONT*BDENS
      DAREA=HSEC*AFRONT*ARATIO
C
C INITIALIZE COUNTERS FOR ADSORPTION OR REGENERATION HALF CYCLE.
11  AMASS=FLOW*DT
      NPASS=INT(TRUN*60./DT)
      TIME=0.
      ADS=0.
      TSUM=0.
      WSUM=0.
      HSUM=0.
      RMASS=AMASS/BMASS
C
C TRANSFER COEFFICIENTS FROM HADLEY AND HEGGS CORRELATION.
13  GA=FLOW/AFRONT
      RK=.02624+7.58E-5*(TIN(M)-27.)
      RMU=1.859E-5+4.32E-8*(TIN(M)-27.)
      H=.58*RK*(DIAM*GA/RMU)**.67/DIAM
      G=H/(CAIR*RLEWIS(M))
C
C MAIN CALCULATION LOOP
      DO 46 N=1,NPASS
        WA1=WIN(M)
        TA1=TIN(M)
        DO 40 II=1,NBED
          IF (M.EQ.1) I=II
          IF (M.EQ.2) I=NBED+1-II
          TB1=TBED(I)
          XB1=XBED(I)
C
C MASS TRANSFER CALCULATION: COUNTER-FLOW EXCHANGER METHOD.
C THE AMOUNT OF WATER TRANSFERED IN A SINGLE TIME STEP IS
C CALCULATED USING EQUATIONS ANALOGOUS TO THOSE FOR A
C STEADY STATE COUNTER-FLOW HEAT EXCHANGER. THE QUANTITY
C "DYDMS" IS THE PARTIAL DERIVATIVE OF THE DESICCANT LOADING
C FRACTION WITH RESPECT TO THE EQUILIBRIUM MASS FRACTION
C OF WATER IN THE AIR AT THE INTERFACE. THIS IS ANALOGOUS TO
C THE SPECIFIC HEAT IN THE HEAT TRANSFER PROBLEM AND REPLACES
C THE INVERSE OF HENRY CONSTANT USED IN GAS-LIQUID MASS EXCHANGE
C PROBLEMS.
          PSAT=PS(TB1)
          CALL PROPS(ICORR,XB1,TB1,PSAT,PVE,HSHV)
          RMS=.622*PVE/(PATM-.378*PVE)
          RMA1=WA1/(1.+WA1)
          CA=AMASS*(1.+WA1)/DT
          CALL DERIV(ICORR,XB1,TB1,RMS,HSHV,PATM,PSAT,DYDMS)
          CB=FRAC*BMASS*(1+XB1)*DYDMS/DT
          CMIN=AMIN1(CA,CB)
          CMAX=AMAX1(CA,CB)
          CC=CMIN/CMAX
          RNTU=G*DAREA/CMIN
          EFF=(1.-EXP(-RNTU*(1.-CC)))/(1.-CC*EXP(-RNTU*(1.-CC)))
          RMA2=RMA1-EFF*(RMA1-RMS)
          WA2=RMA2/(1.-RMA2)
          WATER=AMASS*(WA1-WA2)
          XB2=(XB1*FRAC*BMASS+WATER)/(FRAC*BMASS)
C
C ENERGY BALANCE
C A NEW TEMPERATURE IS CALCULATED FOR THE BED SECTION WHILE THE
C AIR IS ASSUMED TO REMAIN AT ITS INITIAL TEMPERATURE. THE DIFFERENCE
C BETWEEN THE HEAT OF ADSORPTION AND THE HEAT OF VAPORIZATION IS
C ACCOUNTED FOR. HSHV IS THE RATIO OF THE HEAT OF ADSORPTION TO

```

```

C THE HEAT OF VAPORIZATION AND IS RETURNED BY SUBROUTINE PROPS.
  HVAP=2358500.-2460.*(TB1-60.)
  TBINT=(TB1*BMASS*(CBED+FRAC*XB1*CWATER)
1    +AMASS*(ENTH(TA1,WA1)-ENTH(TA1,WA2))+WATER*HVAP*
2    (HSHV-1.))/(BMASS*(CBED+FRAC*XB2*CWATER))
C
C HEAT TRANSFER CALCULATION:
C THE MODEL ASSUMES THAT THE FINAL TEMPERATURES OF THE AIR CHUNK
C AND THE BED SECTION AT THE END OF THE TIME STEP ARE THE SAME AS
C THE STEADY STATE OUTLET TEMPERATURES FROM A SIMPLE COUNTER FLOW
C HEAT EXCHANGER THAT HAS STEADY FLOWS OF AIR AND DESICCANT MATERIAL
C WITH INLET CONDITIONS EQUAL TO THE INITIAL CONDITIONS OF THE AIR
C CHUNK AND THE BED SECTION. THE EFFECTIVENESS OF THIS HEAT
C EXCHANGE PROCESS IS DETERMINED BY THE HEAT TRANSFER COEFFICIENT,
C THE TOTAL SURFACE AREA IN THE BED SECTION, AND THE HEAT CAPACITY
C RATES OF THE AIR AND BED MATERIAL.
  CA=AMASS*DHDT(TA1,WA2)/DT
  CB=BMASS*(CBED+FRAC*XB2*CWATER)/DT
  CMIN=AMIN1(CA,CB)
  CMAX=AMAX1(CA,CB)
  CC=CMIN/CMAX
  RNTU=H*DAREA/CMIN
  EFF=(1.-EXP(-RNTU*(1.-CC)))/(1.-CC*EXP(-RNTU*(1.-CC)))
  HEAT=EFF*CMIN*(TB2-TA1)*DT
  TA2=TA1+HEAT/(DHDT(TA1,WA2)*AMASS)
  TB2=TBINT-HEAT/(BMASS*(CBED+FRAC*XB2*CWATER))
  ADS=ADS+WATER
  TBED(I)=TB2
  XBED(I)=XB2
  WA1=WA2
  TA1=TA2
40  CONTINUE
C
C OUTLET CONDITIONS ARE STORED AT THE END OF EACH TIME STEP
  TIME=TIME+DT
  TSUM=TSUM+TA2
  WSUM=WSUM+WA2
  HSUM=HSUM+ENTH(TA2,WA2)/1000.
46  CONTINUE
  TAVE=TSUM/FLOAT(NPASS)
  WAVE=WSUM/FLOAT(NPASS)
  HIN=ENTH(TIN(M),WIN(M))/1000.
  HAVE=HSUM/FLOAT(NPASS)
  DELH=HAVE-HIN
  ADFRAC=ADS/(FRAC*BMASS*NBED)
  IF (NCYCLE.GT.100) GO TO 47
  IF ((ABS((ADS+ADSOLD)/ADS).LT.ADSERR).AND.(M.EQ.1)) GO TO 47
  IF (FLAG2) GO TO 47
  GO TO 54
47  IF (M.EQ.2) GO TO 48
  WRITE(6,98)
  T(7)=TAVE
  W(7)=WAVE
  HS(7)=HAVE
  GO TO 49
48  WRITE(6,99)
  T(5)=TAVE
  W(5)=WAVE
  HS(5)=HAVE
49  WRITE(6,100) ARATIO,AFRONT,HEIGHT,DIAM,BDENS,FRAC,
1  TIN(M),WIN(M),FLOW,TRUN,DT,NBED,RMASS,RLEWIS(M),ICORR
  WRITE(6,101) NCYCLE,TAVE,WAVE,HIN,HAVE,DELH,ADS,ADFRAC
  IF (FLAG2) GO TO 60
  FLAG2=.TRUE.
54  ADSOLD=ADS
  IF (M.EQ.1) NEXT=2
  IF (M.EQ.2) NEXT=1
  M=NEXT
  NCYCLE=NCYCLE+1
  GO TO 11

```

C

C FINAL SYSTEM PERFORMANCE CALCULATIONS

```

60 CADS=FLOW*DHOT(T(7),W(7))
   CREG=FLOW*DHOT(T(2),W(2))
   CMIN=AMIN1(CADS,CREG)/1000.
   QEXCH=EHX*CMIN*(T(7)-T(2))
   W(8)=W(7)
   HS(3)=HS(2)+QEXCH/FLOW
   HS(8)=HS(7)-QEXCH/FLOW
   T(3)=TH(HS(3),W(3))
   T(8)=TH(HS(8),W(8))
   HS(4)=ENTH(T(4),W(4))/1000.
   DHREG=HS(4)-HS(3)
   QREGEN=FLOW*DHREG
   CALL WETBLB(T(8),W(8),HS(8),TWB,PATM)
   PSAT=PS(TWB)
   WSTAR=.622*PSAT/(PATM-PSAT)
   T(9)=T(8)+EC2*(TWB-T(8))
   W(9)=W(8)+EC2*(WSTAR-W(8))
   HS(9)=ENTH(T(9),W(9))/1000.
   HROOM=ENTH(TROOM,WROOM)/1000.
   DHCOOL=HROOM-HS(9)
   CAP=DHCOOL*FLOW
   COP=CAP/QREGEN
   WRITE(6,106)
   IF (MODE.EQ.1) WRITE(6,107) EC1,EHX,EC2
   IF (MODE.EQ.2) WRITE(6,108) EC1,EHX,EC2
   WRITE(6,109)
   DO 80 I=1,9
80  WRITE(6,110) I,T(I),W(I),HS(I)
   WRITE(6,111) DHCOOL,DHREG,QREGEN,CAP,COP

91  CONTINUE
   STOP
98  FORMAT("1",////,1X,15HADSORPTION MODE)
99  FORMAT("1",////,1X,17HREGENERATION MODE)
100 FORMAT(//,1X,15HBED PARAMETERS:,10X,22HSURFACE AREA (M2/M3) =,
1 F6.0,/,26X,22HFRONTAL AREA (M2) =,F5.3,
2/,26X,14HBED DEPTH (M)=,F6.4,/,26X,22HPARTICLE DIAMETER (M)=,F8.6,
3/,26X,22HBED DENSITY (KG/M3) =,F5.0,/,26X,19HDESICCANT FRACTION=,
4 F6.3,
5//,1X,19HCONDITIONS FOR RUN:,6X,8HTIN (C)=,F5.1,/,26X,4HWIN=,F6.5,
6/,26X,17HFLOW RATE (KG/S)=,F8.5,/,
726X,13HPERIOD (MIN)=,F8.1,/,26X,
814HTIME STEP (S)=,F5.0,/,26X,5HNBED=,I2,
9/,26X,11HMASS RATIO=,F5.3,
1/,26X,22HLEWIS NUMBER =,F4.1,
2/,26X,22HPROPERTY CORRELATION =,I2)
101 FORMAT(//,1X,7HNCYCLE=,I3,10X,5HTAVE=,F5.1,10X,5HWAVE=,F6.5,/,
121H ENTHALPY IN (KJ/KG)=,F8.4,5X,13HENTHALPY OUT=,F8.4,
25X,7HCHANGE=,F8.4,/,
31X,18HWATER CYCLED (KG)=,F10.5,5X,23HFRACTION OF BED CYCLED=,F6.4,
4 /)
106 FORMAT(//,1X,34HSYSTEM PERFORMANCE CHARACTERISTICS)
107 FORMAT(/,1X,"VENTILATION MODE: 1-ROOM, 6-AMBIENT.",
1 " 9-DELIVERED",//,1X,"EFFECTIVITIES: EC1-",F3.2," EHX-",F3.2,
2 " EC2-",F3.2)
108 FORMAT(/,1X,"RECIRCULATION MODE: 1-AMBIENT, 6-ROOM.",
1 " 9-DELIVERED",//,1X,"EFFECTIVITIES: EC1-",F3.2," EHX-",F3.2,
2 " EC2-",F3.2)
109 FORMAT(//,1X,"STATE POINTS:",12X,"I",11X,"TEMP (C)",6X,
1 "HUMIDITY (KG/KG)",3X,"ENTHALPY (KJ/KG)",//)
110 FORMAT(26X,I1,7X,F10.3,9X,F10.5,8X,F10.3)
111 FORMAT(////,26X,"DHCOOL=",F8.3," KJ/KG DRY AIR",/,
1 26X,"DHREG =",F8.3," KJ/KG DRY AIR",/,
3 26X,"QREG =",F8.0," KW",/,
4 26X,"CAP. =",F8.3," KW",/,
5 26X,"COP =",F8.3)
END

```

```
C
C
C SATURATION VAPOR PRESSURE AS A FUNCTION OF TEMPERATURE.
C CORRELATION FROM MACLAINE-CROSS THESIS.
  FUNCTION PS(T)
    TK=T+273.
    PS=EXP(23.28199-3780.82/TK-225805./TK**2)
    RETURN
  END

C
C ENTHALPY OF AIR AS A FUNCTION OF TEMPERATURE AND HUMIDITY
C CORRELATION FROM MACLAINE-CROSS THESIS
  FUNCTION ENTH(T,W)
    ENTH=(1005.22+.02615*T)*T+W*(2500800.+1868.*T)
    RETURN
  END

C
C FUNCTION FOR TEMP. FROM ENTHALPY AND HUMIDITY RATIO.
C FROM MACLAINE-CROSS THESIS
  FUNCTION TH(H,W)
    D=(1005.22+1868.*W)/.0523
    TH=-D+SQRT(D*D+(H*1000.-2500800*W)/.02615)
    RETURN
  END

C
C FUNCTION FOR THE SPECIFIC HEAT OF AIR FROM MACLAINE-CROSS
  FUNCTION DHOT(T,W)
    DHOT=1005.22+.0523*T+1868.*W
    RETURN
  END

C
C
C SUBROUTINE FOR WET BULB TEMP. GIVEN DRY BULB TEMP. AND HUMIDITY
C BASED ON EQUATIONS FROM ASHRAE CHAPTER ON PSYCHROMETRICS
  SUBROUTINE WETBLB(TDB,W,H,TWB,PATM)
    H0=H+20.1
    TSTART=(-13.9+.5696*H0-.001665*H0**2)
    THI=TSTART+3.
    TLO=TSTART-3.
    DO 5 I=1,20
      TWB=(THI+TLO)/2.
      PSAT=PS(TWB)
      WSTAR=.622*PSAT/(PATM-PSAT)
      TF=TWB*1.8+32.
      TDF=TDB*1.8+32.
      WCHECK=((1093.-.556*TF)*WSTAR-.24*(TDF-TF))/(1093.+ .444*TDF-TF)
      IF (WCHECK.GT.W) THI=TWB
      IF (WCHECK.LT.W) TLO=TWB
    5  CONTINUE
    RETURN
  END

C
C SUBROUTINE FOR THE EQUILIBRIUM PROPERTIES OF REGULAR DENSITY
C SILICA GEL. CORRELATIONS BASED ON EXPERIMENTAL DATA ARE USED
C TO CALCULATE THE EQUILIBRIUM VAPOR PRESSURE AT THE DESICCANT
C SURFACE AND TO CALCULATE THE RATIO OF THE HEAT OF ADSORPTION
C TO THE HEAT OF VAPORIZATION. THREE CORRELATIONS ARE INCLUDED,
C AND THE PASSED INTEGER "ICORR" DETERMINES WHICH ONE IS USED.
C
C      ICORR=1    BULLOCK AND THRELKELD FIT TO HUBARD'S DATA
C                  AND CLOSE AND BANKS EQNS FOR HADS/HVAP.
C
C      ICORR=2    CLOSE AND BANKS FIT TO HUBARD'S DATA.
C                  F(X)=2.009*X AND LINEAR EQNS FOR HADS/HVAP ARE USED.
C
C      ICORR=3    FIT TO DATA OF F. ROJAS FOR DAVISON PA-30
C                  SILICA GEL. LINEAR EQNS FOR HADS/HVAP.
C
C      SUBROUTINE PROPS(ICORR,X,TC,PSAT,PVE,HSBV)
C      GO TO (10,30,40) ICORR
C
C ICORR=1
```



```

C
10  T=TC*1.8+32.
    IF(X.GT..05) GO TO 11
    PVE=((((4.02263E-4*X+1.186214E-5)*T-8.938272E-2*
1X-3.267901E-3)*T+7.068827*X+.322929)*T-182.1523*X-
210.41436)*X
    GO TO 17
11  IF (X.GT..1) GO TO 12
    PVE=(((-7.808642E-6*X+1.989198E-6)*T+4.312037E-3*X-
1 6.024537E-4)*T-.484787*X+.058058)*T+17.20448*X-1.836323
    GO TO 17
12  IF (X.GT..15) GO TO 13
    PVE=((((2.083333E-5*X-8.75E-7)*T-3.825E-3*X+2.1125E-4)*T
1+.255417*X-.015963)*T-4.6825*X+.352375
    GO TO 17
13  IF (X.GT..2) GO TO 14
    PVE=((((5.333333E-5*X-5.75E-6)*T-1.38E-2*X+1.7075E-3)
1*T+1.264667*X-.16735)*T-38.*X+5.35
    GO TO 17
14  IF (X.GT..25) GO TO 15
    PVE=(((-8.166667E-5*X+2.125E-5)*T+2.135E-2*X-5.3225E-3)
1*T-1.752333*X+.43605)*T+47.6*X-11.77
    GO TO 17
15  IF (X.GT..3) GO TO 16
    PVE=((((4.E-5*X-9.16667E-6)*T-8.1E-3*X+2.04E-3)
1*T+.599*X-.151783)*T-14.1*X+3.655
    GO TO 17
16  PVE=((((2.E-5*X-3.166667E-6)*T-3.7E-3*X+7.2E-4)
1*T+.291*X-.059383)*T-6.9*X+1.495
17  PVE=PVE*101325./29.92
    IF (X.GT..04) GO TO 21
    HSHV=8533.*X**3-542.*X*X+11.79*X+1.1557
    GO TO 50
21  IF (X.GT..1) GO TO 22
    HSHV=45.4*X*X-8.97*X+1.5922
    GO TO 50
22  HSHV=-9.1553*X**3+7.048*X*X-1.8966*X+1.2789
    GO TO 50

C
C ICORR=2
C
30  IF (X.GT..1) GO TO 31
    HSHV=1.3-1.75*X
    GO TO 32
31  HSHV=1.14-.15*X
32  PVE=(101325./29.91)*(29.91*2.009*X*PSAT/101325.)*HSHV
    GO TO 50

C
C ICORR=3
C
40  IF (X.GT..1) GO TO 41
    HSHV=1.3-1.75*X
    GO TO 42
41  HSHV=1.14-.15*X
42  R=(.616238*X+16.7916*X*X-74.34228*X**3+116.6834*X**4)
1 /((1.-(TC-40.)/300.)
    PVE=R*PSAT
50  RETURN
    END

```

```

C
C
C
C SUBROUTINE FOR CALCULATING THE PARTIAL DERIVATIVE OF THE MASS
C FRACTION OF WATER IN THE DESICCANT WITH RESPECT TO THE MASS
C FRACTION OF WATER IN THE AIR AT EQUILIBRIUM. THREE CORRELATIONS
C ARE INCLUDED, AND THE PASSED INTEGER "ICORR" DETERMINES WHICH
C CORRELATION IS USED.
C DERIVATIVES OF THE EQUATIONS GIVEN IN SUBROUTINE PROPS ARE USED.
C
      SUBROUTINE DERIV(ICORR,X,TC,RMS,HSHV,PATM,PSAT,DYDMS)
      GO TO (10,20,30) ICORR
C
C ICORR=1
C
      T=TC*1.8+32.
      IF (X.GT..05) GO TO 11
      DPVDX=((8.0453E-4*X+11.862E-6)*T-.17876*X+32.679E-4)*T
      1      +14.138*X+.32293)*T-364.34*X-10.414
      GO TO 50
11      IF (X.GT..1) GO TO 12
      DPVDX=(-7.8086E-6*T+43.12E-4)*T-.48479)*T+17.204
      GO TO 50
12      IF (X.GT..15) GO TO 13
      DPVDX=((20.833E-6*T-38.25E-4)*T+2.5542)*T-4.6825
      GO TO 50
13      IF (X.GT..2) GO TO 14
      DPVDX=((53.333E-6*T-.0138)*T+1.2647)*T-38.
      GO TO 50
14      IF (X.GT..25) GO TO 15
      DPVDX=(-81.667E-6*T+.02135)*T-1.7523)*T+47.6
      GO TO 50
15      IF (X.GT..3) GO TO 16
      DPVDX=((4.E-5*T-81.E-4)*T+.599)*T-14.1
      GO TO 50
16      DPVDX=((2.E-5*T-37.E-4)*T+.291)*T-6.9
      GO TO 50
C
C ICORR=2
C
20      C1=3388.
      C2=5.93E-4*PSAT
      C3=-1.75
      IF (X.GT..1) C3=-.15
      DPVDX=C1*(C2*HSHV*(C2*X)**(HSHV-1.))+C3*(C2*X)**HSHV*ALOG(C2*X))
      GO TO 50
C
C ICORR=3
C
30      DPVDX=PSAT*(.616238+33.5832*X-223.027*X*X+466.734*X**3)
      1      /(1.-(TC-40.)/300.)
50      DYDMS=.622*PATM/((1.+X)**2*(.622+.378*RMS)**2*DPVDX)
      RETURN
      END

```

Document Control Page	1. SERI Report No. TR-631-1330	2. NTIS Accession No.	3. Recipient's Accession No.
4. Title and Subtitle Analysis of the Adsorption Process and of Desiccant Cooling Systems -- A Pseudo-Steady-State Model for Coupled Heat and Mass Transfer		5. Publication Date December 1982	
		6.	
7. Author(s) Robert S. Barlow		8. Performing Organization Rept. No.	
9. Performing Organization Name and Address Solar Energy Research Institute 1617 Cole Boulevard Golden, Colorado 80401		10. Project/Task/Work Unit No. 1131.00 and 1132.11	
		11. Contract (C) or Grant (G) No. (C) (G)	
12. Sponsoring Organization Name and Address		13. Type of Report & Period Covered Technical Report	
		14.	
15. Supplementary Notes			
16. Abstract (Limit: 200 words) This report documents a computer model to simulate the adiabatic adsorption/desorption process. Developed to predict the performance of desiccant cooling systems, the model has been validated through comparison with experimental data for single-blow adsorption and desorption. The report also contains a literature review on adsorption analysis, detailed discussions of the adsorption process, and an initial assessment of the potential for performance improvement through advanced component development.			
17. Document Analysis a. Descriptors Adiabatic processes ; Adsorption ; Computerized simulations ; D codes ; Dessicants ; Packed beds ; Silica gel ; Solar cooling systems b. Identifiers/Open-Ended Terms c. UC Categories 59c			
18. Availability Statement National Technical Information Service U. S. Department of Commerce 5285 Port Royal Road Springfield, Virginia 22161		19. No. of Pages 156	
		20. Price \$8.00	